Republic of Iraq
Ministry of Higher Education and Scientific Research
University of Babylon
College of Sciences for Women
Department of Laser Physics

Theoretical Investigation of Organic Molecules as a Candidate for Optoelectronic Applications

A Thesis

Submitted to the Council of the College of Sciences for Women,

University of Babylon

In Partial Fulfillment of the Requirements for the Degree of

Doctor of Philosophy in Laser Physics and its Applications

By

Saba Razaq Salman Fahad

B.Sc., Laser Physics, University of Babylon (2008)
M.Sc., Physics, University of Babylon (2011)

Supervised by

Assistant. Prof. Dr. Oday A. Al-Owaedi

University of Babylon
College of Science for Women
Laser Physics Department

2022 A.D ***1443A.H***

جمهورية العراق
وزارة التعليم العـالي والبحث العلـمي
جامـــعة بـــابـــل
كليـــة العلـوم للبنات
قســـم فيزيـــاء الليزر

دراسة نظريه لجزيئات عضويه مرشحه للتطبيقات الكهروضوئيه

أطروحة

مقدمه الى مجلس كلية العلوم للبنات في جامعة بابل

وهي جزء من متطلبات نيل درجة الدكتوراه فلسفة في علوم فيزياء الليزر وتطبيقاته

من قبل الطالبه

صبا رزاق سلمان فهد

بكالوريوس في علوم فيزياء الليزر (جامعة بابل - ٢٠٠٨)

ماجستير في علوم الفيزياء (جامعة بابل - ٢٠١١)

بأشراف

أ.م. د. عدي اركان عباس العويدي

كليه العلوم للبنات /قسم فيزياء الليزر

١٤٤٣هـ ٢٠٢٢م

بسم الله الرحمن الرحيم

﴿ قَالُوا سُبْحَانَكَ لَا عِلْمَ لَنَا إِلَّا مَا

عَلَّمْتَنَا إِنَّكَ أَنْتَ الْعَلِيمُ الْحَكِيمُ ﴾

صدق الله العلي العظيم

سورة البقرة :الآية ٣٢

Supervisor certificate

I certify that this thesis entitled **"*Theoretical Investigation of Organic Molecules as a Candidate for Optoelectronic Applications*** " was prepared by the student **(Saba Razaq Salman)** under my supervision at the department of Laser physics, College of Science for Women, University of Babylon, as a partial fulfillment of the requirements of the degree of Doctorate of philosophy in laser physics and its applications.

Signature:

Name: ***Oday A. Al-Owaedi***
Title: **Assistant. Prof. Dr.**
(Supervisor)
Date: / / 2022

Head of the Department Certificate

In view of the available recommendations, I forward this dissertation for debate by the examining committee.

Signature:
Name: ***Jinan Ali Abd***
Title: **Assistant. Prof. Dr.**
(Head of Laser Physics Department)
Date: / /2022

Examination Committee Certification

We certify that after reading this thesis, entitled: **"*Thoretical Investigation of Organic Molecules as a Candidate for Optoelectronic Applications*"**, and as committee, examined the student **"Saba Razaq Salman"** its contents and that in our opinion it meets the standards of a thesis for the Degree of Philosophy of Doctorate in Laser Physics and its Application.

Signature:
Name: **Dr. Ahmed Kamal Ahmed**
Title: Professor
Date: /10 / 2022
(Chairman)

Signature:
Name: **Dr. Jenan M. AL-Mukh**
Title: Professor
Date: /10 / 2022
(Member)

Signature:
Name: **Dr. Khalid Haneen Abass**
Title: Professor
Date: / 10 /2022
(Member)

Signature:
Name: **Dr. Sadiq Hassan Lefta**
Title: Assistant Professor
Date: / 10 / 2022
(Member)

Signature:
Name: **Dr. Amer K. H. AL-Nafiey**
Title: Assistant Professor
Date: /10 / 2022
(Member)

Signature:
Name: **Dr. Oday A. Al-Owaedi**
Title: Assistant Professor
Date: /10 / 2022
(Member/Supervisor)

Approved by the Dean of College
Signature:
Name: **: Dr. Abeer Fawzi AL-Robayi**

Title: Professor
Address: Dean of the College of Science for Women.
Date: / / 2022

الخلاصة

تتضمن هذه الدراسة عملين علميين جديدين،ويمكن تلخيصهما على النحو التالي: توضح الدراسة الأولى ان الوصلات الجزيئية للثيوفين /فنيلين المشترك (TPCOs) لها اهميه خاصه بسبب مميزاتها الإلكترونية والتركيبية ، والتي تقدم كمرشح مناسب للتطبيقات البصرية والكهروحراريه . تم استخدام نظريه كثافه الحالات مع نظريه كرين لحساب الخصائص التركيبية والبصرية والإلكترونية والكهروحراريه لجزئيات الثيوفين /فنيلين المشترك (TPCOs) باطوال جزيئيه مختلفة حيث ان زياده وحدات الثيوفين /فنيلين المشترك(TPCOs) من (P3T-P11T) ينتج عنها زياده في قوة مذبذب الانبعاث من (4.5 - 1.6) .وفي هذا السياق تم الحصول على قيم منخفضه للتوصيل الكهربائي (0.1×10^{-7}) عند اطول طول جزيئي (5.561nm) بينما تظهر هذه الجزيئات اعلى قدره حرارية (μVK-1 23.42-) مما يؤدي بدوره الى اعلى معامل جوده (1.93×10^{-2}) . هذا كله يساعد في ابتكار مرشحات واعده لتصميم اجهزه كهروحراريه بالإضافة الى كونها تصلح كأوساط ليزر فعاله .

تعرض الدراسة الثانية لهذه الأطروحة تحقيقًا نظريًا باستخدام طرق نظرية الكثافة الوظيفية للخصائص الإلكترونية والطيفية لعائلة من وحدات أوليغو (فينيلين-إيثينيلين) OPEs مع مجموعات ربط بيريديل ، مع نقاط ربط مختلفه para، ortho و meta. حيث تبين من هذه الدراسه ان اختلاف مواقه ربط الذرات من para الى ortho الى meta تغيير في شدة الامتصاص من اعلى قيمه (84248.a.u) للجزيئه نوع PPP مع ثلاث نقاط ربط نوع para إلى (40809.a.u) للجزيئه نوع MMM مع ثلاث نقاط ربط نوع meta ، وأقل قيمة (a.u. 5964) لكثافة الامتصاص تم تقديمها بواسطة جزيئه منوع PMP ، في حين أن أعلى قيمة (87102 a.u) تم إدخالها عبر جزيئه نوع OPO. بالإضافة إلى ذلك ، يمكن ملاحظة أن اطول طول جزيئي (λ_{max}) لجميع الجزيئات يكون ضمن المنطقة المرئية ، حيث يتذبذب من

317 نانومتر لـ PMP إلى 372 نانومتر لـ365.4 نانومتر. بناءً على هذه النتائج ، يمكننا أن نستنتج أن تغيير اختلاف مواقع ربط الذرات من para الى ortho الى meta لا يؤثر فقط على شدة الامتصاص ، بل يؤدي أيضًا إلى إزاحة في الأطوال الموجية. بلاضافه الى ان الجزيئات نوع PPP و MPM و OPO تنتج أعلى قوه مذبذب انبعاث (2.08، 2.145 ، 5.15 على التوالي) ، بينما تظهر MMM و PMP أدنى قوه مذبذب انبعاث (0.154، 0.145 على التوالي).

Declaration

I hereby declare that the thesis is my own work and effort and has not been submitted in substantially the same form for the award of a higher degree elsewhere. Other sources of information have been used, they have been acknowledged. This thesis documents work carried out between September 2020 and September 2022 at the University of Babylon, Iraq, under the supervision of Assistant Prof. Dr. Oday A. Al-Owaedi.

Saba

Dedications

To

My parents who have provided me with confidence and support

My brothers whose love motivated me to challenge myself and work harder

My husband for his understanding enduring ,patience and encouragement through this hard work.

To my children

((Ridha, Qassem, zahraa)

To my friends and colleagues who helped me

Saba

Acknowledgment

This thesis would never completed without the excellent supervision and guidance I received from **Assistant Prof. Dr. Oday A. Al-Owaedi.** There are no words in English books can express my gratitude to you. Really you were excellent supervisor.

I am deeply indebted to the Head of the Laser Physics Department, the staff and the dean of the College of Science for Women for the support that provided.

Also I would like to pay my regards to all relatives and friends for the help they showed at the Department of Laser Physics.

I would like to express my very deep respect and sincere appreciation to my family, whose patience and moral encouragement gave me so much hope and support.

Above all, my great thanks to **ALLAH** for his mercy and blessing.

Saba

Abstract

This work involves two novel scientific works, and can be abstracted as follows: The first study demonstrates thiophene/phenylene co-oligomers (TPCOs) molecular junctions of particular interest because of its electronic and structural features, which introduce it as a suitable candidate for optical and thermoelectric applications. Utilizing the density functional theory (DFT) methods, and the Green's function formulism, this work involves a theoretical investigation of optical, structural, electronic and thermoelectric properties of thiophene/phenylene co-oligomers (TPCOs) with different molecular lengths. This work predicates an important result, which is an increase of the (TPCOs) units (P3T–P11T), and leads to a significant increase the emission oscillator strength (fem) (1.6– 4.5). In contrast, the lowest electrical conductance (0.1×10^{-7}), is presented via the longest molecular length (5.561 nm), while it exhibits the highest thermopower (-23.42 μVK-1) which in turn leads to high ZT_e (1.93×10^{-2}). This may aid in innovate promising new candidates for the design of optical and thermoelectric devices, as well as the active mediums for lasers.

The second study of this thesis exhibits a theoretical investigation using the density functional theory methods of electronic and spectral properties for a family of Oligo (phenylene-ethynylene) OPEs with pyridyl linker groups, with different transport connections para, ortho and meta.

These showed changing the transport connections from para to meta or ortho result changing the intensity of the absorption from (84248 a.u.) for the molecule PPP with three para transport connection point to (40809 a.u.) for the molecule MMM with three meta transport connection point, and lowest value (5964 a.u.) of the absorption intensity is presented by PMP molecule, whereas the highest value (87102 a.u.) introduced via OPO molecule. In addition, it could be observed that the maximum wavelength (λ_{max}) for all molecules lies in the visible region, and there is also a fluctuation from (317) nm for PMP to (372) nm for MMM of (365.4 nm). Based on these results, it can be concluded that changing the transport connections from para to meta or ortho not only affects the intensity of the absorption, but also leads to a displacement in wavelengths. In contrast, PPP, MPM and OPO produce the highest f_{em} (2.08, 2.145 and 5.15 respectively),while MMM and PMP, show the lowest f_{em} (0.154 and 0.145 respectively).

List of Figures

Table of Contents

Chapter 1 : Introduction

Chapter 2 : Density Functional Theory

List of Tables

List of Symbols

Symbol	Physical Meaning
m_n	Mass
Z_m	Atomic number
R_n	Position
T_e	Kinetic energy for the electron
T_n	Kinetic energy for the nuclei
U_{ee}	Interaction energy between all electrons
f_{em}	Emission oscillator strength
Ψ	Wave function
n(r)	Ground-state density
H	Hamiltonian operator
M	Nuclei number
$\boldsymbol{N}$	Electrons number
r_i	Position of the *i-th* electron
R_I	Position of the I-th nucleus
E_i	Numerical value of the energy of the i^{th} state
U_{nn}	Interaction energy terms between the nuclei
U_{en}	Interaction between electrons and nuclei
m_e	Mass of the electron

m_n	Mass of the nucleus
e	Electron charge
Z_n	Nuclear charge
r_i	Position of the electrons
R_n	Position of the nuclei
∇_i^2	Laplacian operator
$V_{ext}(\vec{r})$	External potential
H_{eff}	Effective Hamiltonian
V_{eff}	Effective external potential
$F_{K-S}[n(\vec{r})]$	Energy functional of the Kohn-Sham
E_{xc}	Exchange-correlation energy
E_X	Exchange energy of an electron
E_C	Correlation energy of an electron
$s = \frac{\lvert V\rho \rvert}{2k_{F\rho}}$	Dimensionless density gradient
k_{T-F}	Thomas-Fermi screening wavenumber
r_s	Local Seitz radius
r_c	Core radius
r	Outside of the core radius
V_{nl}^{ps}	Pseudo-potential
R_{nl}^{ps}	Radial pseudo-wavefunction

$\Psi^I_{nlm}(r)$	Single basis function
R^I_{nl}	Radial wavefunction
Y^I_{lm}	Spherical harmonic
φ_i	Molecular orbitals (basis functions)
μ_L	Chemical potential in the left
μ_R	Chemical potential in the *right*
T(E)	Probability the transition
R	Probability the reflection
δI^{in}	Incident electric current
ε_o	on-site energies
$-\gamma$	Hopping parameters
k	Wavenumber
ε_1	Single site energy
ε_2	Two site energy
$\Gamma_{L,R}(E)$	Level broadening due to the coupling between right (R) and left (L) electrodes
$\mathcal{T}_L$	Temperature left
$\mathcal{T}_R$	Temperature right
Γ	Number of transfer electrons
e_J	Number of electron on nitrogen atoms when molecule in a junction
e_N	Number of electron on nitrogen atoms when molecule in

	gas-phase
δV	Voltage associated with the chemical potential mismatch
$\mathcal{G}$	conductance
S	Matrix, it connects states coming from the left lead to the right lead and vice versa:
$\Delta \mathcal{T}$	Temperature
ΔV	Potential drop
I	Charge current
$\mathcal{Q}$	Heat current
$g(z, z')$	Retarded Green's function
$-\alpha$	Coupling element
G_+	(advanced) Green's function
G_-	retarded Green's function
ZT_e	Electronic figure of merit
E_F	Fermi energy
$f(E)$	Fermi-Dirac function
f_L	Fermi distribution from the left
f_R	Fermi distribution from the right
$S(T)$	Thermopower
G/G_0	Electrical conductance
G_o	Quantum of conductance

H	Planck’s constant
K_B	Boltzmann constant
ε	Absorption intensity
λ_{Max}	Maximum wavelength
A	Absorption intensity
E	Emission intensity

1.1. Introduction

Molecular electronics has attracted great attention from a wide variety of researchers, due to promising applications in nanoscale electronic devices such as transistors [1], switches [2], rectifiers, interconnects [3], organic photovoltaic and chemical sensors. Using molecules as electronic elements has many advantages due to their small sizes, their ability to be self-assemble onto surfaces and the low cost of producing large numbers of identical molecules. However, realizing and controlling the connection between the molecule and electrodes has remained challenging due to small molecular size [4].

The use of individual molecule as functional electronic devices was first proposed in the 1970s [5]. In order to design and realize molecular devices it is essential to have a good understanding of the properties of an individual molecule. Within the framework of molecular electronics, the most important property of a molecule is its conductance and the major question in this field is how electrons transfer through molecules. To address this question, extensive experimental and theoretical studies have been carried out. Various measurement techniques have been developed [6].

The field is currently attracting attention from a broad cross-section of the scientific community in response to both fascinations with the fundamental scientific challenges associated with the measurement of the

electrical properties of molecules, and manipulation of electronic phenomena via molecular processes, and growing concerns over the technological challenges and ultimate limits facing solid state semiconductor technology. The use of organic materials for electronic applications in which the bulk electronic or optoelectronic response arises from ensembles of several millions of molecules, and for which properties are measured or observed on the macroscopic level, is at a mature stage of development and application. The most obvious examples of molecular materials readily available in the electronics mass market are the use of liquid crystals and organic light emitting diodes (OLEDs) in flat video displays [7]. This sector of the electronics industry continues its steady development driven by the promises of transparent, flexible, non-toxic, printable electronics, with improved consumer. In molecular electronic junctions the electrical signal comes in and out of the molecules via contact-coupled electrodes. The electrodes can be classified as metal or nonmetal electrodes. The development of molecular electronics initially started from the use of metal electrodes. Hence, the development of molecular devices based on metal electrodes will summarized [8].

1.2. Single Molecule Junctions

The initial idea of using individual molecules as active electronic elements provided the impetus to develop a variety of experimental platforms to probe their electronic transport properties. Among these platforms, single-molecule junctions based on metal−molecule−metal architecture have received considerable attention and contributed significantly to the fundamental understanding of the physical phenomena required to develop molecular-scale electronic devices. The scanning probe microscopy, SPM, technique is regarded as a milestone in the history of molecular electronics because it has made a great contribution to the development of molecular electronics and continues to promote the advancement of molecular electronics in the future. In addition to SPM technique, Scanning Tunnelling Microscopy Break Junctions (STM-BJ) [9-11] and Mechanically Controllable Break Junctions MCBJ [12,13] have been used widely.

Generally, materials used as electrodes in molecular junctions should have superior properties in four aspects. The first premise is good electrical conductivity, which can maintain its high value with dimension scale-down. The second is the stability of the material composition and configuration, which is of great importance for resisting external perturbation/oxidation and ensuring the success of forming molecular

junctions. The third is the abundant availability using either bottom-up or top-down approaches [14]. The fourth is the ease of material processing, which should be compatible with industrial micro/nanofabrication techniques. On the basis of these considerations, the past two decades have witnessed a large variety of materials being used in molecular electronics, ranging from conventional noble metals to novel carbon allotropies, which continuously and creatively update the paradigms for device architecture and operation. In addition to the materials mentioned above, there were also other attempts to expand the research regimes of molecular electronics, including silicon and polymer-based nanoelectrode systems as Silicon-based electrodes [13], and CMOS-compatible electrodes, such as Pt and Pd [14].

1.3. Integrating Molecular Functionalities into Devices

Undoubtedly, the substantial experimental and theoretical progress detailed above lays the foundation for both the measurement capabilities and a fundamental understanding of the various physical phenomena of molecular junctions. Despite these considerable achievements, there are still no commercially available molecular electronic devices [14]. To satisfy the requirements for actual applications, the development of practical molecular devices with specific functions is a prerequisite. In fact,

recent experimental developments have demonstrated conductance switching/modulation and rectification as well as how quantum interference effects play a critical role in the electronic properties of molecular junctions [15].

The focus of these experiments illustrates the engineering of functionalities that are beyond conventional electronic transport properties using a rational chemical design in single-molecule junctions. The developing trends of integrating molecular functionalities into electrical circuits based on single molecules is including a wiring toward nanocircuits; rectification toward diodes; modulation toward transistors; switching toward memory devices; and transduction toward sensors [16]. For different functions resulted from individual molecules, both molecular cores and molecular tails are equally important due to the fact that the proposed functions could be affected not only by molecular electrical characteristics but also by the electrode−molecule bonding. In summary, with the rapid development of molecular-scale electronics, using molecular devices as the future of next-generation electrical circuit units with lower power consumption, higher speed, and higher level of integration has received significant attention [17].

1.4. Organic Molecules

Organic molecules are chemical compounds with complicated structures. Composed of many atoms, apart from electronic properties they also exhibit special physicochemical features [18]. When organic molecules create molecular solid-state devices with crystal or amorphous structures, the properties of these devices follow from organic molecule interactions. Therefore in molecular solid-state structures, the energy levels of individual molecules form continuous bands of energy. Due to the weak interactions between the molecules, molecular solid-state structures exhibit the properties of the individual molecules to a greater degree than the properties characteristic for solid-state materials [19]. A special feature of the molecular solid state is the fact that singlet and triplet states are excited due to light interaction being able to move across the material. These mobile quasi-particles are called excitons. Furthermore, excitons can be generated not only by light but also from the recombination process of charge carriers with opposite signs, electrons and holes injected into the system [20]. This has important implications and enables the application of organic materials to light-emitting devices able to produce any colour. Owing to the excitation of the organic material by electromagnetic waves

with energy, carriers are generated. Taking into account these features of organic materials, it could be conclude that they have significant potential in many fields of science and technology. Therefore an understanding of their properties is salient, and our current knowledge remains insufficient [21].

1.5. Electrical Pumping of Organic Laser Active Medium

Organic solid-state lasers (OSSL) have received a lot of attention in recent years due to their ease of manufacture and ability to cover a broad range of lasing wavelengths from near infrared to ultraviolet. Optically pumped OSSL have progressed to the point that they can reach impressively low thresholds for laser and/or amplified spontaneous emission (ASE), as well as operation that is almost constant. However, the ultimate aim in the field of OSSL is to achieve electrically pumped lasing, which will allow for the development of low-cost, portable, and flexible solid OSSL devices [6,7].

Because of the following considerations, electrically pumped OSSL lasing is far more difficult than optically pumped OSSL lasing. First, according to spin statistics, three-quarters of excitons generated during current injection are triplets, which have a lengthy decay period [22].

Second, polarons, excitons, and other species that are not engaged in optical pumping will cause repeated annihilation and absorption losses when electrical pumping is used. The recent advances have reported promising signs of current injection OSSL, which has opened up the possibility of developing small and low-cost electrically powered organic laser systems [23]. Regardless of these organic laser gain medium, electrical pumping was used to investigate light amplification. As a result, it's crucial to conduct theoretical analysis and forecast potentially good electrical pumping options, which must have a large stimulated emission cross section, low annihilation or absorption losses, and a short lifetime, ideally with high mobility [7]. In this context, the purpose of this communication is to offer an universal computational approach for systematically screening out electrically pumped lasing molecules over a broad spectrum of organic solid-state luminous materials using efficient electronic structure computations based on density functional theory (DFT) and time-dependent DFT (TD-DFT) [23,24].

Organic dyes absorb light in the ultraviolet (UV) to near-infrared (NIR) spectral range. Multiple conjugated double bonds are present in all of these compounds, limiting their spectral characteristics and chemical reactivities. The large range of chemical configurations that may operate as laser dyes is one of the major reasons for dye lasers' surge in popularity. Laser dyes

emit light over the whole visible spectrum, as well as the NUV and NIR spectral regions. more than 500 distinct dyes with varying absorption and emission bands may be discovered. Laser dyes are typically classified according to their chemical structures [24].

1.6. Literature Review

Changsheng Wang et al, in 2009 **[25],** have used STM-molecular break junction methods in Au|molecule|Au configurations, the electrical conductivity of the oligoyne molecular wires Py-(CtC)n-Py (n) 1, 2 and 4; Py) 4-pyridyl) was investigated at the single molecule level. Multiple series of peaks can be seen in the conductance histograms, which can be attributed to different contact geometries between the pyridyl head groups and the gold electrodes. Higher conduction groups are linked to pyridyl group adsorption at more strongly coordinated places such as step edges or adjacent gold adatoms, according to both experimental and theoretical data.

Pavel Moreno-García et al, in 2013 **[26],** have reported that the electrical conductivity of a series of oligoyne molecular wires in single-molecule junctions with gold contacts was investigated using a combination of experimental and theoretical methods. The synthesis and characteristics of diaryloligoynes with n = 1, 2, and 4 triple bonds, as well as the anchor dihydrobenzo[b]thiophene, are the subjects of their experiments (BT). The aurophilic anchor groups cyano (CN), amino (NH2), thiol (SH), and 4-

pyridyl were also investigated for comparison (PY). To explore single-molecule conductance characteristics, researchers used scanning tunneling microscopy break junction (STM-BJ) and mechanically controlled break junction (MCBJ) methods.

Oday A. Al-Owaedi et al in 2016 **[27],** introduced a theoretical and experimental studies of trans-Ru complexes. They interpreted the electronic properties of such molecules in terms of the transport mechanisms (LUMO-dominated conductance). These results have significant implications for the future design of organometallic complexes for studies in molecular junctions.

Oday A. Al-Owaedi et al in 2017 [28], have highlighted research on the critical role of metal complexes in preventing orthogonal contacts, which helped to explain why some organometallic compounds had very high conductance values.

Mohsin K. Al-Khaykanee et al in 2018 **[29],** have work that comprised a study of the charge transport of 4,4-bipyridine molecules with a variety of sterically-induced twist angles between the two pyridyl rings, which was done using density functional theory DFT and Green's function formalism. Different molecular orientations within the junctions were shown to be the cause of high and low conductance peaks, according to one experiment. The conductances of both geometries were proportional to twisted angle

demonstrating that the electrical current travels through the C-C bond joining the pi systems of the two rings.

Guang-Ping Zhang et al in 2019 **[30],** optimizing the conductance switching performance in photo switchable dimethyldihydropyrene/cyclophanediene single-molecule junctions. Designing molecular switches with high stability and performance is still a great challenge in the field of molecular electronics. For this aim, key factors influencing the charge transport properties of molecular devices require to be carefully addressed.

Masoud Baghernejad et al in 2020 **[31],** have mentioned that the influence of heteroatoms on electron transport via asymmetric and symmetric alkyne-terminated benzodichalcogenophene compounds has been investigated using a combination of experimental and theoretical methods. Experiments, DFT-based theory, and a simple tight binding model were all in excellent agreement. The decreased conductance of the asymmetric molecule is caused by the asymmetry created by differing bond lengths in the two 5-membered rings of the molecule, as demonstrated by the tight-binding modeling of heteroatom replacement in these non-bipartite cores. In addition, they discover that the differing overlap integrals of the CO and C-S bonds must be taken into consideration in the tight binding model.

Yi Jiang et al in 2020 **[32],** have studied a variety of gain materials including organic dyes, fluorescent semiconductor emitters, triplet gain media, and biological materials, covering a wide spectrum from UV to NIR. Some gain media are already commercial available, including some laser dyes, i.e. TDAF-1 (79), PFO (203), F8BT (225) and bis-styrylbenzene), introducing branched flexible chains, constructing triplet gain media and triplet harvesters, may be beneficial to the development of robust organic gain media for OSLDs. They hope that in the future, intense efforts will be paid to explore various successful ways to realize electrically pumped organic lasers and promote their practical application, inspired by the recent advancements.

Baraa A. Al-Mammory et al in 2021 **[33],** thermoelectric Properties of Oligoyne-Molecular Wires. Oligoynes are prototype molecular wires due to their conjugated system and the coherent tunneling transport, which aids this type of wires to transfer charges over long distances. The electric and thermoelectric characteristics for a series of Oligoyne molecular wires ((n) 3, 5, 7 and 9) are studied to explore the fundamental transport mecha nisms for electrons crossing through single molecules, our probed both the electrical conductance and Seebeck coefficient for Au|molecule|Au configurations using (DFT).

Rasool M. Al-Utayjawee et al in 2021 **[34],** we use Single-molecule porphyrin applications gain attention by using molecules as elementary blocks of electronic components involving metallic atoms. Theoretically, one type of molecular-scale porphyrin device is used in this article, consisting of organometallic single molecules with different metals (Zn, Mg, Cu and Fe), sandwiched between gold electrodes bound by thiol anchor groups. The transmission and Seebeck coefficients for Au|molecule|Au configurations were computed by using (DFT).

M. Naher, et al., in 2021 [35], have studied a series of 12 conjugated molecular wires, 6 of them contain either a ruthenium or platinum center centrally placed within the backbone. The measurements and calculations have demonstrated a small positive Seebeck coefficient, and the transmission coefficient through these molecules takes place by tunneling through the tail of the HOMO resonance near the middle of the HOMO–LUMO gap in each case.

1.7. Thesis Outline

The outline of this thesis can be summarized as follows; this chapter is followed by chapter 2 which presents a brief overview of density functional theory (DFT), which is one of the main theoretical techniques that has used in this thesis to study and understood the electronic properties of single-molecule junctions. Chapter 3 describes the single particle transport theory. This chapter involves a Green's function scattering formalism and all related topics such as the Landauer formula, Green's function of infinite leads, some of examples of scattering.

Chapter 4 and 5 represent the results and discussions of the electronic, thermoelectric, optical and spectral properties of variety of molecles.

1.8. The Aims of the Study

This research is aiming to investigate the electronic and thermoelectric properties of organic molecular junctions. Also, one of the main goals of this study is the exploring of some of optical characteristics such as HOMO-LUMO gap of these devices; Therefore, the goals of this work can be summarized as following:

1. Study of electronic, electric, thermoelectric and some of optical properties of a series of all molecules in this work.
2. Obtaining the fundamental understanding of the effect of many factors and their impact on the characteristics of these simple prototypical systems such as the molecular length, position of anchor groupes, and roles of quantum interference.
3. Conducting analysis of work results and providing forecasts for the use of these nanostructures in the field of optoelectronics applications

2.1. Introduction

In an attempt to explore and understood the electronic properties of molecules, many theories have emerged; one of the most important of these theories and most common is the density functional theory (DFT). Nowadays, DFT can be presented as a powerful tool for computations of the quantum state of atoms, molecules and solids, and of ab-initio molecular dynamics. In 1927, immediately after the foundation of quantum mechanics, an initial and approximate version of density functional theory was conceived by Thomas and Fermi [36]. Later, using the basics of quantum mechanics, Hohenberg, Kohn, and Sham, developed density functional theory of the quantum ground state to be superior to both Thomas-Fermi and Hartree-Fock theories, which opened a wide door to the applications for realistic physical systems [37,38]. From that time on, density functional theory (DFT) has grown vastly, and it has become one of the main tools in theoretical physics and molecular chemistry.

This chapter presents a brief summary of DFT and SIESTA (Spanish Initiative for Electronic Simulations with Thousands of Atoms) code [39], which has been used to study the electronic, electric, spectral and thermoelectric properties of the molecules that are the subject of research in this thesis [40].

2.2. The Many-Body Problem

This is an approach which aims to solve any system consisting of a large number of interacting particles. In a microscopic system consisting of charged nuclei surrounded by electron clouds these interactions such as electron-nuclei, electron-electron, nuclei-nuclei and electron correlations are described via Schrödinger equation [40].

The full Hamiltonian operator of a general system describing these interactions is

$$\mathrm{H} = \overbrace{-\frac{\hbar^2}{2m_e}\sum_{i=1}^{N}\nabla_i^2}^{T_e} \overbrace{-\frac{\hbar^2}{2m_n}\sum_{n=1}^{M}\nabla_n^2}^{T_n} \overbrace{-\frac{1}{4\pi\varepsilon_o}\sum_{i=1}^{N}\sum_{n=1}^{M}\frac{1}{\left|\vec{r}_i-\vec{R}_n\right|}Z_n e^2}^{U_{en}}$$

$$+\frac{1}{4\pi\varepsilon_o}\frac{1}{2}\overbrace{\sum_{i=1}^{N}\sum_{i\neq j}^{N}\frac{e^2}{\left|\vec{r}_i-\vec{\vec{r}}_j\right|}}^{U_{ee}} + \overbrace{\frac{1}{4\pi\varepsilon_o}\frac{1}{2}\sum_{n=1}^{M}\sum_{n\neq n'}^{M}\frac{1}{\left|\vec{R}_n-\vec{R}_{n'}\right|}Z_n Z_{n'}e^2}^{U_{nn}} \tag{2.1}$$

Here i and j denote the *N*-electrons while n and n' run over the *M*-nuclei in the system, m_e and m_n are the mass of electron and nucleus respectively, e and Z_n are the electron and nuclear charge respectively. The position of the electrons and nuclei are denoted as $\vec{r}_i$ and $\vec{R}_n$ respectively,

Approximately, the mass of nucleons is a few orders of magnitude higher than that of electron, and in terms of their velocities, the nuclei could be considered as a classical particle which creates an external potential, and the electrons as quantum particles are subjected to this potential.This concept is known as the Born-Oppenheimer approximation [40], together with an assumption that the nucleon wavefunction is independent of the electron position, equation (2.1) can then be written as follows:

$$H = T_e + U_{e-e} + V_{e-nuc} \tag{2.2}$$

The first part of equation (2.2) presents the kinetic energy of all electrons, which is described by;

$$T_e = \sum_n \frac{\hbar 2}{2me} \nabla_i^2 \tag{2.3}$$

The electron-electron interaction is represented in the second part of equation (2.2), which is given by;

$$U_{e-e} = \sum_{i,j,i\neq j} \frac{e^2}{4\pi\varepsilon_0} \frac{1}{|\vec{r}_i - \vec{r}_j|} \tag{2.4}$$

$Ue{-}e$ describes the sum of all potentials acting on a given electron at position $r_i$by all other electrons at position r_j .

The third part of equation (2.2) describes the interactions between electrons and nuclei, which is expressed by;

$$V_{e-nuc} = \sum_i \sum_n \ v_{nue}(r_i \ - R_n \ ) \tag{2.5}$$

v_{e-nue} is the interaction between electrons and nuclei; it depends on the positions of electrons r_i and nuclei R_n .

The employment of a Born-Oppenheimer approximation [40], allows the electron and nucleon degrees of freedom to be decoupled

2.3. The Hohenberg-Kohen Theorems

Essentially, density functional theory (DFT) evolved significantly depending on two ingeniously simple theorems put forward and proved by Hohenberg and Kohn in 1964 [37]. These theorems are two powerful statements:

Theorem I: For any system of interacting particles in an external potential V_{ext}, the density is uniquely determined. In other words, the external potential is a unique functional of the density. To prove this theorem, assume that there are two external potentials $V_{ext}{}^{(1)}$ and $V_{ext}{}^{(2)}$ differing by more than a constant, and giving rise to the same ground state density, $\rho_0(r)$. It is clear that these potentials belong to different Hamiltonians, which are denoted H^1 and H^2 they give rise to distinct ground-state wavefunctions $\psi^{(1)}$ and $\psi^{(2)}$. Since $\psi^{(2)}$ is not a ground state of $H^{(1)}$, so:

$$E^{(1)} = \langle \psi^{(1)} | H^{(1)} | \psi^{(1)} \rangle < \langle \psi^{(2)} | H^{(1)} | \psi^{(2)} \rangle \qquad (2.6)$$

and, similarly:

$$E^{(2)} = \langle \psi^{(2)} | H^{(2)} | \psi^{(2)} \rangle < \langle \psi^{(1)} | H^{(2)} | \psi^{(1)} \rangle \qquad (2.7)$$

Assuming that the ground states are non-degenerate [41,42], one could rewrite equation (2.6) as follows:

$$\langle \Psi^{(2)} \left| H^{(1)} \right| \Psi^{(2)} \rangle = \langle \Psi^{(2)} \left| H^{(2)} \right| \Psi^{(2)} \rangle + \langle \Psi^{(2)} \left| H^{(1)} - H^{(2)} \right| \Psi^{(2)} \rangle$$

$$= E^{(2)} + \int \left(V_{ext}^{(1)}(r) - V_{ext}^{(2)}(r) \right) \rho_0(r)\, dr \qquad (2.8)$$

and assuming that $|\Psi^{(1)}\rangle$ has the same density $\rho_0(r)$ as $|\Psi^{(2)}\rangle$:

$$\langle \psi^{(1)} \left| H^{(2)} \right| \psi^{(1)} \rangle = E^{(1)} + \int \left(V_{ext}^{(2)}(r) - V_{ext}^{(1)}(r) \right) \rho_0(r)\, dr \qquad (2.9)$$

Combining of equations (2.8) and (2.9) leads to,

$$E^{(1)} + E^{(2)} < E^{(1)} + E^{(2)} \qquad (2.10)$$

This equation proves the two different external potentials cannot produce the same ground-state density.

Theorem II: A universal functional $F[\rho]$ for the energy $E[\rho]$ could be defined in terms of the density. The exact ground state is the global minimum value of this functional. In other words, the ground state energy of the system is given by the functional $F[\rho]$. If the input density and ground-state density are the same, the functional $F[\rho]$ would deliver the lowest energy. Hence, the functional could be minimised by varying the density to obtain the ground-state energy for the external potential [41].

The second theorem could be proven by considering the expression for the total energy, *E*, of the system with density ρ.

$$E[\rho] = T[\rho] + E_{\text{int}}[\rho] + \int V_{\text{ext}}(r)\rho(r)dr \qquad (2.11)$$

The kinetic term, T, and internal interaction of the electrons, E_{int}, depend only on the charge density, and so are universal[42].

The first theorem reported that the ground-state density (ρ_0) for a system with external potential (V_{ext}) and wavefunction (Ψ_0), determines the Hamiltonian of that system, so for any density, ρ, and wavefunction, Ψ, other than the ground state, it could be found:

$$E_0 = \langle \Psi_0 | H | \Psi_0 \rangle < \langle \Psi | H | \Psi \rangle = E \qquad (2.12)$$

Hence, the ground-state density, $\rho 0$, minimizes the functional (equation 2.11). If the functional $T[\rho]+E_{int}[\rho]$ is known, then by minimizing equation 2.11, the ground-state of the system could be obtained, and then all ground-state characteristics could be calculated, which are the subject of the interest [42].

2.4. The Kohn-Sham Method

The Kohn-Sham method has been used in solid state physics for about fifty years. By now, largely due to the development of increasingly accurate density functionals, the method has also gained a large popularity among physicist and chemists, especially as it allows in many cases, accurate treatments of molecular systems unattainable by the more traditional quantum mechanical methods [43,44].

It has been reported in the previous section that obtaining the ground-state density leads to calculating the ground-state energy. However, the precise form of the functional shown in equation (2.11) is not known. Generally,

the kinetic term and internal energies of the interacting particles cannot be expressed as functionals of the density.

Kohn and Sham in 1965 [38], came up with the idea, that it possible to replace the original Hamiltonian of the system by an effective Hamiltonian of non-interacting particles in an effective external potential, which gives rise to the same ground state density as the original system [45,46].

The form of energy functional of the Kohn-Sham ansatz is:

$$E_{KS}[\rho] = T_{KS}[\rho] + \int V_{ext}(r)\,\rho(r)dr + E_H[\rho] + E_{xc}[\rho] \qquad (2.13)$$

Here, T_{KS} is the kinetic energy of the non-interacting system. The kinetic energy, T, in equation (2.11) has been used for the interacting system. This discrimination is due to the exchange correlation, E_{xc}, functional, which is described in equation (2.15). E_H is the Hartree functional, which describes the electron-electron interaction using the Hartree-Fock method [47-51], and it is given by:

$$E_{\mathrm{H}}[\rho] = \frac{1}{2}\iint \frac{\rho(r)\rho(r')}{|r-r'|}\,dr\,dr' \qquad (2.14)$$

This is an approximated version of the internal interaction of the electrons, E_{int}, as defined previously. Again, the difference referred to the exchange correlation, E_{xc}. Therefore, the differences between the exact and approximate solutions for the kinetic energy, and electron-electron interaction terms were represented via E_{xc}, which is expressed by:

$$E_{xc}[\rho] = (E_{int}[\rho] - E_H[\rho]) + (T[\rho] - T_{KS}[\rho]) \qquad (2.15)$$

Consequently, the Kohn-Sham method could be a powerful approach to obtain an accurate ground-state density if the exchange correlation, E_{xc}, is known precisely [51].

2.5. The Exchange-Correlation Functionals

The biggest challenge of Kohn-Sham DFT is the finding of accurate approximations to the exchange correlation energy, Exc. The best understanding of exact functional could be obtained by the best approximation could be designed it [52]. Many efforts have been spent to find the best approximation for the exchange-correlation functional, and numerous forms have been proposed. This section presents a brief summary of two of the most popular approximation forms. The first one is the local density approximation (LDA) [53]. Secondly, the generalized gradient approximation (GGA) [54]. The comparison in terms of the accuracy between LDA and GGA, reported that the GGA is more accurate approximation, because it is designed based on density and the density gradients, while LDA is the simplest, because it is based on the local density.

2.5.1. Local Density Approximation (LDA)

The simplest approximation is to assume that the density can be treated as a uniform electron gas. Based on this approximation, which was initially proposed by Kohn and Sham [38], the exchange-correlation energy for a density ρ is given by:

$$E_{XC}^{LDA}[\rho] = \int \rho(r)(\epsilon_x^{hom}(\rho(r)) + \epsilon_c^{hom}(\rho(r)))dr \qquad (2.16)$$

Here, the terms ϵ_x^{hom} and ϵ_c^{hom} are the exchange and correlation energy densities for the homogeneous electron gas. The analytical exchange energy, ϵ_x^{hom}, can be found in the literature [55]:

$$\in_x^{hom} = -\frac{3}{4\pi}\sqrt[3]{3\pi^2\rho} \qquad (2.17)$$

Ceperley and Alder [56] calculated numerically the correlation energy $\in_C^{hom}$ using the quantum Monte-Carlo method, then Perdew and Zunger [57] fitted the numerical data to analytical expressions, and found:

$$\in_c^{hom} = \begin{cases} -0.048 + 0.031\,ln(r_s) - 0.0116\,r_s + 0.002\,ln(r_s) & \text{rs} < 1 \\ -\dfrac{0.1423}{(1 + 1.9529\sqrt{r_s} + 0.3334\,r_s} & r_s > 1 \end{cases} \qquad (2.18)$$

Here, $r_s = (\frac{3}{4\pi\rho})^{-1/3}$ is the radius of a sphere in a homogeneous electron gas of density, ρ that contains one electron.

The LDA is often surprisingly accurate and for systems such as graphene and carbon nanotubes or where the electron density slowly varies, generally gives very good results. Despite the remarkable success [58,59], of the LDA, care should be taken in its application. For example, LDA predicts a wrong ground state for the titanium atom and it gave a very poor description for hydrogen bonding [60,61], as well as it gives an incorrect value of the band gap in semiconductors and insulators [62,63].

2.5.2. Generalized Gradient Approximation (GGA)

The pitfalls of the local density approximation (LDA) and a fact that real systems are inhomogeneous, means that there is a need to find an alternative approximation, which is the generalized gradient approximation (GGA). Basically, there is no analytical form for the exchange energy in GGA, and therefore it has been calculated along with the correlation term, numerically. Nowadays, there are various parameterizations which are used in this approximation; one of the most popular and most reliable is the PBE functional form, which was proposed in 1996 by Perdew, Burke and Ernzherhof [64]:

$$E_{XC}^{GGA} = E_X^{GGA}[\rho] + E_C^{GGA}[\rho] \qquad (2.19)$$

The exchange part is given by:

$$E_X^{GGA} = \int \in_X \left(\rho(r)\right) V_X \left(\rho(r), \nabla\rho(r)\right)\rho(r)dr \qquad (2.20)$$

Where,

$$V_X(\rho, \nabla\rho) = 1 + k - \frac{K}{1+\frac{\mu S^2}{K}}$$

The values of k and μ parameters are 0.804 and 0.21951, respectively and $s = \frac{|\nabla\rho|}{2k_F\rho}$ is the dimensionless density gradient and k_F is the Fermi wavelength and $V_x(\rho,\nabla\rho)$ represents the enhancement factor[61].

The correlation energy form is given by:

$$E_C^{GGA}[\rho] = \int \rho(r)[\epsilon_c(\rho(r)) + F(\rho(r), \nabla\rho(r))]dr \qquad (2.21)$$

$$F(\rho, \nabla\rho) = \frac{\gamma e^2}{a_0} \ln\left[1 + \frac{\beta t2}{\gamma}\left(\frac{(1+At^2}{1+At^2+A^2t^4}\right)\right],$$

$$A = \frac{\beta}{\gamma}\frac{1}{(\exp -\frac{\epsilon_c(\rho)}{\gamma} - 1)}$$

β = 0.066725, $\gamma = \frac{(1-\ln 2)}{\pi^2}\gamma$, $a_0 = \frac{\hbar}{m^2}$, and the dimensionless gradient is $=\frac{|\nabla\rho|}{2K_{TF}\rho}$, where $K_{TF} = \sqrt{12/\pi}\Big/\sqrt{r_s}$ is known as the Thomas-Fermi screening wavelength and rs is defined as the local Seitz radius. The PBE-GGA functional has been extremely influential, both for performing actual calculations and as the basis for functionals involving higher derivatives and exact exchange [65]. It has been used in all studies of this thesis, and it gives a good agreement with experiment [66 – 68].

2.6. SIESTA

SIESTA is an acronym derived from the *Spanish Initiative for Electronic Simulations with Thousands of Atoms* [67] is both a method and computer program implementation, to perform electronic structure calculations and *ab-initio* molecular dynamics simulations of molecules and solids. One of the main characteristics of SIESTA, that it uses the standard Kohn-Sham self-consistent density functional method in the local density (LDA) and, or generalized gradient (GGA) approximations. In addition, it utilizes norm-conserving pseudopotentials in their fully nonlocal form, and a linear combination of atomic orbital basis set to achieve efficient calculations [67].

In this thesis, the SIESTA code has been used to perform all DFT calculations. It is used to obtain the optimized geometries of the molecules which are the subject of this research, and a Hamiltonian describing their properties.

2.6.1. The Pseudopotential Approximation

In terms of time and computer memory, the investigation of the properties of typical systems of molecules consist of a large number of atoms containing complex potentials could be expensive. Although, the splitting of a large interacting problem into a large effective non-interacting problem as shown previously simplifies the problem; still there is a need

for more simplification, which could be obtained by using the proposed pseudopotential approximation by Fermi in 1934 [69,70]. The fundamentals of this concept are the removing of the core electrons, which lie within filled atomic shells, and replace them by an external potential known as apseudopotential, while valance electrons are arranged in the partially filled outer shells, and they are only contribute in the formation of molecular orbitals. The advantages of this kind of approximations could be summarized in two points; first it decreases the electrons number of the system significantly, and that lowers the cost (time and memory) to perform the calculations of the system. The second benefit is the numerical stability, because these pseudopotentials are smooth.

In this section, a special type of *ab-initio* pseudopotential is presented, which is used in the SIESTA code, a norm-conserving pseudopotential [71]. The calculation of the pseudopotential based on the Kohn-Sham formalism to solve the many-electron problem for a single atom, could replace the effect of the core electrons. The definition of the valance electron wavefunctions is the product of radial and spherical harmonic wavefunctions:

$$\psi_{nlm}^{ae}(r) = \frac{1}{r} R_{nl}^{ae}(r) Y_{lm}(\varphi, \vartheta) \qquad (2.22)$$

Here, $n = 1, 2, \ldots, l = 0, \ldots n - 1$ and $m = -l, \ldots l$ are quantum numbers, $Y_{lm}(\varphi, \vartheta)$indicates to normalized spherical harmonics and $R_{nl}^{ae}(r)$

is the solution to the radial Schrödinger equation (equation 2.23) that contains the all-electron potential , V_{nl}^{ae},, which includes all core-and valence-electron interactions.

$$\in_{nl}^{ae} \quad R_{nl}^{ae}(r) = [-\frac{1}{2}\frac{d^2}{dr^2} + \frac{l(l+1)}{2r^2} + V_{nl}^{ae}]R_{nl}^{ae}(r) \qquad (2.23)$$

To reduce the size of the system, the core electrons were removed and replaced the all-electron potential with an effective potential: $V_{nl}^{eff}[\rho](r)$, where $\rho(r)$ is the electron density given by the filled Kohn-Sham orbitals [71]:

$$\rho(r) = \rho(r,\varphi,\vartheta) = \Sigma f_{nlm}|\Psi_{nlm}(r,\ \varphi,\vartheta)|^2 \qquad (2.24)$$

f_{nlm}=0,1,2 is the occupancy factor indicating whether an orbital is empty, half-filled or full. In general, $\rho(r)$ is not spherically symmetric, but for an isolated atom, it is possible to integrate out the angular dependence:

$$\rho(r) = \int \rho(r,\varphi,\vartheta)r^2 sin\vartheta d\vartheta d\varphi =$$

$$\Sigma_{nlm} f_{nlm}\,|R_{nl}(r)|^2 \int |Y_{lm}(\varphi,\vartheta|^2 sin\vartheta d\vartheta d\varphi$$

$$= \Sigma\, f_{nlm}|R_{nl}(r)|^2 \qquad (2.25)$$

This purely radially-dependent density generates an effective potential that is also only radially dependent. Hence, the Kohn-Sham equation takes the form:

$$\in_{nl} \quad R_{nl}(r) = [-\frac{1}{2}\frac{d^2}{dr^2} + \frac{l(l+1)}{2r^2} + V_{nl}^{eff}]R_{nl}^{ae}(r) \qquad (2.26)$$

The attractive nuclear potential is also included into the effective potential. This is the Kohn-Sham orbitals and the self-consistent effective potential that involves all of the interaction between electrons.

The pseudowavefunction, $R_{nl}^{ps}(r)$, and eigen-energies, $\in_{nl}^{ps}$ are obtained from the solution to equation (2.26), after replacing the central potential V_{nl}^{ps} by a pseudopotential V_{nl}^{eff} which is given by [71]:

$$V_{nl}^{eff} = \in_{nl}^{ps} - \frac{l\ (l+1)}{2r^2} + \frac{1}{2\,R_{nl}^{ps}(r)} \frac{d^2}{dr^2} R_{nl}^{ps}(r) \qquad (2.27)$$

The formula (2.27) is obtained by inverting the Schrödinger equation for known valence wavefunctions (or pseudowavefunction), $R_{nl}^{ps}(r)$, and eigenvalues, $\in_{nl}^{ps}$. Therefore, the pseudopotential depends on the *n* and *l* quantum numbers and are parameterized to be smooth and continuous outside the given cut-off radius.

In this thesis, all DFT calculations were achieved using SIESTA with pseudopotentials generated using the Troullier-Martins method [72,73]. In this method, the radial part of the pseudowavefunction described by two formulas and depends on a given cut-off radius rc as follows:

$$R_{nl}^{ps} = \begin{cases} R_{nl}(r) & r > r_c \\ re^{p(r)} & r < r_c \end{cases} \qquad (2.28)$$

Where , $p(r)$ is given by:

$$p(r) = a_0 + a_2r^2 + a_4r^4 + a_6r^6 + a_8r^8 + a_{10}r^{10} + a_{12}r^{12} \qquad (2.29)$$

The a_i coefficients are determined by the following conditions[73]:

1. Norm-conservation refers to the charge in as sphere less than r_c has to be same for the pseudopotential and all valence electron wavefunctions.

$$\int_0^{r_c} |R_{nl}(r)|^2 dr = \int_0^{r_c} |R_{nl}^{ps}(r)|^2 \, dr$$

2. The corresponding valence eigenvalues are the same.

$$\in_{nl}^{ps} = \in_{nl}$$

3. Smoothness of the pseudowavefunctions leads to a smooth pseudopotential

$$R_{nl}(r_c) = R_{nl}^{ps}(r_c), \quad and \ For \ i = 1,2,3,4$$

$$: \left[\frac{d^i R_{nl}(r)}{dr^i}\right]_{r=r_c} = \left[\frac{d^i R_{nl}^{ps}(r)}{dr^i}\right]_{r=r_c}$$

From these conditions, it is possible to parameterize $R_{nl}^{ps}(r)$ (equation (2.28)), and then substitute this into equation (2.27), to obtain the explicit form of the pseudopotential:

$$V_{nl}^{ps}(r) = \begin{cases} V_{nl}^{ps}[n](r) & r > r_c \\ \in_{nl}^{ps} + \frac{(\mathrm{L}+1)\mathrm{p}\prime(\mathrm{r})}{r} + \frac{1}{2}(p'(r) + p''(r)) & r < r_c \end{cases}$$

(2.30)

The resulting pseudopotential would be smooth and nodeless, if these conditions are satisfied [72]. $V_{nl}^{ps}(r)$ is known as a screened pseudopotential because it involves the effects of both core and valence

electrons. The employing of this pseudopotential in other environment such as molecules, any screening from the valence electrons should be removed, which could be performed by subtracting the exchange-correlation and Hartree potentials, and that yielded the bare ion potential, $V_{nl}^{ion}(r)$, which would be transferable to different environments [72].

$$V_{nl}^{ion}(r) = V_{nl}^{ps}(r) - V_H[n^{val}(r)] - V_{xc}[n^{val}(r)] \qquad (2.31)$$

Here, $n^{val}(r)$ denotes the valence components of the self-consistent charge density. A huge number of real-space points is required to calculate the potential matrix directly. Secondly, the number of matrix elements per *l* value is scaled by $n(n+1)$, where *n* represents the orbital number. To optimize this procedure, the pseudopotential could be consider in two parts; the first one is called a local potential, V^{loc}, which is the same for all *l* components. The second one is called a semi-local potential, $V_n^{sl} = V^{ion} - V^{loc}$, which differs for each *l*, and it is constructed inside region less than the given cut-off radius, r_c , otherwise it is zero outside this region [72].

The expression of this potential is given by:

$$V_n^{ion} = V_n^{loc}(r) + \sum_{l=0}^{n-1} V_n^{sl} + \sum_{m=-1}^{l} \delta V_{nl} \quad |Y_{lm}\rangle \langle Y_{lm}| \qquad (2.32)$$

V_n^{sl} is the second part of equation (2.32), where δV_{nl} is constructed in a way that it is zero beyond the cut-off radius. This is reasonable since, beyond the cut-off radius, the pseudopotential is the original effective potential, which is local.

The semi-local part of equation (2.32) has been represented as a fully non-local potential in terms of Kleinmann-Bylander projectors [74]:

$$V_n^{sl} = \sum \frac{|\delta V_{lm} \Psi_{lm}^{ps}\rangle\langle \Psi_{lm}^{ps} \delta V_{lm}|}{\langle \Psi_{lm}^{ps}|\delta V_{lm}|\Psi_{lm}^{ps}\rangle} = V^{KB} \qquad (2.33)$$

Here, $|\Psi_{lm}^{ps}\rangle$, δV_{lm} and $|\delta V_{lm}\Psi_{lm}^{ps}\rangle$ are the spherical harmonic, the semi-local part of the pseudopotential, and the pseudowavefunction respectively.

Hence, the non-local parts could be calculated by implementing Kleinmann-Bylander projectors, which decreases the number of matrix elements per l from n(n+1) to n [74]. In addition, the non-local pseudopotential matrix elements could be calculated in k-space rather than a real space grid, which dramatically lowers the computational expenses for the large systems.

2.6.2. SIESTA Basis Sets

A basis set is a mathematical description of the orbital within a system used to perform the theoretical calculations. One elegant and popular choice of basis sets in periodic system calculations is the plane-wave basis set. However, one of the main reasons for applying the SIESTA code for my calculations is that it used localised basis sets (which are not implicitly periodic) and therefore can be used to construct a tight-binding Hamiltonian, this is not easy to achieve using a plane wave based code.

The type of basis set is one of the most important aspects for calculations using SIESTA. For example, to perform efficient calculations,

the Hamiltonian should be sparse, and therefor SIESTA utilizes a linear combination of atomic orbital basis sets (LCAOs), which are constrained to be zero outside of a certain radius (cut-off radius), and are constructed from the orbitals of the atoms. This generates the desired sparse form for the Hamiltonian, and it reduces the overlap between basis functions, and therefore a minimal size basis set creates characteristics similar to that of the system under investigation[75].

The simplest basis set for an atom is called a single-ζ basis, which corresponds to a single basis function, $\psi_{\mathrm{nlm}}(\mathrm{r})$ per electron orbital (i.e. 1 for an *s*-orbital, 3 for a *p*-orbital, etc...). In this case each basis function consists of a product of one radial wavefunction, $\emptyset_{nl}^{1}$, and one spherical harmonic, Y_{lm}:

$$\psi_{\mathrm{nlm}}(\vec{r})=\emptyset_{nl}^{1}(r)\quad Y_{lm}(\varphi,\vartheta) \tag{2.34}$$

The small number of the expected basis function is one, and therefore a single-ζ basis uses single atomic orbitals as a basis function. Therefore, the radial part in equation (2.34) is found by using the Sankey method [75], because the component of the real orbital is described by an infinitely long tail, which is not suitable for a localized basis function.

This method uses a modified version of the Schrödinger equation, which is solved for an atom placed inside a spherical box, and the radial wavefunction equals zero at the cut-off radius, r_c . This restriction yields an

energy shift δE within the Schrödinger equation such that eigenfunction has a node at the cut-off radius, r_c :

$$\left[-\frac{d^2}{dr^2}+\frac{l(l+1)}{2r^2}+V_{nl}^{ion}(r)\right]\emptyset_{nl}^{1}(r)=(\in_{nl}+\delta E)\varphi_{nl}^{1}(r) \qquad (2.35)$$

The energy shift δE satisfies the previous constraint and the corresponding pseudopotential is $V_{nl}^{ion}(r)$.To obtain high accuracy basis sets (multiple-ζ), additional radial wavefunctions could be included for each electron orbital. The split-valence method has been used to calculate the additional radial wavefunctions, $\emptyset_{nl}^{i}$, for $i > 1$. This involves defining a split-valence cut off for each additional wavefunction r_s^i. Thus, it is split into two piecewise functions: a polynomial below the cut-off and the former wavefunction above it:

$$\emptyset_{nl}^{i}=\begin{cases} r^1(a_{nl}-b_{nl}r^2 & r>r_s^i \\ \emptyset_{nl}^{i} & r_s^i<r<\ r_s^{i-1} \end{cases} \qquad (2.36)$$

The additional parameters are found at the point r_s^i where the wavefunction and its derivative are assumed continuous.

The polarization of a real orbital due to the electrical field of the neighbour atoms, is taken into account to calculate the basis set function. This kind is called double-ζ polarized(DZP), which is used to achieve all calculations in this thesis. Table (2.1) shows the number of basis of orbitals for a selected number of atoms for single-ζ polarized (SZP), double-*ζ(DZ)* and double-ζ polarized (DZP) [75].

Table 2.1: Examples of the radial basis functions per atom as used within the SIESTA for different degrees of precisions[75]

Atom	SZ	SZP	DZ	DZP
H	1	4	2	5
C	4	9	8	13
S	4	9	8	13
N	4	9	8	13
O	4	9	8	13
Au	6	9	12	15

2.7 Time-Dependent Density Functional Theory (TD-DFT)

The time-dependent density functional theory (TD-DFT) extends the ground-state density functional theory by allowing for the examination of a system's excited-state features in the presence of time-dependent potentials, such as electric or magnetic fields. TD-DFT may be used to investigate the influence of fields on molecules by calculating representative excitation energies, oscillator strength, wavelength, molecular orbital character, and electronic transitions of the molecules [76]. The theoretical of TD-DFT based on the Runge-Gross theorem (R-G theorem) in 1984. The R-G theorem explained the association between the time-dependent external potential $\hat{V}_{ext}(\vec{r})$ and $\rho(\vec{r}\,,t)$ of the system. R-G theorem designated that when two external potentials $\hat{V}_{ext}(\vec{r})$ and $\widehat{V'}_{ext}(\vec{r})$ have an alteration of more than a time-dependent function, their own electron densities $\rho(\vec{r}\,,t)$ and $\rho'(\vec{r}\,,t)$ are also dissimilar [77].

Runge and Gross discussed how excited states are obtained using TD-DFT. The starting point of studying time-dependent systems is the time-dependent Schrodinger equation. The TD-DFT is straight related to the Schrodinger equation $\left[i\,\hbar\,\frac{\partial}{\partial t}\,\Psi\,(\,\vec{r}\,,t\,) = \hat{H}\,\Psi\,(\,\vec{r}\,,t\,)\right]$ where the Hamiltonian is known to be [78]:

$$\hat{H} = \hat{T} + \hat{V}_{\text{elec.elec}} + \hat{V}_{\text{ext.}}(\vec{r}\,) \tag{2.37}$$

Here, $\hat{H}$ consists of the kinetic energy operator $\hat{T}$ electron-electron repulsion $\hat{V}_{\text{elec.elec}}$ (Coulomb operator) and the external potential $\hat{V}_{\text{ext.}}(\vec{r})$. Where $\hat{V}_{\text{ext.}}(\vec{r})$ is given in the following operators:

$$\hat{V}_{\text{ext.}}(\vec{r})=\sum_{i=1}^{N} V_{ext.}\,(\vec{r_i}\,) \tag{2.38}$$

The densities of the system rise from a fixed first state $\Psi\,(\,t_o) = \Psi\,(\,0\,)$. The first state, $\Psi\,(\,0)$ is arbitrary, it must not be the ground-state or some other eigen state of the first potential $\hat{V}\text{ext.}(\vec{r}) = \hat{V_o}\,(\vec{r})$. The R-G theorem indicates that there exists an one-to-one correspondence between the time-dependent external potential $\hat{V}\text{ext.}(\vec{r})$, and the time-dependent electron density $\rho(\vec{r}\,,t)$, for systems developing from a fixed first many-body state. Translation to it, the density determines the external potential, and next helps in obtaining the time-dependent many-body wave functions [79,80]. As this wave-function controls all observables of the system as an important, the saying point is that all observables are functionals of $\rho(\vec{r}\,,t)$.

The statement of the theorem is the "densities $\rho(\vec{r},t)$ and $\rho'(\vec{r},t)$ evolving from the same initial state $\Psi(0)$ under the effect of two potentials $\hat{V}_{\text{ext.}}(\vec{r})$ and $\widehat{V'}_{ext}(\vec{r})$ are always different provided that the potentials differ by additional than a chastely time-dependent function [76,78]:

$$\hat{V}_{\text{ext.}}(\vec{r},t) = \widehat{V'}_{ext}(\vec{r},t) + C(t) \qquad (2.39)$$

Where the $C(t)$ allows increase to wave functions that are different only by a phase factor $e^{-iC(t)}$, therefore, the same electronic density is stable. R-G theorem states that the density is a functional of the external potential and of the first wave function on the space of potentials differing by more than the addition of C(t).

2.8 Gaussian 09 Program (G09)

The Gaussian program is a computational software package initially published by John Pople in 1970. Gaussian program is a very high-end quantum mechanical software package. The "09" mentions to the year 2009 in which the software was published[81].

Gaussian is capable of running all of the major methods in molecular modeling, including molecular mechanics, ab-initio, semi-empirical, HF and DFT. Moreover, excited state computes can be done by different methods in this program[82].

The name originates Gaussian comes from the use of the Gaussian Type Orbitals that Gaussian's originator, John Pople, used to try to

overcome the computational difficulties that get up from the use of Slater Type Orbitals. A number of researchers, such as S.F. Boys and Isaiah Shavitt, Pople, quite brilliantly, recognized that the (relatively) simple, substitution of a series of Gaussian functions for the Slater function, would greatly simplify the rest of the calculation of the Schrödinger equation. Pople (1998) was awarded the Nobel Prize in chemistry (along with Walter Kohn) for this work [81,82].

2.9. Gaussian Basis Set

In theoretical physics and chemistry, a basis set is a collection of mathematical functions that are used to explain the form of molecular orbitals. Both ab-initio and DFT approaches make use of basis sets to specify the molecular orbitals in a system quantitatively. While it is possible to develop a basis set from scratch, the vast majority of calculations are performed using pre-existing basis sets. The correctness of the results is dependent on the type of calculation used and the basis sets used. Slater-type orbitals (STOs) and Gaussian-type orbitals (GTOs) are two forms of basis sets [83].

2.9.1. Slater Type Orbitals (STO's)

Slater type functions show a correct behavior near the nuclei at r → 0 with an intermittent behavior. The Slater type orbitals have the form [81]:

$$X^{STO} = N\, r^{n-1}\, e^{-\xi r}\, Y_{lm}(\theta, \varphi) \qquad (2.40)$$

Where, n is a major quantum number and ξ is a constant related to the effective charge of the nucleus. Y_{lm} is a spherical harmonic which describes the angular part of the wave function.

2.9.2. Gaussian Type Orbitals (GTO's)

The Gaussian type orbitals (GTOs) basis function is widely used in HF and related approaches because it enables the calculation of many-center integrals analytically. In terms of Cartesian coordinates, Gaussian type orbitals can be written as [82]:

$$X^{GTO} = N\, x^{lx}\, y^{ly}\, z^{lz}\, e^{-\xi\, r^2} \tag{2.41}$$

N is a normalization factor; the sum of l_x, l_y and l_z determines the type of orbitals; and ξ represents the orbital exponent that shows compact large ξ or diffuse small ξ is the resulting function, r^2 dependence in the exponential is insufficiency of the GTO's related to the Slater-type orbitals STO's.

One of the negative aspects of STO's is that many-center integrals such as Coulomb and HF-exchange terms are hard to compute with STO's. For this reason, it plays no role in modern wave function based quantum chemistry codes. As a result, for the calculations of Coulomb and HF-exchange terms, the analytical solution is available for the Gaussian functions. In order to improve the GTO basis sets, one usually. employs a

contracted GTO basis set, in which several primitive Gaussian functions are mixed to give a contracted Gaussian function (CGF) as [83,84]:

$$X_j^{CGF} = \sum_i^M C_{ij}\, X_a^{GTO} \tag{2.42}$$

M is the number of Gaussian primitives employed in a linear combination in this case. Gaussian uses a variety of different basis sets, including minimum basis sets, split valence sets, polarization and diffuse functions, and others [84].

3.1. Introduction

Electrical conductance is one of the most important properties of single molecules in the field of molecular electronics. Many theoretical descriptions of electron transport properties (including conductance) through single molecule systems are based on the Landauer formula, which is a simple expression for the relation between the transmission probability of the electron and the electronic conductance in one-dimensional structures with two terminals. The Landauer formula was later generalized by Buttiker to the case of multi-terminal devices. According to the Landauer formalism, the conductance can be calculated from a transmission probability, which in turn can be evaluated using Green‘s functions [85].

In this chapter, we will start Landauer and Buttiker formulas. Then we will discuss scattering theory and Green‘s functions for different transport regimes. As an example, a one dimensional structure with an arbitrarily scattering region will be used to present the general methodology used to describe the transmission coefficient *T(E)* in a molecular junction for electrons with energy traversing from one electrode to another. Thereafter different types of resonances will be discussed that characterize the conductance within a general theory of electronic transport [86].

3.2. The Landauer Formula

The Landauer formula [86,87] was first suggested by Rolf Landauer in 1957 [88] for two terminals. To illustrate the formula, consider a scattering region connected to two electrodes (leads) as sketched in Figure 3.1. The leads are assumed to be ballistic conductors, i.e. conductors with no scattering and thus the transmission probability equals one [89]. Each lead, in turn, is coupled to a reservoir where all inelastic processes take place.Suppose that the chemical potentials of the reservoirs on the left and right hand sides are μ_l , μ_r respectively, and let the temperature be equal to zero (T = 0)

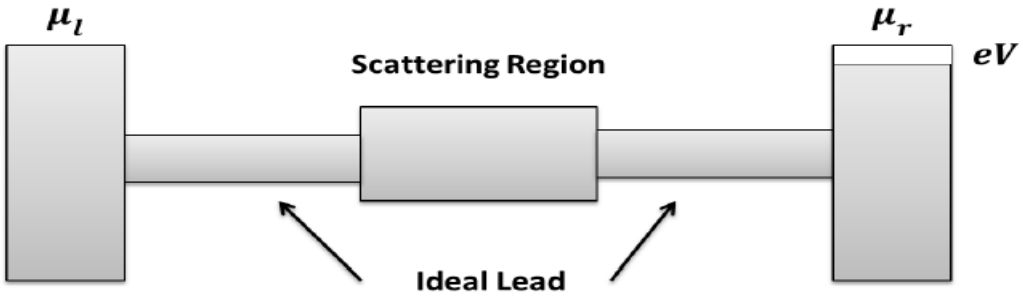

Figure 3.1. Schematic view of a 1D scattering region connected to two reservoirs with different chemical potentials μ_L and μ_R via ideal leads

Consider the case of a 1-dimensional system. When the scattering region is an ideal 1-dimensional lead, so that the two reservoirs are connected by a perfect 1-d lead with no scattering, the current through this system, which flows due to the chemical potential difference between the reservoirs is,

$$I = (-e)v\,\frac{\partial n}{\partial E}(\mu_l - \mu_r) \qquad (3.1)$$

Here v is the group velocity, e is the electronic charge and $\frac{\partial n}{\partial E}$ is the density of states per unit length of the electrons which is given by $\frac{\partial n}{\partial E} = \frac{1}{\pi \hbar v}$ It is worth mentioning that the Landauer formula describes the linear response conductance, hence it only holds for small bias voltages, $\delta V \to 0$ Thus,

$$I = \frac{-e}{\pi \hbar} (\mu_l - \mu_r) \tag{3.2}$$

In the presence of the scatter, these electrons have a transmission probability T to traverse the scattering region, therefore, the current flow is [89]:

$$I = \frac{-2e}{h} T (\mu_l - \mu_r) \tag{3.3}$$

Since the chemical potentials difference between the reservoirs is given by ,$-eV = (\mu_l - \mu_r)$, the conductance between the two terminals is obtained as:

$$G = \frac{I}{V} = \frac{2e^2}{h} \mathrm{T} = G_0 T \tag{3.4}$$

Where $G_0 = \frac{2e^2}{h}$. This relation is called Landauer formula for a one-dimensional system [86,87]. For a perfect conductor where $T = 1$, the Landauer formula becomes:

$$G = G_0 \approx 12.9(k\Omega)^{-1} \tag{3.5}$$

Where G_0, is the conductance quantum. At a finite temperature the Landauer formula (3.3) is transformed into the more general formula for the current [88]:

$$I = \frac{2e}{h} \int T(E)[f(E - \mu_l) - f(E - \mu_R)]dE \tag{3.6}$$

Where f is the Fermi-Dirac distribution $f(E-\mu) = 1/(1+e^{\frac{E-\mu}{k_B T}})$ related to the chemical potential μ , T is temperature and k_B is Boltzmann's constant. In the case of the linear response regime (i.e. at low bias eV), the Fermi-Dirac functions in eq. (3.6) can be Taylor expanded around the Fermi energy [89] resulting in:

$$I = \frac{2e^2V}{h}\int_{-\infty}^{\infty}\left[-\frac{\partial f(E)}{\partial(E)}\right]\ T\ (E)\ \ dE \tag{3.7}$$

Last equation shows that when the voltage is small, the current is linearly proportional to the voltage, and then we can write:

$$I\ = G\ V \tag{3.8}$$

Where G is the conductance of the two terminals device. Thus:

$$G = G_0\int_{-\infty}^{\infty}\left[-\frac{\partial f(E)}{\partial(E)}\right]\ T\ (E)\ \ dE \tag{3.9}$$

As mentioned above, the current in equation (3.8) is linearly proportional to the voltage and because of this linearity, this system of transport is called linear response regime.

3.3. Landauer-Buttiker formalism

Landauer original result was obtained for two-terminal systems and then its idea was extended by Buttiker to the case of multi-terminal devices where the matrix form of the full formalism including the transmission probability is needed. Buttiker suggested that the Landauer formula, equation (3.3), can be generalized to structure with many terminals by writing the current I_i at the i_{th} terminal as [90]:

$$I_i = \frac{2e^2}{h}\sum_j (T_{ji}\ \mu_i - T_{ij}\ \mu_j) \tag{3.10}$$

Where T_{ji} (T_{ij}) is the transmission probability from terminal $j(i)$ to terminal $i(j)$. We therefore define:

$$G_{ij} = G_0\, T_{ij} \tag{3.11}$$

And rewrite Eq. (3.10) as:

$$I_i = \sum_j (G_{ji}\ \mu_i - G_{ij}\ \mu_j) \tag{3.12}$$

Current conservation gives some conditions for currents and conductance, because

$$\sum_i I_i = 0 \tag{3.13}$$

Furthermore all currents should be zero, when the potential μ_i of all the terminals are equal

$$\sum_j \left(G_{ji} - G_{ij}\right) = 0 \tag{3.14}$$

This allows us to rewrite equation (3.12) as:

$$I_i = \sum_j (G_{ij}\ (\mu_i - \mu_j) \tag{3.15}$$

This is the so-called Landauer-Buttiker formula for the multi-terminal structures [90].

3.4. Green's Functions

Green's function (GF) is a useful tool for studying the properties of nano-scale structures because it can be used to express all of the observable properties of the system of interest [91]. In this section we will first discuss how to construct the Green's function for some separate lattices. Then we will briefly discuss how to connect the Green's functions of these separable lattices together to construct the Green's function of the whole system using Dyson equation.

3.4.1. Green's Function of Doubly Infinite Chain

In this section we will derive the one dimensional doubly infinite Green's function of the electrodes, where these electrodes are described as a perfect one dimensional chain as shown in Figure 3.2 In order to obtain the scattering amplitudes we need to calculate the Green's function of the system[92].

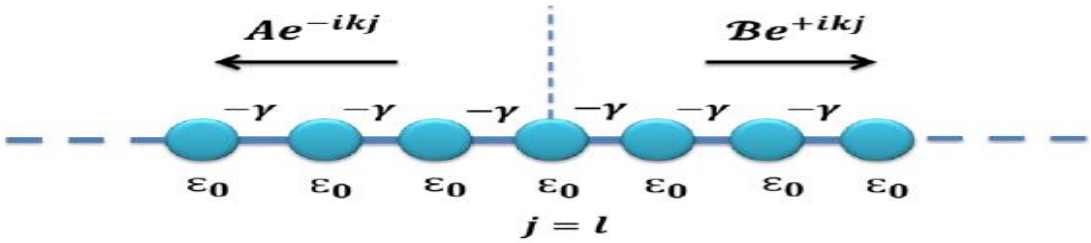

Figure 3.2 Tight-binding representation of a one-dimensional infinite lattice with on-site energies ε_0 and couplings γ [92].

The Green's function for a system obeying the Schrodinger's equation

$$(EI - H)\psi = 0 \tag{3.16}$$

is defined as:

$$(E - H)G = I \tag{3.17}$$

The solution for this equation can be written as:

$$G = (E - H)^{-1} \tag{3.18}$$

Where G, is the retarded Greens function g_{jl}, describes the response of a system at a point *j* due to a source at *l*. This source causes excitation which raises two waves, travelling to the left and right as shown in Figure 3.2. Where,

$$g_{jl} = \begin{cases} A\, e^{-ikj}, & j < l \\ \mathcal{B}\, e^{+ikj}, & j > l \end{cases} \tag{3.19}$$

Here, *A* and *B* are the amplitudes of the two outgoing waves travelling to the left and right, respectively. Green's function must be continuous at $j = l$. As a result we can write:

$$g_{jl|j=l} = \begin{cases} A\, e^{-ikj}, & ,let \dots A = Ce^{+ikl} \\ \mathcal{B}\, e^{+ikj}, & ,let \dots B = Ce^{-ikl} \end{cases} \tag{3.20}$$

Therefore:

$$A\, e^{-ikj} = \mathcal{B}\, e^{+ikj} = C \tag{3.21}$$

Substituting from equation (3.21) into equation (3.19) results in:

$$g_{jl} = Ce^{ik|j-l|} \tag{3.22}$$

In order to obtain the constant C , equation (3.17) has to be satisfied using equation (3.22), thus:

$$C = \frac{1}{2i\gamma\, sink} = \frac{1}{i\hbar v} \tag{3.23}$$

Combining the last two equations yields:

$$g_{jl} = \frac{e^{ik|j-l|}}{i\hbar v} \tag{3.24}$$

This equation represents Green's function of a doubly infinite one-dimensional chain [89,92,93].

3.4.2. Green's Function of Semi-Infinite One-Dimensional Chain

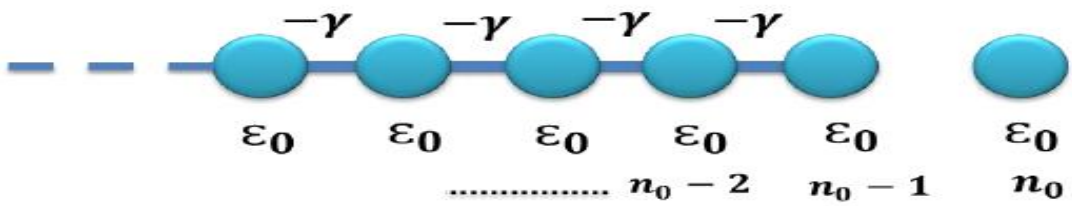

Figure 3.3. Tight-binding representation of a one-dimensional semi-infinite lattice with on-site energies ε_0 and couplings γ .

In order to obtain Green's function of a semi-infinite chain from Green's function of a doubly infinite chain, an appropriate boundary condition should be introduced. Let consider one dimensional lattice with site energies and hopping elements $-\gamma$ as shown in Figure 3.3. The chain must be terminated at a given point, n_0 so all points for which $n \geq n_0$are missing, that means that the Green's function should vanish at site n_0 . This can be achieved by adding a wave function to the Green's function of the doubly infinite chain[94,95]. The proper wave function in this case is:

$$\Psi_{jl} = -\frac{e^{-ik(j+l-2n_0)}}{i\hbar v} \tag{3.25}$$

Therefore:

$$g_{jl} = \frac{e^{ik|j-l|}}{i\hbar v} - \frac{e^{-ik(j+l-2n_0)}}{i\hbar v} \tag{3.26}$$

Satisfying the boundary condition ($j = l = n_0 - 1$) yields:

$$g_{n_{0-1}, n_{0-1}} = \frac{1}{i\hbar v} - \frac{e^{2ik}}{i\hbar v} \tag{3.27}$$

Hence, the Green's function at site $j=n_0-1$ due to a source at site $l=n_0-1$ is:

$$g_{n_{0-1},n_{0-1}} = \frac{e^{ik}}{\gamma} \tag{3.28}$$

3.4.3 Green's Function of A Finite One-Dimensional Chain

To derive the Green's function of a finite one-dimensional lattice, consider a linear chain of *N* atoms as expressed in Figure 3.4. Green's function should vanish at site *n=0* and site *n=N+1*.

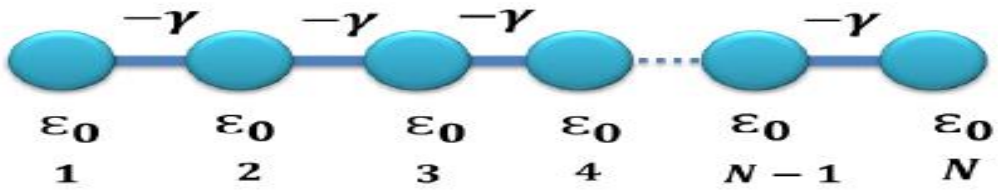

Figure 3.4. Tight-binding representation of a one-dimensional semi-infinite lattice with on-site energies ε_0 and couplings γ [97].

To achieve that, Green's function should take the following expressions:

$$g_{jl} = \begin{cases} A\sin kj, & j < l \\ B\sin k\big(j-(N+1)\big), & j > l \end{cases} \tag{3.29}$$

So the boundary conditions will be satisfied [96,97]. The Green's function must be continuous at j = l, so

$$g_{jl} = \begin{cases} A\sin kl, & A = C\sin kl(l-(N+1)) \\ B\sin k(l-(N+1), & B = C\sin kl \end{cases} \tag{3.30}$$

Therefore:

$$g_{jl} = \begin{cases} C\ \sin k\big(l-(N+1)\big)\sin kj & ,j \le l \\ C\ \sin k\big(j-(N+1)\big) & ,j \ge l \end{cases} \tag{3.31}$$

Then C can be obtained as:

$$C = \frac{1}{\gamma\ \sin k\ \sin k\ (N+1)} \tag{3.32}$$

This gives the Green's function of a finite one-dimensional chain containing atom 1 and N at the opposite ends:

$$g_{N1} = \frac{-sink}{\gamma\ sink\ (N+1)} \tag{3.33}$$

3.4.4 One Dimensional Scattering

To construct the Green's function of the whole system we have to connect the Green's functions of the separable lattices together. Let us first consider the case of decoupled leads (α=0) shown in Figure 3.5.The total Green's function of the system can be given by the decoupled Green's function[98]:

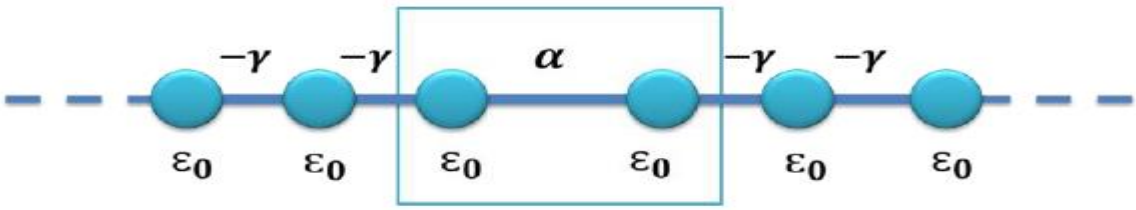

Figure 3.5. Tight-binding representation of a one dimensional scattering region attached to one dimensional leads [98].

$$g = \begin{pmatrix} -\frac{e^{ik}}{\gamma} & 0 \\ 0 & -\frac{e^{ik}}{\gamma} \end{pmatrix} = \begin{pmatrix} g_L & 0 \\ 0 & g_R \end{pmatrix} \tag{3.34}$$

For the case of coupled system[99], Green's function of the whole system can be obtained using Dyson's equation:

$$G = (g^{-1} - V)^{-1} \tag{3.35}$$

Here the operator V describes the interaction connecting the two leads and has the form:

$$V = \begin{pmatrix} 0 & V_c \\ V_c^{\dagger} & 0 \end{pmatrix} = \begin{pmatrix} 0 & \alpha \\ \alpha^* & 0 \end{pmatrix} \tag{3.36}$$

The solution to Dyson's equation is:

$$G = \frac{1}{\gamma^2 e^{-2ik} - \alpha^2} \begin{pmatrix} -\gamma e^{-ik} & \alpha \\ \alpha^* & -\gamma e^{-ik} \end{pmatrix} \tag{3.37}$$

This expression is Green‘s function for the whole system under consideration.

3.5. Transport Through an Arbitrary Scattering Region

As mentioned previously, once the Green‘s function is calculated the transmission probability is easy to obtain. In this section we will derive the most general formula for the transmission probability for an arbitrarily shaped scattering structure. Here we will use a different approach starting with the wave functions leading to the surface Green‘s function and ending up with a general formula for the transmission probability [100].

Considering the system in Figure 3.6, where an arbitrary scattering region with Hamiltonian H is connected to two one dimensional leads. On-site energies of the left and right leads are ε_0 and the coupling in the two leads is $-\gamma$ [101].

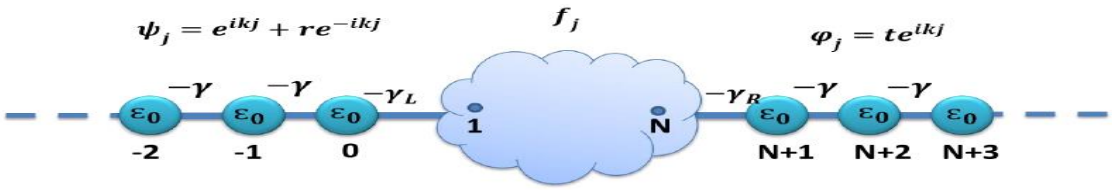

Figure 3.6. Tight-binding representation of a one dimensional arbitrarily scattering region attached to one dimensional leads [100].

The leads are connected to the site (1) and (2) of the scattering region with the couplings$-\gamma_L$ and $-\gamma_R$. The Hamiltonian for this system is:

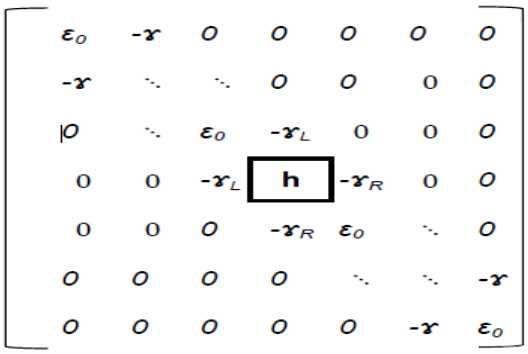

If the wave function in the left, the right and the scattering region are:

$\psi_j = e^{ikj} + r\, e^{-ikj}$ $, \varphi_j = te^{ikj}$ and f_j respectively.

The Schrodinger equations in left, right, scattering region and connection points could be written as[100,101]:

$$\varepsilon_0\psi_j - \gamma\psi_{j-1} - \gamma\psi_{j+1} = E\psi_j \qquad for\ j \le -1 \qquad (3.38)$$

$$\varepsilon_0\psi_0 - \gamma\psi_{j-1} - \gamma_L f_1 = E\psi_0 \qquad for\ j = 0 \qquad (3.39)$$

$$\sum_{j=1}^{N} h_{ij}f_j - \gamma_L\psi_0\delta_{i1} - \gamma_R\,\varphi_{N+1}\delta_{iN} = Ef_i \qquad for\ 0 \le j \le N+1 \qquad (3.40)$$

$$\varepsilon_0\varphi_{N+1} - \gamma_R f_N - \gamma\varphi_{N+2} = E\,\varphi_{N+1} \qquad for\ j = N+1 \qquad (3.41)$$

$$\varepsilon_0\varphi_J - \gamma\varphi_{J-1} - \gamma\varphi_{J+1} = E\,\varphi_j \qquad for\ j > N+1 \qquad (3.42)$$

Equation 3.40 could be re-written as $|\,f\,\rangle\, g|\,x\rangle$ where $g = (E-H)^{-1}$ is the Green's function and $|\,x\rangle$ called source which is a zero vector with non-zero elements only in the connection points at site $j = 0$ and $j = N + 1$, $|f\,\rangle$ has only two non-zero elements due to the source,

$$\begin{pmatrix} f_1 \\ f_N \end{pmatrix} = \begin{pmatrix} g_{11} & g_{1.N} \\ g_{N,1} & g_{N,N} \end{pmatrix} \begin{pmatrix} x_0 \\ x_{N+1} \end{pmatrix} \qquad (3.43)$$

Where $x_0 = \gamma_L \psi_0$ and $x_{N+1} = \gamma_R \varphi_{N+1}$

Using recurrence relation gives:

$$\gamma \varphi_N = \gamma_R f_N \tag{3.44}$$

$$\gamma \psi_1 = \gamma_L f_1 \tag{3.45}$$

$$\varphi_N = \varphi_{N+1} e^{-ik} \tag{3.46}$$

$$\psi_1 = 2i \sin k + e^{-ik} \psi_0 \tag{3.47}$$

Combining last four equations with equation (3.43) gives:

$$\begin{pmatrix} -g_{11}\ \gamma_L - \frac{\gamma}{\gamma_L} e^{-ik} & -g_{1N}\ \gamma_R \\ -g_{N1}\ \gamma_L & -g_{NN}\ \gamma_R \frac{\gamma}{\gamma_R} e^{-ik} \end{pmatrix} \begin{pmatrix} \psi_0 \\ \varphi_{N+1} \end{pmatrix} = \frac{\gamma}{\gamma_L} 2isink \begin{pmatrix} 1 \\ 0 \end{pmatrix} \tag{3.48}$$

Thus

$$\begin{pmatrix} \psi_0 \\ \varphi_{N+1} \end{pmatrix} = 2isink \frac{\gamma}{\gamma_L} \frac{1}{d} \begin{pmatrix} g_{NN}\ \gamma_R - \frac{\gamma}{\gamma_R} e^{-ik} \\ -g_{N1}\ \gamma_L \end{pmatrix} \tag{3.49}$$

Therefore the transmission t and reflection r amplitudes could be obtained [102,103,104].

$$t = iv[\gamma_L g \left(\frac{g_{N1}}{\Delta}\right) \gamma_R g] \tag{3.50}$$

Where

$$g = -\frac{e^{ik}}{\gamma} \tag{3.51}$$

is the Green‘s function of semi-infinite chain and

$\Delta = 1 - \sum_L g_{11} - \sum_R g_{NN} + \sum_L \sum_R (g_{11} g_{NN} - g_{N1}\ g_{1N}\ )$

Where $\sum_{R,L} = \gamma_{L,R}^2\ g$ are the self energies due to the left and right contact.

The transmission probability is $T(E) = |t|^2$ then

$$T(E) = v^2 \left[\left[\frac{\gamma_L}{\gamma} \frac{|g_{N1}|^2}{|\Delta|^2} \left(\frac{\gamma_R}{\gamma}\right)^2\right]\right] \quad (3.52)$$

This is the most general formula to calculate the transmission probability for any scattering region connected to identical leads.

3.6. Features of the Transport Curve

The main feature of electron transport through single molecules and phase-coherent nanostructures is the appearance of transport resonances associated with quantum interference. Deep understanding of the transmission process can be achieved by looking at the properties of these resonances. Here, we will briefly discuss different kinds of resonances, including Breit−Wigner resonances [105], anti-resonances [106,107], and Fano resonances [108,109].

3.6.1 Breit-Wigner Resonance

For electrons of energy E passing through a single molecular orbital, the transmission probability could be expressed by a Lorentzian function, via the Breit-Wigner formula [105]:

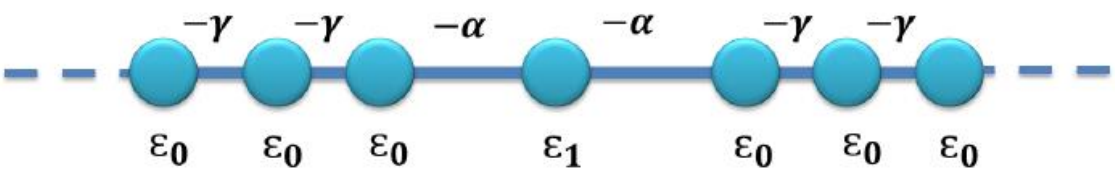

Figure 3.7. Tight binding model to possessing a Breit-Wigner resonance. Two one-dimensional semi-infinite chains coupled to a scatting region of site energy by hopping elements – γ.

$$T(E) = \frac{4\Gamma_1\Gamma_2}{[(E-\varepsilon_n)^2+(\Gamma_1+\Gamma_2)^2]} \quad (3.54)$$

Within this formula, the transmission coefficient T(E) of the single molecular junction can be described by two parameters: (Γ) and (ε_n) where (Γ) is the strength of the coupling between the molecule and the electrodes (labeled 1 and 2) and $\varepsilon_n = E_n - \sum$ is the eigen energy E of the molecular orbital shifted slightly by an amount $\sum$ due to the coupling of the orbital to the electrodes. Transmission coefficient $T(E)$ has Breit-Wigner-type resonances showing the maximum value when the electron resonates with the molecular orbital (i.e. when $E = \varepsilon_n$). Figure (3.7) shows a scattering region with a single impurity placed between two one-dimensional semi-infinite chains. Where, Figure 3.10 shows the tight binding representation of the transmission probability (blue curve) for this system. The formula is valid when the energy of the electron is close to an eigen energy of the isolated molecule, and if the level spacing of the isolated molecule is larger than ($\Gamma_1+\Gamma_2$) In the case of a symmetric molecule attached symmetrically to identical leads (i.e. $\Gamma_1=\Gamma_2$ and again when ($E = \varepsilon_n$)) , *T(E)* equals one. The width of the resonance depends on the coupling component where if the coupling element α is large, the resonances are wider.

3.6.2. Fano Resonances

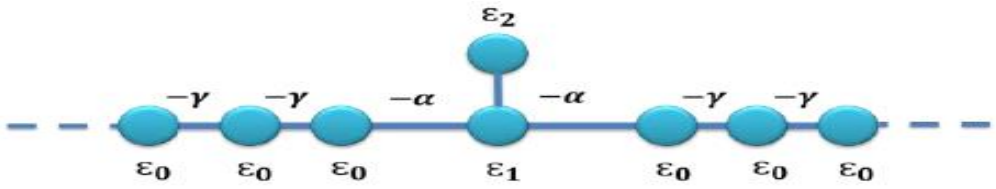

Figure 3.8. Tight binding model to study Fano resonances. Two one-dimensional semi-infinite chains coupled to a scattering region of site energy ε_0 by hopping elements where an extra energy level is attached to the scattering region $-\gamma$ [108].

In contrast to the Breit-Wigner resonance (a symmetric shape line); Fano resonance was explained as a phenomenon of constructive and destructive interferences between a bound state and the continuum where the corresponding spectral lines are asymmetric. For example, a molecule with a side group produces a Fano resonance when the energy of the incident electron is close to an energy level in the side group. Fano resonances have been observed in various systems including quantum dots, nanowires, tunnel junctions and more [108]. Figure 3.8 expresses a simple example of a system contains two one-dimensional semi-infinite chains with site energies ε_0 and hopping elements $-\gamma$ coupled to a scattering region with two site energies ε_1 and ε_2. The red curve in Figure 3.10 shows the transmission probability for this system using tight binding model [108,109].

3.6.3. Anti-Resonances

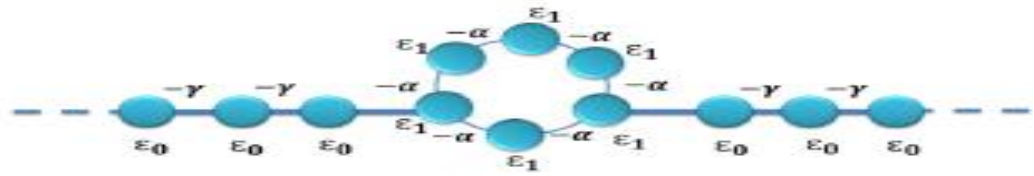

Figure 3.9. Tight binding model to study anti-resonance. Two one-dimensional semi-infinite chains coupled to the scattering region[106].

This kind of resonance appears in the transmission probability spectrum when the system is multi-branched and destructive interference occurs between propagating waves. A simple example is shown in Figure 3.9, where two one-dimensional semi-infinite chains with site energies ε_0 and hopping elements $-\gamma$ are coupled to a scatting region with six site energies (ε_1). The magenta curve in Figure 3.10 shows the general shape of the transmission probability related to this kind of resonance [106,107].

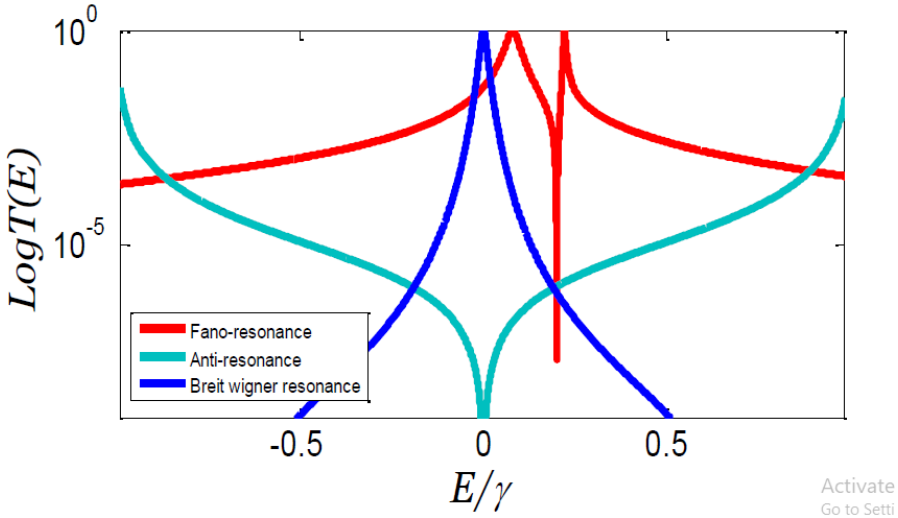

Figure 3.10. Tight binding representation of the transmission coefficients for the above systems showing different kind of resonances [107].

3.7. Gollum Program

Charge, spin, and electronic contributions to the thermal transport properties of multi-terminal junctions are calculated using the GOLLUM program. GOLLUM has a simpler structure, is faster, and consumes less memory since it is based on nonequilibrium transport theory.

The software has been developed for ease of use, and it represents a significant step forward in the implementation of ab-initio multi-scale simulations of traditional and more advanced transports functions. GOLLUM's simplified interface allows it to read model tight bound Hamiltonian's [110]. Furthermore, GOLLUM is designed to readily interact with any DFT code that employs a localized basis set .It now reads data from all of the most recent public versions of the code SIESTA.

GOLLUM can model these materials' connections using parameterized tight-binding Hamiltonians or DFT[111,112] .

DFT fails to account for the significant electronic correlation effects found in many Nano-scale electrical connections. As a result, GOLLUM provides a number of methods for dealing with high correlations[113,114].

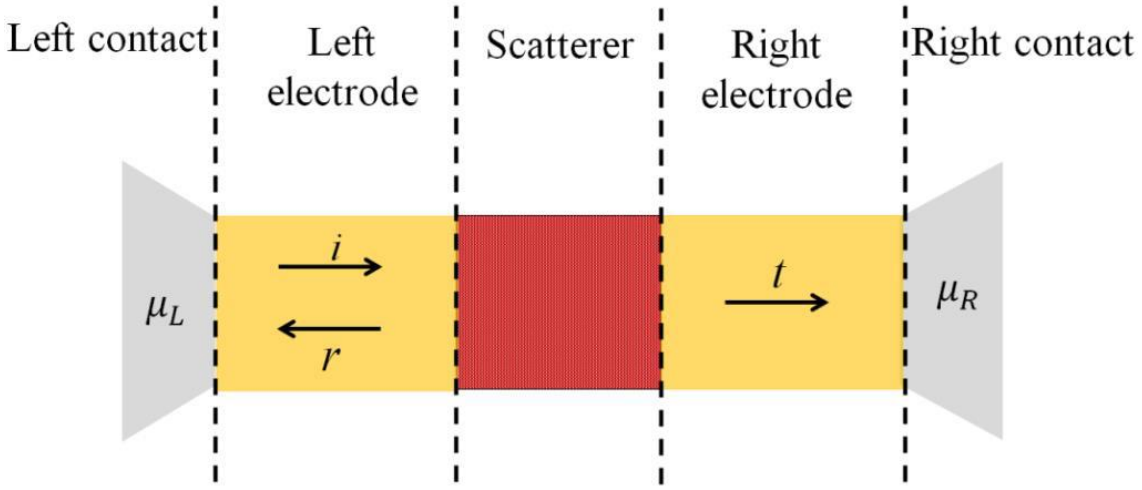

Figure 3.11. illustrates a mesoscopic scatterer connected to contacts by ballistic leads. The μ_L and μ_R represent the chemical potential in the contacts. When an incident wave packet hits the scatterer from the left then it will be transmitted with probability $T = tt*$ and reflected with probability $R = rr*$ where, t, $t*$, r and $r*$ represent the transmission and the reflection amplitudes from the left to the right and vice versa. Charge conservation requires T + R = 1 [114].

4. Results and Discussions

The main goal of this work is the exploring and understanding of novel fundamentals of different molecular junctions, which is the link between the chapters of this thesis, since these studies are aiming to study and realize the electronic, electric, thermoelectric and spectral properties of **Au | organic molecules | Au** nano-molecular junctions. In other words, Chapter four is focusing on different organic molecules to explore some of novel principles such as the emission oscillator strength, electrical conductance and thermopower, as well as to investigate the relation between these properties, and the influence of the most important factors such as the molecular length and quantum interference on these characteristics.

4.1. Optimizing the Emission Oscillator Strength Based on the Molecular Length Manipulation Strategy

4.1.1. Introduction

Over the years, great efforts have been devoted to the development of organic solid-state lasers (OSSL) due to the easy and economic fabrication, covering a wide-range lasing wavelength from near infrared to ultraviolet [115-120]. To date, optically pumped OSSL have been maturely developed, with the achievement of remarkably low laser and/or amplified spontaneous emission (ASE) thresholds and quasi-continuous wave operation [121,122]. The ultimate goal in the field of OSSL is, however, to

realize electrically pumped lasing so as to truly enable the creation of low-cost, portable, and flexible solid OSSL devices. Compared to optically pumped OSSL, lasing under electrical pumping is much more challenging because of the following factors. First, triplet exciton tends to accumulate under electrical pumping based on spin statistics [123], that is, three quarters of excitons formed under current injection are triplets, which usually have a long decay time [119]. Second, under electrical pumping, multiple annihilation and absorption losses will be induced by polarons, excitons, and other species that are not involved in optical pumping [119,120]. Recently, there are encouraging progresses reporting promising indications of current injection OSSL [124], which opened up the opportunities in realizing compact and lowcost electrically driven organic laser devices. Notwithstanding the advancements achieved in previous studies [124], obstacles still remain for organic laser gain media to observe light amplification under electrical pumping. Therefore, it is of significant importance to carry out theoretical evaluation and predict potentially good electrical pumping candidates, which require a large stimulated emission cross section [119,120].

With that in mind, the goal of this study is to propose a general computational protocol to systematically screen out electrically pumped lasing molecules over a range of organic solid-state fluorescent materials, with the assistance of efficient electronic structure calculations based on

density functional theory (DFT) and time-dependent DFT (TD-DFT). The ability of realizing general lasing behavior will be evaluated from one perspective that is closely related to the stimulated emission cross section, which is the emission oscillator strength, and its relationship with other factors such as the molecular length.

4.1.2. Structural Properties of Molecules

The thiophene/phenylene co-oligomers (TPCOs) are ranked as a newly occurring class of organic semiconductors. The materials are characterised by that thiophenes and phenylenes are hybridised at the molecular level with their various mutual arrangements. These molecular arrangements produce peculiar morphological features in the solid state and excellent electronic and optical properties. In this study, those characteristics have been outline in light of the structure/property relationship with central emphasis upon the crystal structure and its relevance to the leading-edge optoelectronic functionalities. These topics are most suitably approached by device studies including field-effect transistors and light-emitting devices. The device characteristics in close connection with current-injected lasers will be described as shown in Figure 4.1 and Table 4.1.

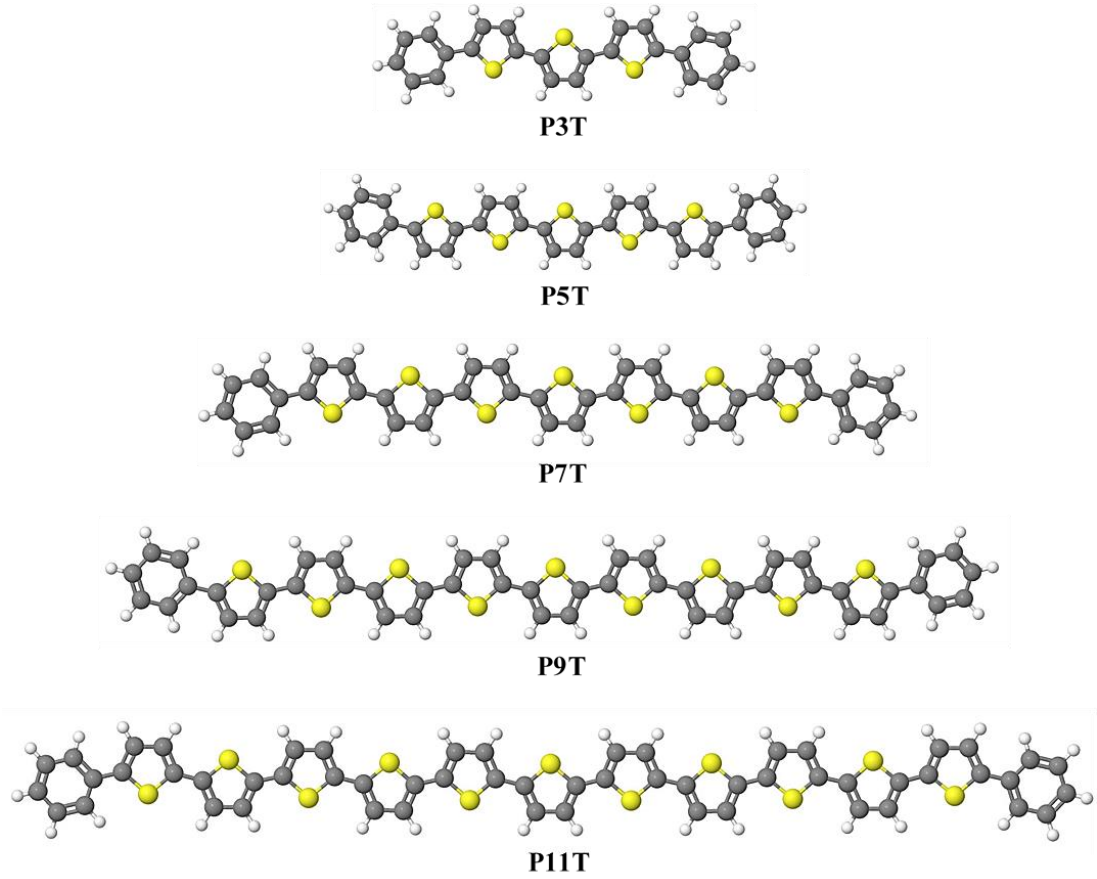

Figure 4.1. The optimized single molecules.

The crystal structure of the thiophene/phenylene co-oligomers (TPCOs) is characterised by the molecular layered structure, this structure being very often observed for crystals of ‘‘direction-defined’’ long molecules with a large aspect ratio [117]. As far as the straight-chain molecules like oligophenylenes are concerned, the layered structure can be seen for the compounds of two aromatic rings or more . In their crystals, the molecules tend to be disposed with the molecular long axes tilting with respect to the bottom crystal plane [117,125,126]. The tilting can be measured by an angle between the molecular long axis and the normal to The bottom crystal plane [127,128]. In the case of the straight-chain

molecules the said angle is around 10–20° [117]. The tilting angles, however, are generally small with the non-straight molecules typified by the TPCOs [127-130]. Here the molecular long axis is defined as a line connecting the terminal carbon atoms of the molecule. In the case of phenyl (thiophene) terminals, the relevant carbon atoms are located at the *p*-position on phenyls (α-position of thiophenes) [127-130]. Figure 4.1 shows optimized molecules under study in this thesis. The structural aspects of these molecules are distinguished by various molecular lengths, since the shortest molecule (P3T) has a molecule length of 2.089 nm, while the longest one (P11T) posses 5.271 nm. All structural aspects are shown in Table 4.1.

Table 4.1. The structural aspect of all molecules. L (H…H), is the molecule length, D (Au…Au), is the molecular length. X is the bond length (Au…C). Z (D – 0.25), is the theoretical electrodes separation. C–C is the carbon-carbon single bond. C=C is the carbon-carbon double bond. C–S is the carbon-sulfur single bond.

Molecule	L (nm)	D (nm)	X (nm)	Z (nm)	C–C (nm)	C=C (nm)	C–S (nm)
P3T	2.089	2.376	0.245	2.126	0.149	0.139	0.168
P5T	2.866	3.155	0.245	2.905	0.149	0.139	0.168
P7T	3.653	3.940	0.245	3.69	0.149	0.139	0.168
P9T	4.442	4.720	0.245	4.47	0.149	0.139	0.168
P11T	5.271	5.561	0.245	5.311	0.149	0.139	0.168

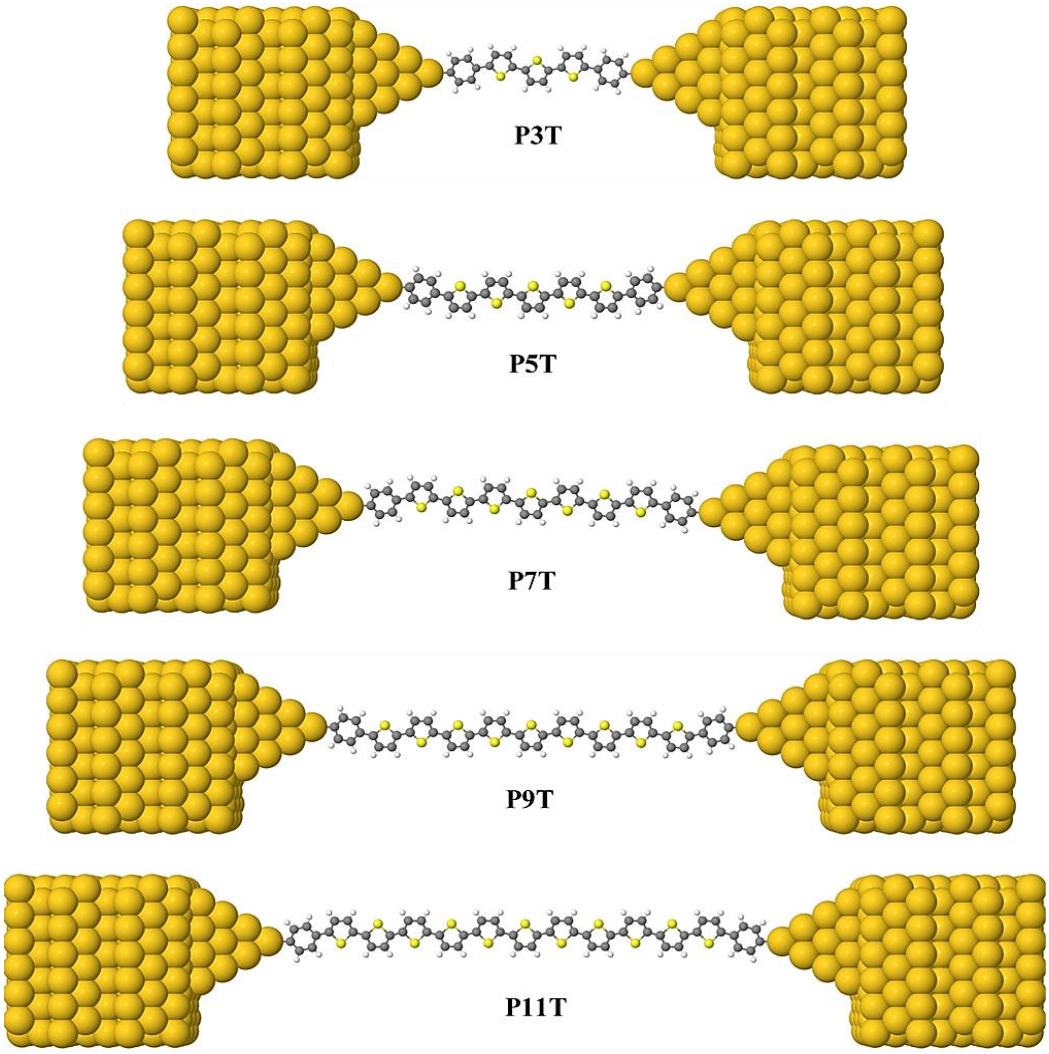

Figure 4.2. The optimized molecular junction of all structures.

To provide further insight, and to better evaluate the properties and behavior of these molecular junctions, calculations using a combination of DFT and a nonequilibrium Green's function formalism were also carried out. Eight layers of (111)-oriented bulk gold with each layer consisting of 6×6 atoms and a layer spacing of 0.235 nm were used to create the molecular junctions, as shown in Figure 4.2. The optimized molecular junction geometries conform well to a description of the phynel-gold contacted compounds forming an angle of 160º contact between the carbon

anchor atom and the undercoordinated gold atoms of the gold electrodes. As expected, Figure 4.2, and Table 4.1 show that the phynel contacted compounds are oriented normal to the idealized pyramidal gold electrode surface within the molecular junction. Also, the molecular length of structures increses with increasing of sulfur atoms from 3 sulfur atoms for the shortest molecule to 11 atom for the longest molecule.

4.1.3. Spectral and Electronic Properties of Molecules

In particular, the emission characteristics are deeply connected with the molecular symmetry and alignment. As already stated previously, the emission oscillator strength value can be subtly and precisely tuned by choosing the TPCO materials with a suitable molecular length and a desired mutual arrangement of thiophenes and phenylenes within the molecule. Because of the nearly upright molecular alignment the emission dominates from crystal edges. Figure 4.3 represents this feature with several molecule length. These results reflect the superior ability of the optical confinement is one of the attractive characteristics of the TPCOs and makes their crystals an excellent candidate for laser media. In relation to the light amplification such emission behaviour is advantageous for causing spectrally narrowed emissions including the laser oscillation.

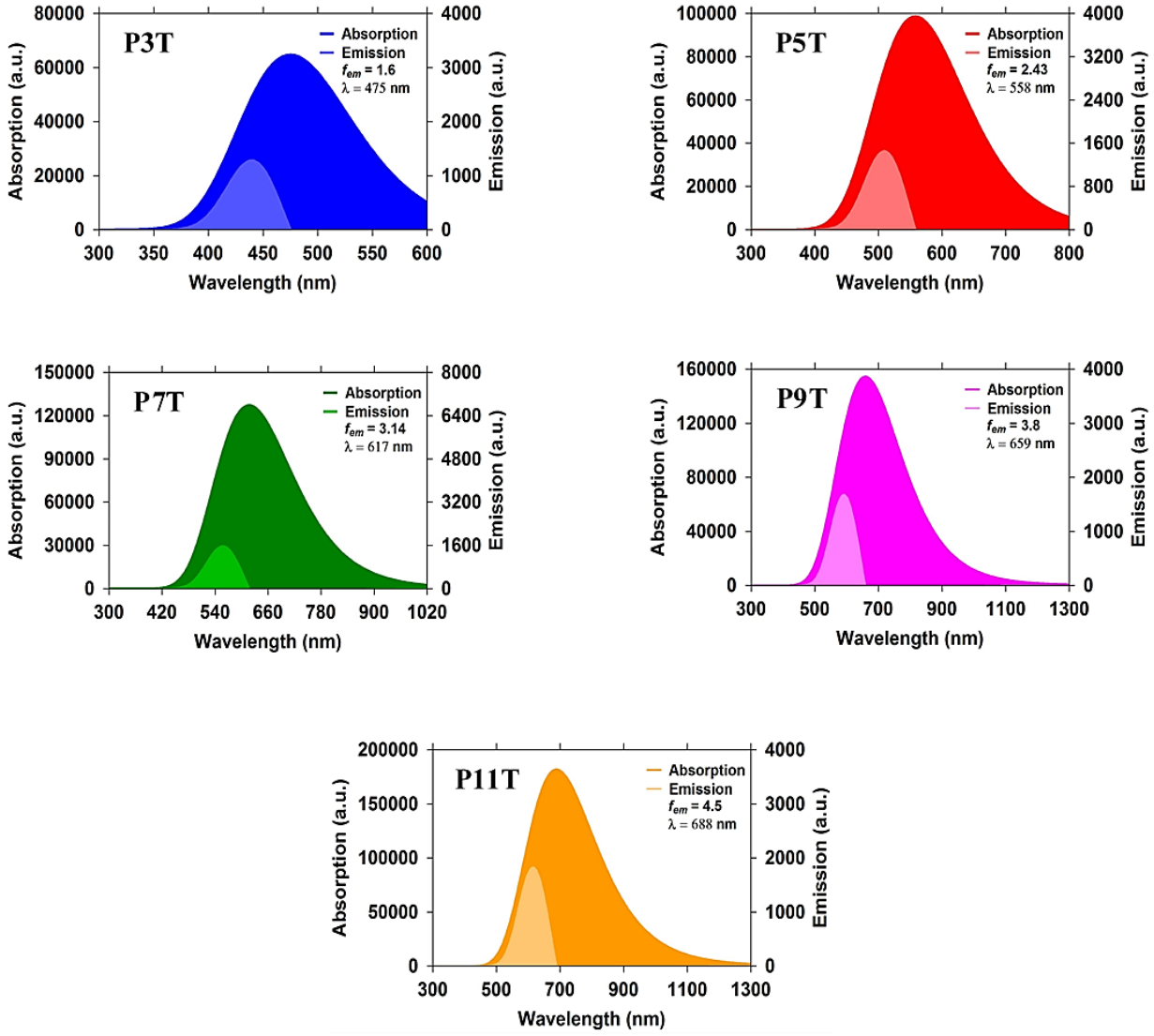

Figure 4.3. Represents the absorption, emission and emission oscillator strength of all molecules.

Figure 4.3 presents the absorption and emission results for all molecules under study in this thesis. Initially, it can be noticed that the absorption intensity of molecules have increased with increasing of the molecule length from 70000 (a.u.) to 180000 (a.u.). In fact, figure 4.3. illustrates that P3T molecule has the smallest emission oscillator strength (f_{em}) (1.6), while, the highest value of f_{em} is intrudesed via P11T molecule as

shown in Figure 4.4 and Table 4.2. It is well known that the light amplification from these structures at room temperature will be difficult, which consistent with previous studies [131]. Since, the calculated emission cross section σ_{em} of a laser transition is consider an important parameter in a laser gain medium. It can affect laser performance in terms of threshold energy, output energy, maximum gain, etc. Under conventional lasing mechanism, a large σ_{em} is a prerequisite of a good laser gain medium [132]. Theoretically, for a given photoluminescence (PL) material, σ_{em} is directly proportional to the emission oscillator strength f_{em} via [132]:

$$\sigma_{em}(v) = \frac{e^2}{4\varepsilon_0 m_e c_0 n_F} g(v) f_{em} \qquad (3.1)$$

where e is the electron charge, ε_0 is the vacuum permittivity, m_e is the mass of electron, c_0 is the speed of light, n_F is the refractive index of the gain material, ν is the frequency of the corresponding emission, and $g(v)$ is the normalized line shape function with $\int g(v)\, dv = 1$. According to the aforementioned facts, all molecules have a high value of f_{em}, which directly leads to high σ_{em}, and therefore any of these materials is possible to be a good optical gain medium in practice. In addition, these results predicate a fact that the molecules with short molecule length properties (see Figure 4.4 and Table 4.2), possess a lower fluorescence, and hence they are not suitable for laser gain media, which is consistent with references [133-135].

On the other hand, molecules with a long molecule length have a good emission oscillator strength (f_{em}), since they owned $f_{em} > 2$, and that means those structures are promising candidates for laser gain medium. Furthermore, most of molecules have produced the maximum emission at wavelengths ranging from 558 to 688 nm, which is in the visible region. These results bring us to an important outcome that those molecules could be powerful for the optoelectronic applications such as light emitting diodes.

Table 4.2. Emission strength oscillator (f_{em}). Maximum wavelength (λ_{Max}).. HOMOs and LUMOs energies. HOMO-LUMO energy gaps.

Molecule	f_{em}	λ_{Max} (nm)	HOMO (eV)	LUMO (eV)	H-L Gap (eV)
P3T	1.6	475	1.4	1.0	2.14
P5T	2.43	558	1.2	0.9	2.1
P7T	3.14	617	1.13	0.8	1.93
P9T	3.8	659	1.1	0.8	1.90
P11T	4.5	688	0.87	0.56	1.43

The electronic structure calculations of any system are an important tool to explore and understand the different properties of molecules. Therefore, the charge distribution, energies, and molecular orbitals (HOMOs and LUMOs), for all molecules have been calculated using the Gaussian package [136,137], as shown in Figure 4.4.

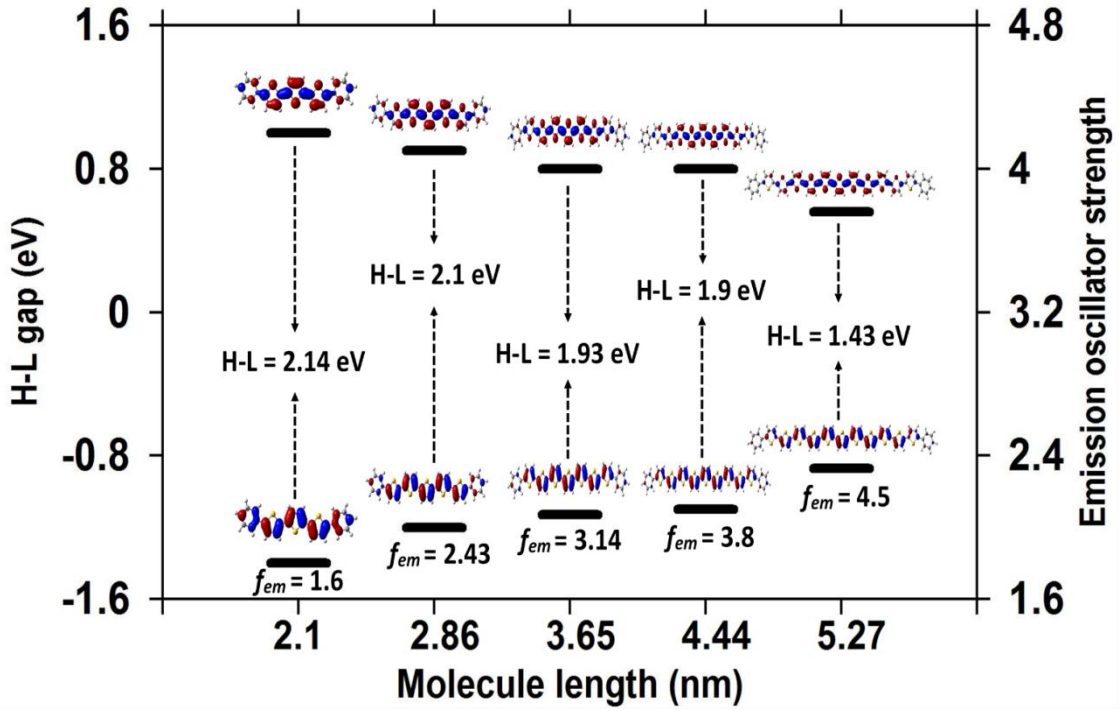

Figure 4.4. Iso-surfaces (±0.02 (e/bohr^3)$^{1/2}$) of the HOMOs and LUMOs, and emission oscillator strength for all molecules.

First of all, these results show that the value of HOMO-LUMO gap has been varied from 2.14 eV for P3T to 1.9 eV for P9T. Then, it dramatically shrinked from 2.14 eV for P3 to 1.43 eV for P11T. These results can be ascribed to the influence of the quantum size effect, which its influence appears due to changing the molecule length from 2.089 nm for P3T to 5.271 nm for P11T. An important point that can be observed from Figure 4.4, that the HOMOs and LUMOs of the first two molecules P3T and P5T are more character over all the backbone of these molecules. While, the rest of structures showed weight less of HOMOs and LUMOs, and that could explain in terms of long tunnelling distance that have been propagated via electrones. These results may aid to put a suitable

interpretation of the emission oscillator strength results shown in Figure 4.4. Since the lowest value of f_{em} (1.6) is introduced by P3T molecule, which has the shortest molecule length (2.089 nm), as shown in Table 4.1 and Figure 4.1, and the biggest HOMO-LUMO gap (2.14eV). Then, the emission oscillator strength increased dramatically with increasing of molecule length to reach the highest value (4.5 nm) for P11T molecule, which possess the longest molecule length (5.271 nm), and the lowest HOMO-LUMO gap (1.43 eV).

Again, in light of the quantum size effect, which appeared due to the relationship between the tunnilling distance and HOMO-LUMO gap, these results could be explained in terms of the contribution of both the charge recombination and emission, which are take place more effectively by switching the gate bias more frequently and more suddenly. Figure 4.4 shows that the long molecule length leads to long tunnilling distance, and the later leads to lowest HOMO-LUMO gap, and vis versa. All these opeartions result to an important consequent, which is the effective charge recombination and emission processes. According to that, the interpretation could be as follows; Suppose at a certain point of time holes are presented predominantly in the molecule. If the next moment the bias of molecule part is made positive, electrons are injected via the other part of molecule which is a more negative. This causes charge recombination and

subsequent light emission. When after this process the polarity of molecules parts is switched to negative, holes are injected from the opposite part, once again leading to the charge recombination and emission. Thus, by alternately switching the molecule parts bias polarity, electrons and holes are injected alternately as well to cause the light emission, which is reflected by the high value of the emission oscillator strength as shown in Table 4.2.

Now, these outcomes are a good example that integrates charge transport and light emission. It could be concluded these molecules could be a powerful candidate for organic current-injected laser device and light-emitting transistors (LETs). Therefore potentially useful for the display technology. When the organic light-emitting diode (OLED) devices are applied to the display, those devices usually require transistors for controlling their luminance. In the LETs, on the other hand, the luminance can be modulated by changing either a drain–source voltage or a gate voltage, without any additional devices. Thus the display panels using the LETs have the great advantage of largely reducing both the number of devices and the circuit complexity. Finally, the results of figure 4.4 indicate to a considerable result that the transport mechanism of charges is LUMO-dominated transport, which is consistent with transmission spectra.

4.1.4. Electric and Thermoelectric Properties of Molecules

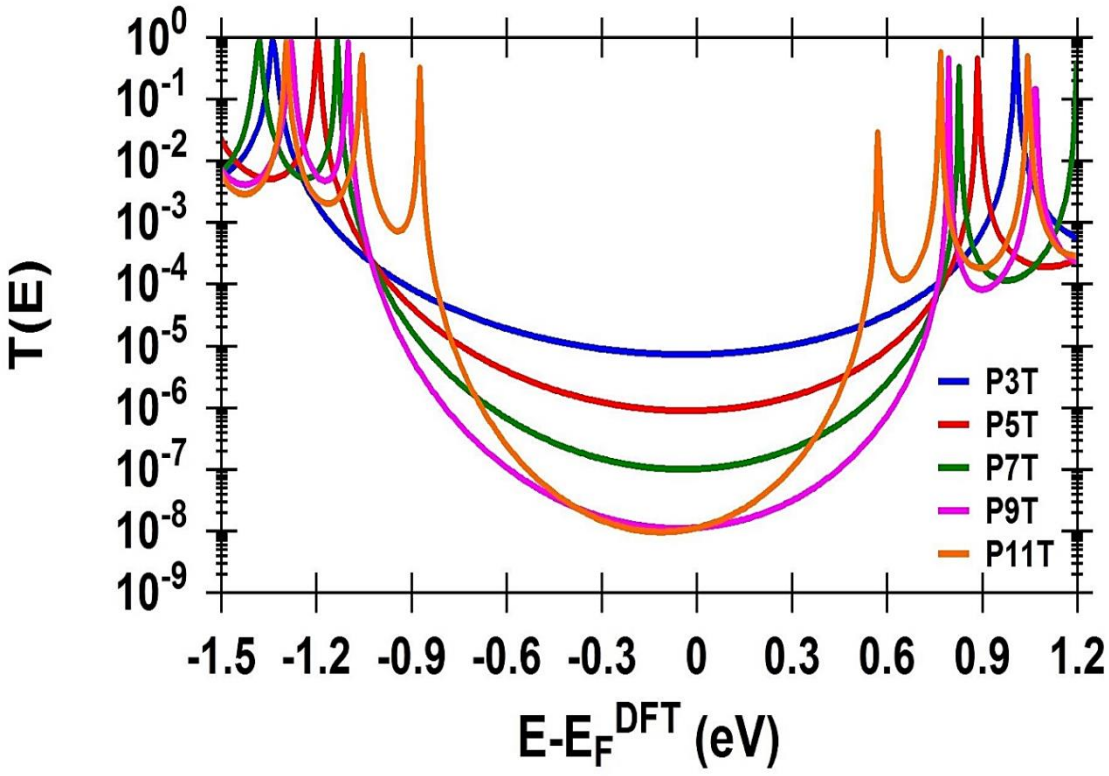

Figure 4.5. Represents the transmission coefficient as a function of the electrons energy of all molecular junctions.

Figure 4.5 reflects an important fact that the molecular length or the number of thiophene unites not only affected the transmission coefficient value but also it influenced the width of HOMO-LUMO gap.

These results can be interpreted in terms of the combation of electrons path and quantum size effects, since the increasing of thiophene unites increased the length of electrons path, which increased the tunnelling distance and that resulted to decrease the transmission coefficient value. In contrast, the width of the HOMO-LUMO gap becomes narrow with

increasing of the molecular length, which ascribed to the impact of the quantum size role. Depending on this, it can be observed that the shortest molecule P3T (2.089 nm) as shown in Figure 4.1, exhibits the highest transmission (7.44×10^{-6}) as shown in Figure 4.4 and the widest HOMO-LUMO gap (2.14 eV), while the longest molecule P11T (5.271 nm) offers the lowest transmission (1.15×10^{-8}) and narrowest gap (1.43eV). In general, the transmission coefficient value of all molecules is high, and that can understand in terms of the quantum interference is a constructive interference and there is no a destructive interference signature within the gap. The order of the transmission is $T(E)_{P3T} > T(E)_{P5T} > T(E)_{P7T} > T(E)_{P9T} > T(E)_{P11T}$. In the same way, the order of HOMO-LUMO gap is $H\text{-}L\ gap_{P3T} > H\text{-}L\ gap_{P5T} > H\text{-}L\ gap_{P7T} > H\text{-}L\ gap_{P9T} > H\text{-}L\ gap_{P11T}$. These results support the previous outcomes and provide a rubest evidence that increasing the molecular length led on the one hand to reduce the HOMO-LUMO gap, which effectively contributed to creating the radiative recombination mechanism of charge carriers, which in turn led to a significant increase in the emission oscillator strength, and a sharp lowering of the electronic transmission coefficient. On the other hand, Figure 4.5 gives a clear picture of the behavior of electrons transfer through the outer orbitals (HOMOs and LUMOs), as well as showing that there is no indication of the destructive quantum interference, and therefore the electrons transfer through these molecules may be governed by the

constructive quantum interference, and the transport mechanism of charge carriers is the LUMO-dominated transport.

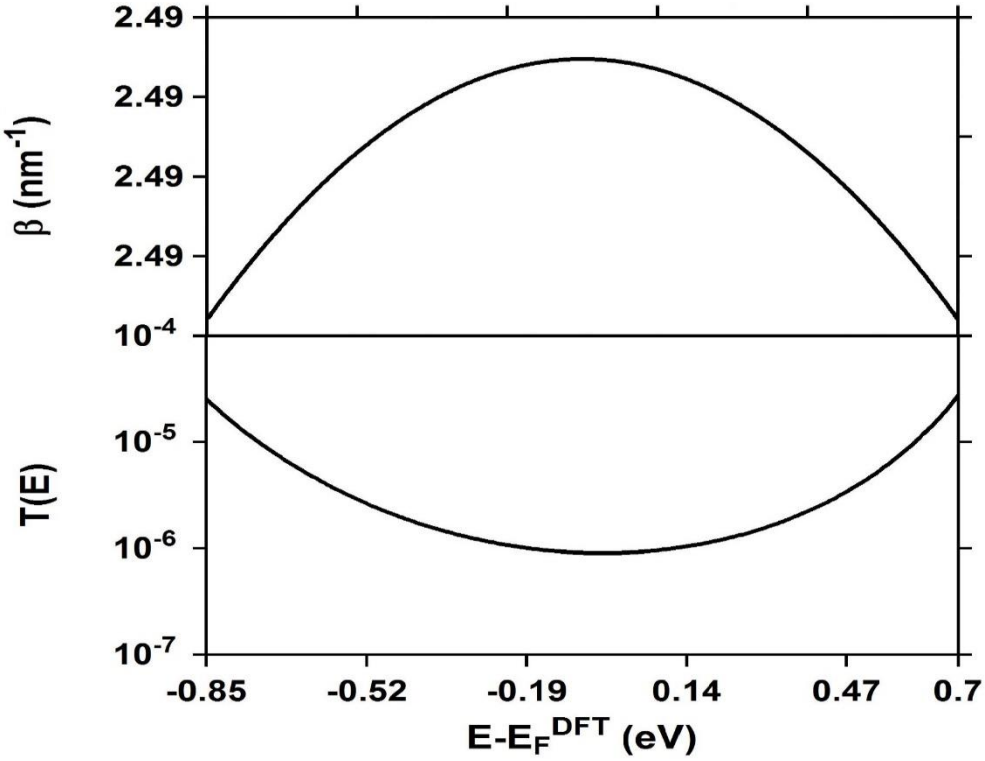

Figure 4.6. Decay constant β (nm^{-1}), and transmission coefficient (T(E)) for the molecular series T3P, T5P, T7P, T9P and T11P as a function of the electrons energy.

Figure 4.6 shows the relationship between the attenuation factor (β) and the electronic transmission coefficient, as the increase in the decay factor as a result of increasing the molecular length led, on the one hand, to a noticeable reduction of the transmission coefficient, and on the other hand, it increased the recombination processes. In addition, DFT computations showed that both the transmission coefficient and the decay constant depend in a very sensitive manner on the position of the contact Fermi energies within the HOMO – LUMO gap, and at the highest value of

the radiative recombination process has been obtained at the theoretical Fermi energy (0.0 eV).

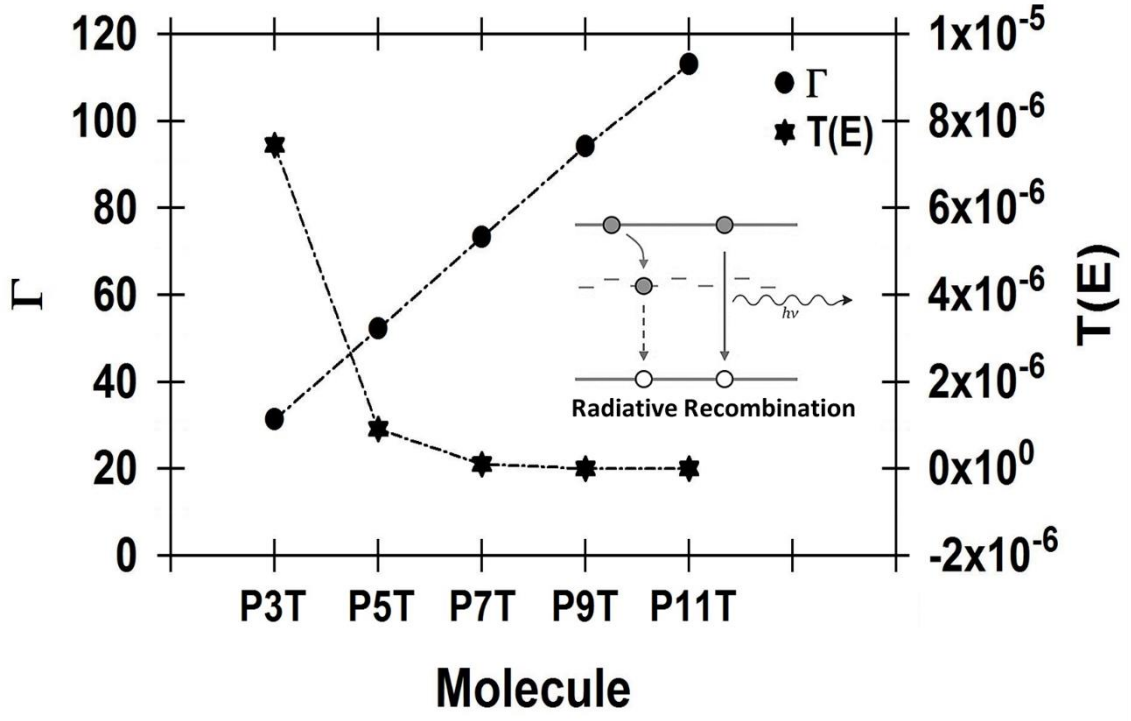

Figure 4.7. The transferred electrons from molecule (Γ), and the electronic transmission coefficient of all molecules.

Figure 4.7 shows a very important result, especially for this kind of molecules, as it is known that increasing the number of tranfered electrons leads to an increase in the transmission coefficient, but the exact opposite is provided by the results presented in Figure 4.7. Notably, the molecule P3T, that posses the lowest Γ value, grants the highest transmission coefficient. The contrary is true for the P11T molecule, which has the highest value of Γ and the lowest value for the transition coefficient. These transport electrons of molecules P5T, P7T, P9T and P11T could be lost only in one way, which is the recombination process. Therefore, these results confirm

and support the previously presented results, which predicted that this type of structures could be an effective organic current-injected laser device and light-emitting transistors (LETs), because the recombination processes of the charge carriers in this type of molecules occur frequently and very effectively as shown in the inset of the Figure 4.7. These processes, in turn, lead to a significant increase emission oscillator strength, as shown in Figure 4.3.

Table 4.3. e_M is the number of electons on molecule in a gas phase. e_J is the number of electons on molecule in a junction. Γ is the transferred electrons. T(E) is the transmission coefficient.

Molecule	e_M	e_J	Γ	T(E)
P3T	48	16.64	31.36	7.44×10^{-6}
P5T	80	27.70	52.29	9.09×10^{-7}
P7T	112	38.77	73.22	1.03×10^{-7}
P9T	144	49.84	94.15	1.20×10^{-8}
P11T	176	62.00	113	1.15×10^{-8}

Now, it is interesting to consider what would happen with the thermoelectric properties of a single molecule junction as a function of the molecular length. Here this study will show that the thermoelectric properties, thermopower (S), electrical conductance (G/G_0) and current-voltage (I-V), characterized by the electronic figure of merit (ZT_e), can be

tuned as a function of the theoretical electrode separation, in a single PT molecule junction (Au/TP/Au). This study also propose a strategy to obtain the maximum ZT of molecular junctions in general.

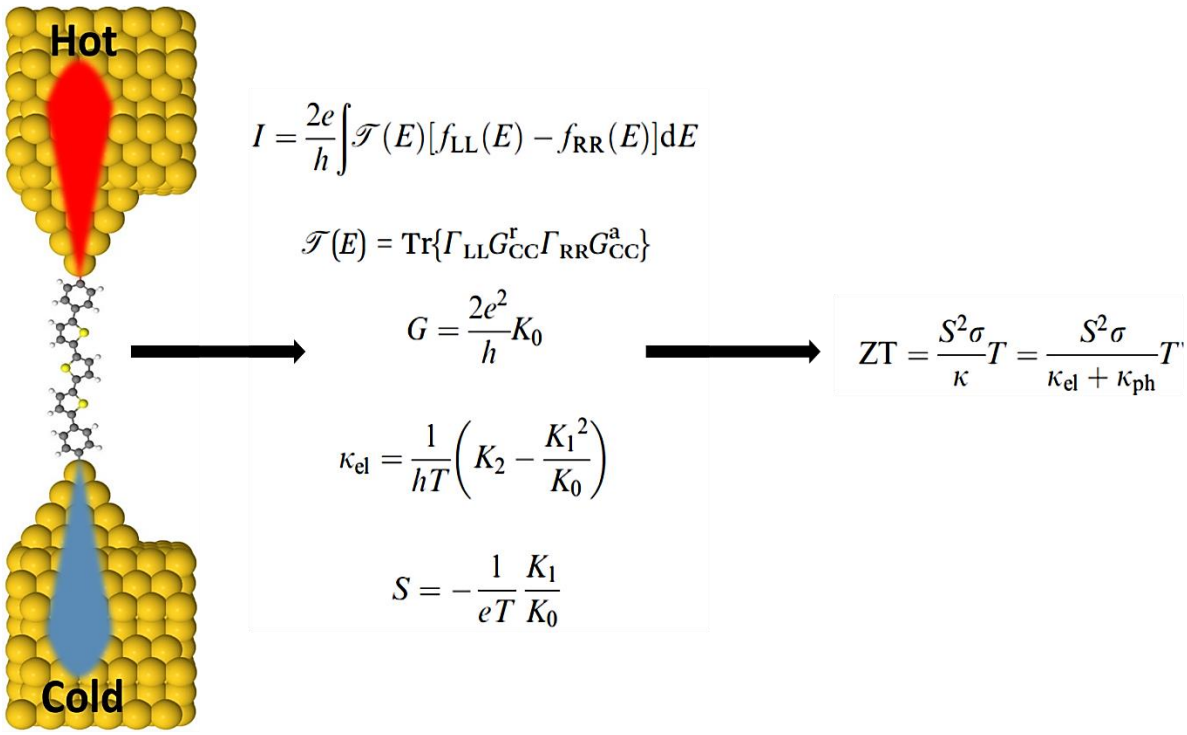

Figure 4.8. Theoretical model to calculate the thermoelectric properties of molecules.

To take out a body of data regard to thermopower behaviour and figure of merit of the representative thiophene/phenylene co-oligomers (TPCOs), P3T, P5T, P7T, P9T and P11T. Figure 4.8 shows a theoretical model to calculate the thermoelectric properties of molecules that connected between a hot lead with a high temperature (T_h), and a cold lead with a low temperature (T_c <<< T_h). This model and according to the Seebeck coefficient equation, as shown in Figure 4.8 confirms S is

proportional to the negative of the slope of lnT(E), evaluated at the Fermi energy.

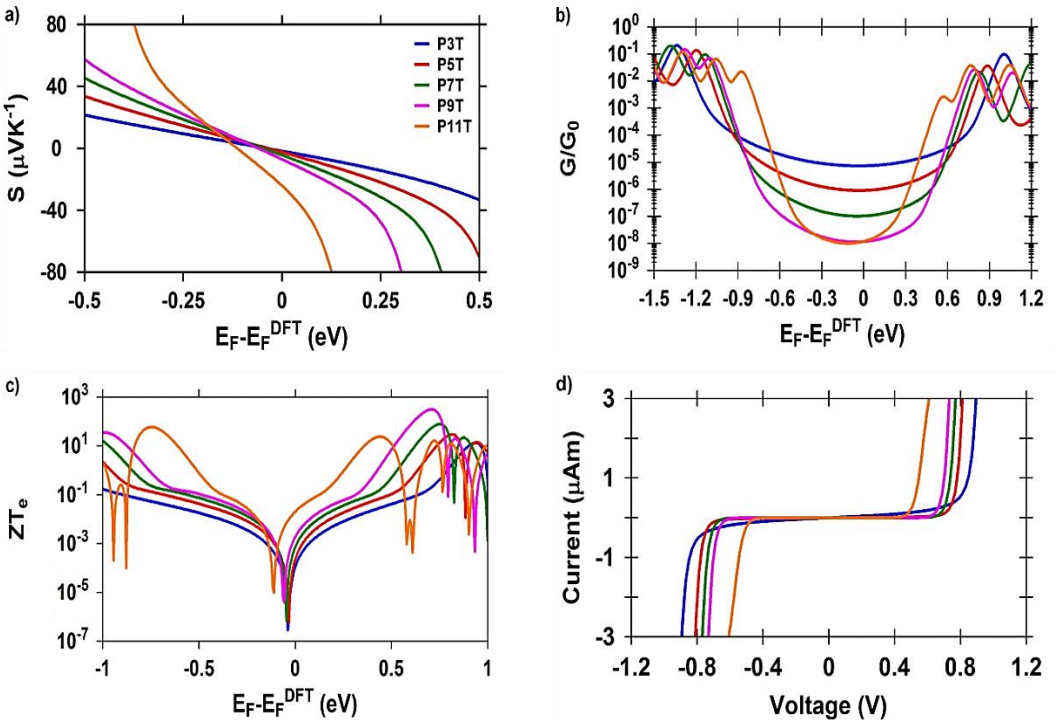

Figure 4.9. a) Thermopower (S) as a function of Fermi energy; b) Electrical conductance (G/G_0) as a function of Fermi energy; c) Electronic figure of merit (ZT_e) as a function of Fermi energy; d) Current-Voltage characteristics.

The computed values of the thermopower were nagative and ranging between -1.55 μVK^{-1} for P3T to -23.42 μVK^{-1} for P11T as shown in figure 4.9a and Table 4.4. These results demonstrate an important role of the occupied molecular orbitals in determine the electrons transport mechanism which is a LUMO-dominated, and so the value and sign of the thermopower for all molecules. The midgap mechanism (see Figure 4.9b) points out that the position of Fermi energy is also a significant parameter because a small change in it could leads to different results for the

conductance and thermopower. Figure 4.9c shows the results of the electronic figure of merit, which is a quantity used to characterize the performance of a device, system or method, relative to its alternatives. Interestingly, the molecule P3T exhibits the lowest figure of merit (9.66×10^{-5}), while the highest value (1.93×10^{-2}) has been shown via molecule P11T. These results prove that the calculated single-molecule conductance value (see Figure 4.9c), at the most probable Fermi energy is the crucial parameter in determining the value of the figure of merit, even if the thermopower value was high. Undoubtedly, the outcomes of conductance (G), thermopower (S) and electronic figure of merit (ZT_e), which illustrated in figures 4.9abc respectively, indicate to an existence of a relation between these parameters. Since the high G results in a low S, which in turn leads to low ZT_e.

Based on our *ab initio* calculations, we show that the thermoelectric properties of a single molecule junction can be tuned by molecular length strategy. For the Au/PT/Au junction. Furthermore, the Seebeck coefficient is negative, indicating that it is dominated by the HOMO, and it increases as the HOMO level, which is associated to the sulphur atom, tends towards energies close to the Fermi energy. These results point out the intense need for further inspection with a goal to more insight and understanding of the thermoelectric properties and their applications.

Primarily, Figure 4.9d shows molecular junctions with current-voltage (I–V) characteristics curves which pass through the second quadrant, which means that they are active components, power sources, which can produce electric power. In addition, these results show threshold voltage (V_{th}), which is one of the most important physical parameters to determine and predicate the appropriate application, such as a field-effect transistor (FET), diodes and light emitting diodes. Threshold voltage is defined as the gate voltage at which the device starts to turn on. The accurate modeling of threshold voltage is important to predict correct circuit behavior from a circuit simulator. Figure 4.9d predicates that the V_{th} of these molecular junction is between 0.5 V to 0.8 V (see Table 4.4), which makes them perfect candidates for electronic and optoelectronic applications.

Table 4.4. Thermopower (S). Electrical conductance (G/G_0). Electronic figure of merit (ZT_e). Threshold voltage (V_{th}).

Molecule	S (μVK^{-1})	G/G_0	ZT_e	V_{th} (V)
P3T	-1.55	0.74×10^{-5}	9.66×10^{-5}	0.8
P5T	-2.19	0.92×10^{-6}	1.91×10^{-4}	0.75
P7T	-4.04	0.1×10^{-6}	6.38×10^{-4}	0.7
P9T	-6.66	0.12×10^{-7}	1.71×10^{-3}	0.65
P11T	-23.42	0.1×10^{-7}	1.93×10^{-2}	0.5

4.2. Theoretical Investigation and Prediction of Promising Organic Molecules for Optical and Electronic Applications

4.2.1. Introduction

One of the success stories in the field of organic optoelectronics is that of the organic light-emitting diode which has already percolated from research laboratories to household electronics [138,139]. Another promising field is that of organic field-effect transistors (OFETs), which has the potential to morph into flexible devices [140-142]. Organic light emitting transistor (OLET) combines both the electrical switching capability of OFETs and the light-generation capability of organic light-emitting diodes (OLEDs) in a single molecule device, in which the intensity and recombination zone of electroluminescence (EL) can be effectively tuned by applying gate voltage [143-146]. A successful development of OLET technology can greatly simplify the display fabrication process and lead to new applications in electrically pumped organic lasers [147-150]. and smart displays [151].

An efficient OLET should exhibit the following characteristics: a large emission oscillator strength (f_{em}), a high charge mobility, a low applied voltage, a high external quantum efficiency (EQE), and tunable recombination zone [143-145]. Moreover, effective ambipolar charge

transport requires materials with proper matching of the highest occupied molecular orbital (HOMO) and lowest unoccupied molecular orbital (LUMO) energy levels with the Fermi energy level of metal electrodes. Unfortunately, strong intermolecular π–π stacking will likely quench luminescence in the solid-state. Thus, organic systems with high solid-state emission quantum yields generally exhibit less planar, but rigid structures, which necessarily impede charge transport and result in low charge carrier mobility [152].

Thus, the development of new materials exhibiting proper energy level alignment, high photoluminescence quantum yield (PLQY), has become critical for further progress in this area. In this study, a family of oligo(phenylene ethynylene) (OPE) with different transport connection points para, meta, and ortho (see Figure 4.10), have been proposed to investigate a new strategy depending on the quantuam interference to enhance and develop the optoelectronic and thermoelectric properties.

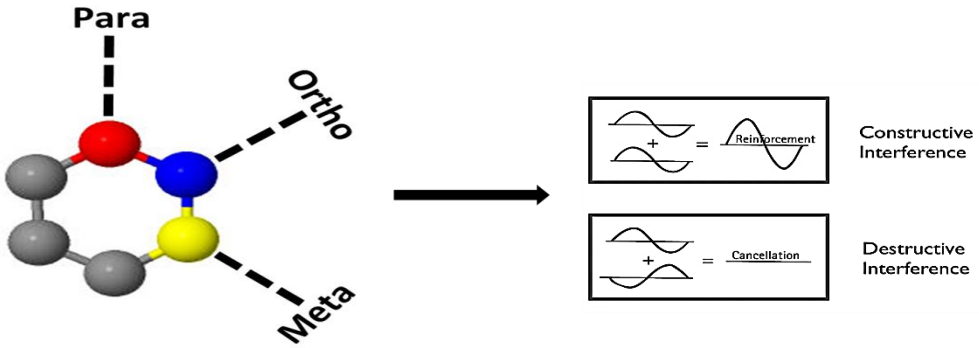

Figure 4.10. Constructive and Destructive Quantum Interferences via Different transport connection points.

4.2.2. Frontier Molecular Orbitals and Electrons Transfer

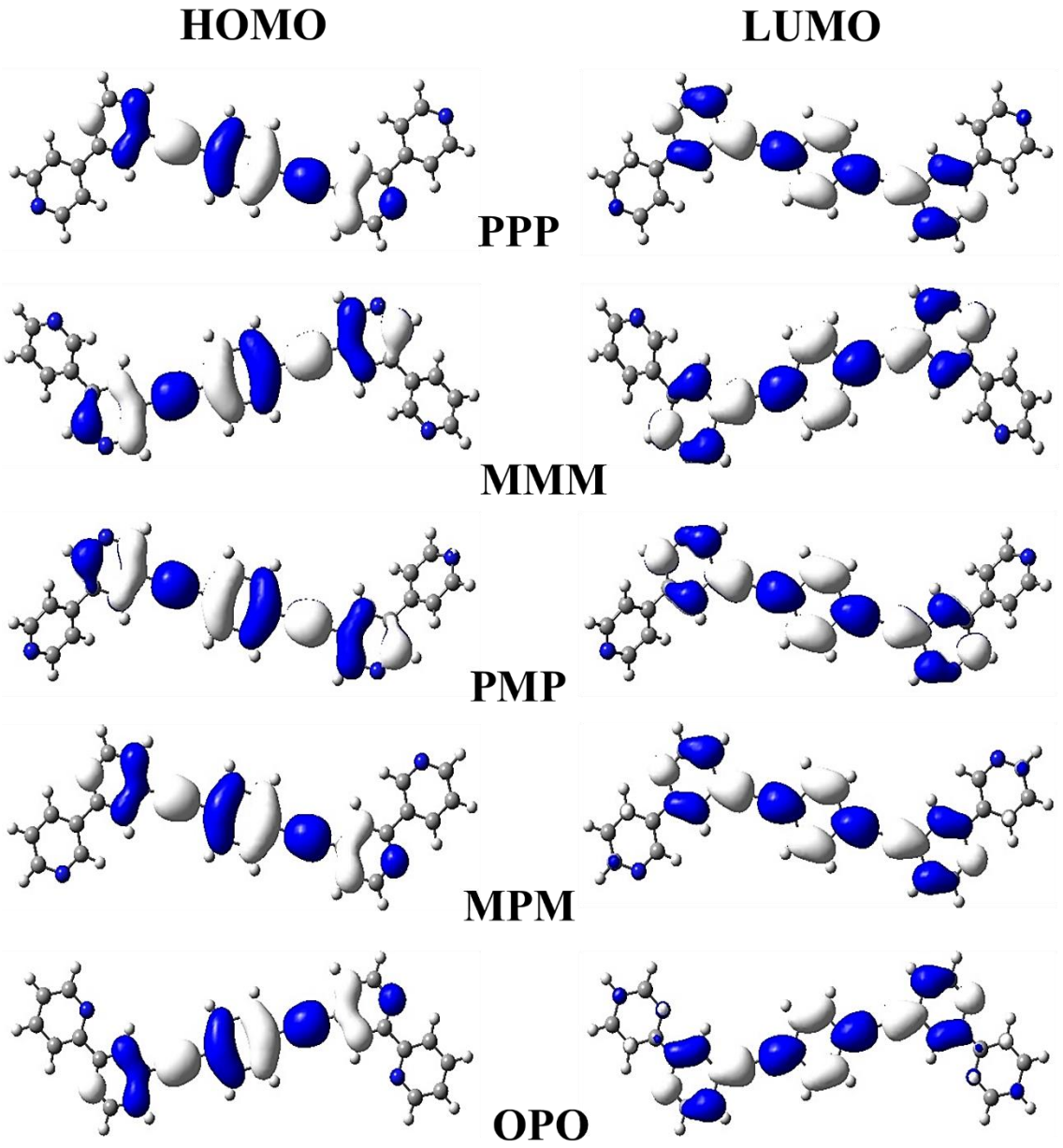

Figure 4.11. Iso-surfaces (± 0.02 $(e/bohr^3)^{1/2}$) of the HOMOs and LUMOs.

The studies of the scattering patterns of the frontier molecular orbital (FMO) is very important to depicted the optoelectronic properties of the designed molecules because these are related to the excitation properties of the molecules. The plots of FMO's of the designed molecules including highest occupied molecular orbital (HOMO) and lowest unoccupied

molecular orbital (LUMO) at the ground states (S_0) are shown in the Figure 4.11 Furthermore, we have investigated distribution patterns for each molecule in terms of partial density of states (PDOS) and the total density of states (TDOS) based on Mullikan population analysis. The percentage contribution of each atom in the composition of molecular orbital have been studied by using Mullikan population analysis approach as shown in Figure 4.12.

These orbitals are real functions and have either a positive or negative [153,154] sign. Crucially, the sign of the HOMOs on the left side of the backbone of molecule are of opposite to the sign on the right side, whereas the LUMOs have the same sign on the left and right the backbone. As discussed in a previous study [153], this means that for each molecule, the HOMO orbital product is negative and the LUMO orbital product is positive. Therefore, their inter-orbital quantum interference is constructive within the HOMO-LUMO gap. In addition, Figure 4.11 shows that the LUMOs of all molecules are extended over the backbone.

Table 4.5. e_M is the number of electron on molecule when molecule in gas-phase. e_J is the number of electron on molecule when molecule in a junction. $\Gamma = e_M - e_J$ is the number of transfer electrons. HOMOs and LUMOs energies. HOMO-LUMO energy gaps.

Molecule	e_M	e_J	Γ	HOMO (eV)	LUMO (eV)	H-L Gap (eV)
PPP	28	22.09	5.91	2.63	1.2	3.83
PMP	28	25.07	2.93	2.77	1.0	3.77
MMM	28	26.02	1.98	2.8	0.96	3.73
MPM	28	21.05	6.95	1.93	1.35	3.28
OPO	28	18.87	9.13	2.04	0.75	2.79

Table 4.5 shows HOMO and LUMO energies and energy gaps between HOMO and LUMO all designed molecules. The trend for HOMO-LUMO energy gaps is $PPP_{H\text{-}Lgap} > PMP_{H\text{-}Lgap} \geq MMM_{H\text{-}Lgap} > MPM_{H\text{-}Lgap} > OPO_{H\text{-}Lgap}$. The smaller energy gap is observed for OPO molecule (2.79 eV). These results could be interpreted in terms of a high electronegativity of the carbon atoms in the backbone of the molecule, so it enhance the delocalization of pi-electrons by pulling the electron density from the side gropus, and therefore an increase in HOMO energy and pronounce increase in LUMO energy is observed. Depending on this, the difference in the HOMO-LUMO gap value of these molecules may be ascribed to the different position of the donor atoms (Nitrogen atoms), which may led to a difference in the value of the electronegativity.

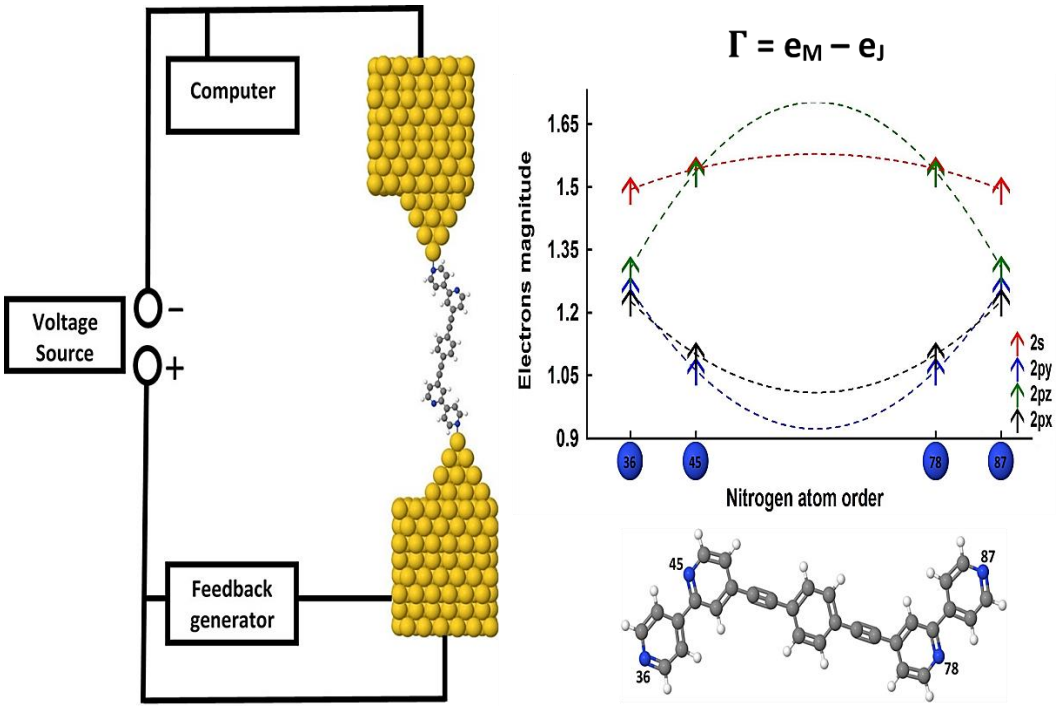

Figure 4.12. Theoretical model of electrons transfer based on Mulliken population analysis approach.

Figure 4.12 exhibits a simple theoretical model of the transfer electrons (Γ) between the molecule atoms themselves, and on onthor hand, between the molecule and electrodes as shown in Table 4.5 and Figure 4.14, based on Mulliken population analysis approach. In this context, it may be worth mentioning, that when a molecular wavefunction is obtained by quantum mechanical calculations, one wishes to extract useful chemical-physics information from it or to interpret it in terms of more intuitive chemical notions. For a molecular wavefunction in the a linear combination of atomic orbitals olecular orbitals (LCAOMO) approximation, the most frequently used method is Mulliken population analysis [155]. At the first stage of the analysis the electron population is

partitioned into individual atoms and bonding regions. The magnitude of the population in a particular bond may be regarded as an indicator of the bond characteristics. At the second stage, the electron populations assigned to bonding regions are divided into individual atomic sites. The result is a point-charge model of the molecule, consisting of a set of gross atomic charges. From a theoretical point of view, it may well be argued that the very notion of atomic charges in a molecule has no concrete theoretical basis.

4.2.3. Emission Oscillator Strength (f_{em})

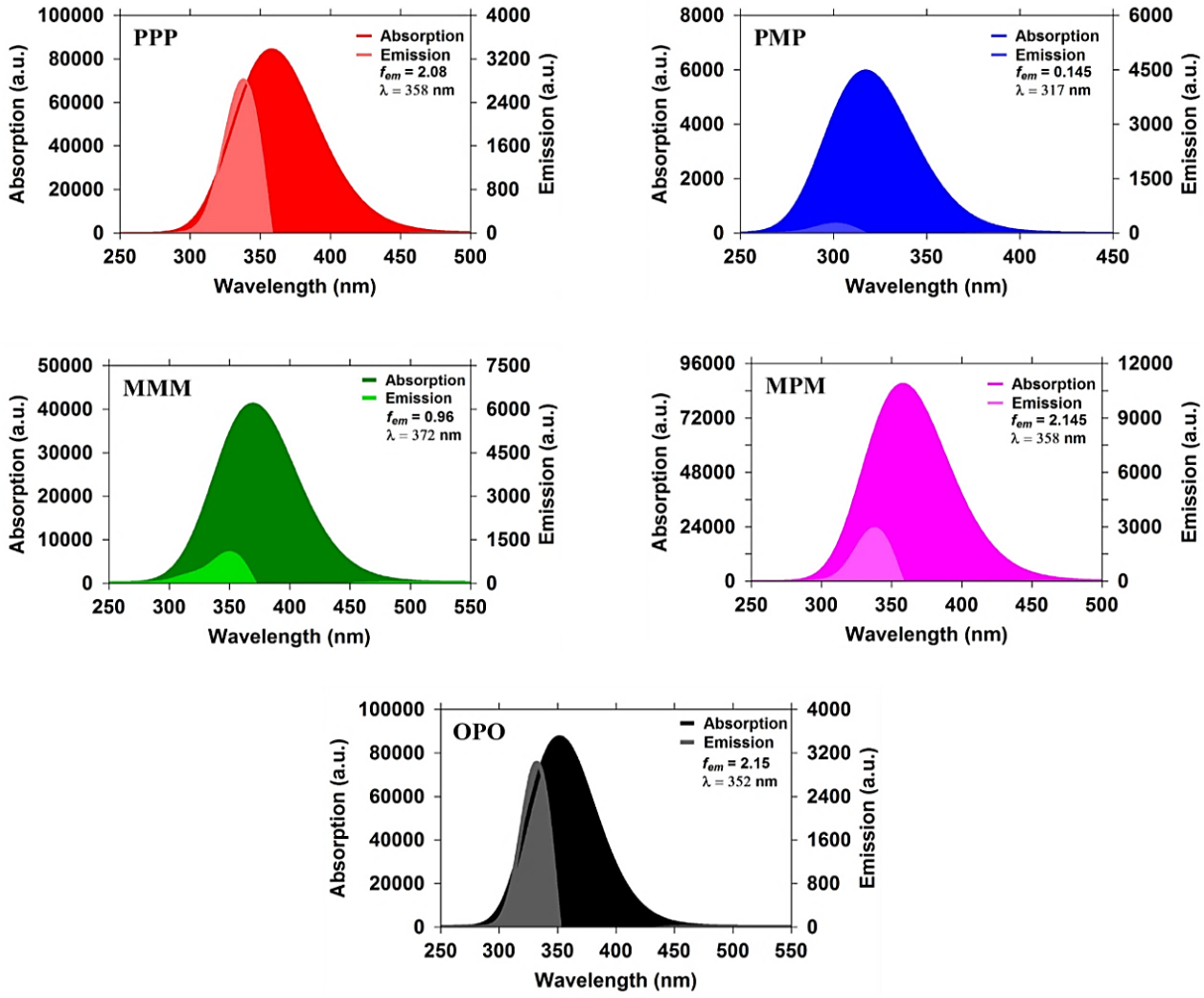

Figure 4.13. Represents the absorption, emission and emission oscillator strength of all molecules.

Figure 4.13 shows that the absorption intensity fluctuated dramatically, since its value was 84248 a.u. for the molecule PPP, with three para transport connection points, then it decresed sharply to 40809 a.u. for the molecule MMM, with with three meta connection points. The lowest value (5964 a.u.) of the absorption intensity is presented by PMP molecule, whereas the highest value (87102 a.u.) introduced via OPO

molecule. In addition, it could be observed that the maximum wavelength (λ_{max}) for all molecules lies in the visible region, and there is also a fluctuation from 317 nm for PMP to 372 nm for MMM. Based on these results, we can conclude that changing the transport connections from para to meta or ortho not only affects the intensity of the absorption, but also leads to a displacement in wavelengths.

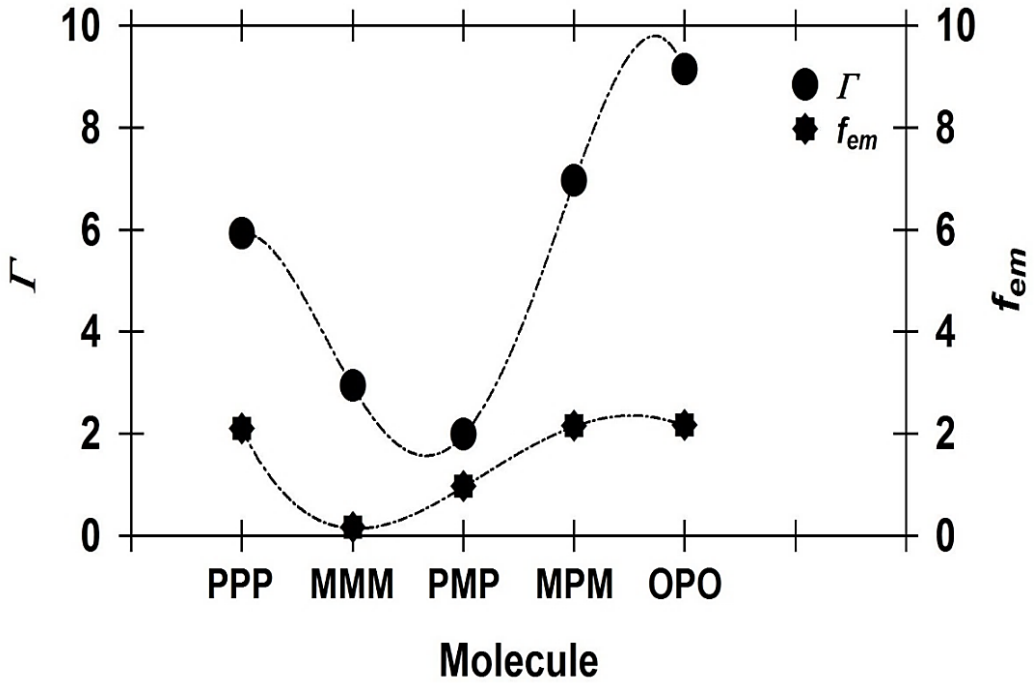

Figure 4.14. The transferred electrons from molecule (Γ), and the emission oscillator strength (f_{em}) of all molecules.

The second important result is exhibited in figures 4.13 and 4.14, and Table 4.6. which is the emission oscillator strength (f_{em}), and it relationship with the electrons transfer and transport connection points. The molecules with para connection in the central part of molecule, PPP, MPM and OPO produce the highest f_{em} (2.08, 2.145 and 5.15 respectively), while the

molecules with meta connection in the central part of molecule, MMM and PMP, show the lowest f_{em} (0.154 and 0.145 respectively).

Table 4.6. Emission strength oscillator (f_{em}). Maximum wavelength (λ_{Max}). Absorption intensity (A). Emission intensity (E).

Molecule	f_{em}	λ_{Max} (nm)	A (a.u.)	E (a.u.)
PPP	2.08	358	84248	2819
PMP	0.145	317	5964	251
MMM	0.154	372	40809	1036
MPM	2.145	358	86884	2911
OPO	2.15	352	87102	3019

The order of emission and absorption intensities and the emission oscillator strength (f_{em}) is OPO > MPM > PPP > MMM > PMP. These results can formulate for us a promising theoretical strategy for choosing the structures and materials that can serve as an active laser medium. Since, the emission cross section (σ_{em}) of a laser transition is consider an important parameter, because it can impact the accomplishment of laser in terms of the threshold energy, output energy, maximum gain, etc.. [156,132]. In other words, the high value of emission cross section (σ_{em}) leads to high gain laser, and since it is a direct proportion between the emission cross section and the emission oscillator strength. Therefore, our

theoretical strategy to enhance the emission via change the transport connection points of molecules can be a powerful way to develop the laser technique.

4.2.4. Junction Formation Probability and Transmission Coefficient

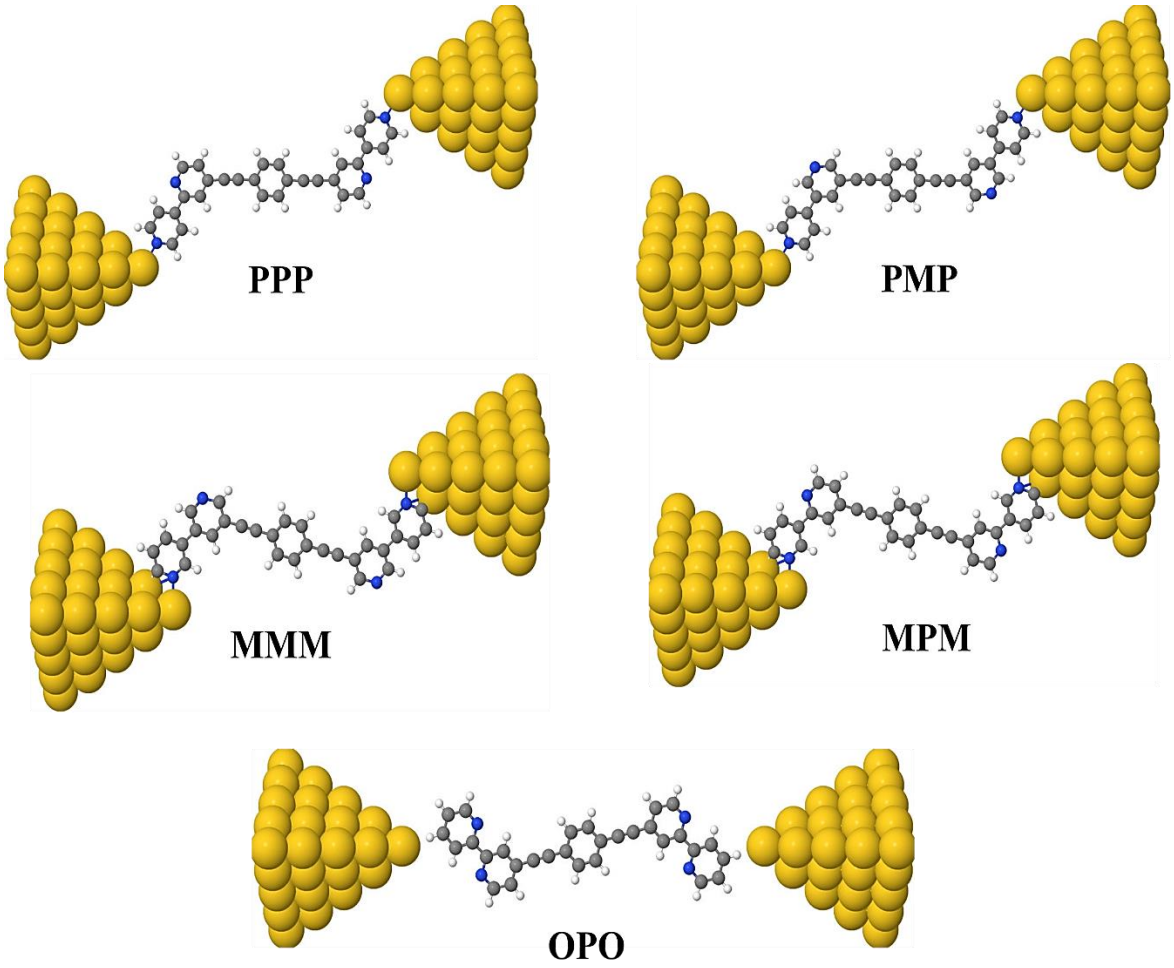

Figure 4.15. The optimized molecular junction of all structures.

To obtain a good insight, and to better evaluate the properties and behavior of these molecular junctions, our results for the structural, electronic and thermoelectric evolutions of the junction Au/OPE/Au are based on functional theory (DFT) calculations [157-159]. We used a PBE-

GGA functional [160] and norm-conserving pseudo-potentials [161] as implemented in the SIESTA code [162,163].

Numerical atomic orbitals were used as basis sets [164]. We employed a double-zeta basis with a polarization function (DZP) for the whole system. The confining energy shift was 0.05 eV and an energy cut-off of 240 Ry was used to the grid integration. For the surface Brillouin zone (BZ) sampling we have used a (111) Monkhorst–Pack set [165]. Moreover, in our calculations the self-consistency is achieved when the change in the total energy between cycles of the SCF procedure is below 10^{-4} eV and the density matrix change criterion of 10^{-4} is also satisfied. These criteria are enough to ensure convergence in the calculated total energy of 0.05 eV.

To obtain the geometries as shown in Figure 4.15, the supercell was such that the molecule would be connected to the two sides of the Au slab. The Au slab was modelled by a (6×6) surface unit cell and eight layers of gold. In all calculations the positions of the OPE atoms and the Au atoms on the first two layers at either side were allowed to relax until the forces were smaller than 0.02 eV $Å^{-1}$.

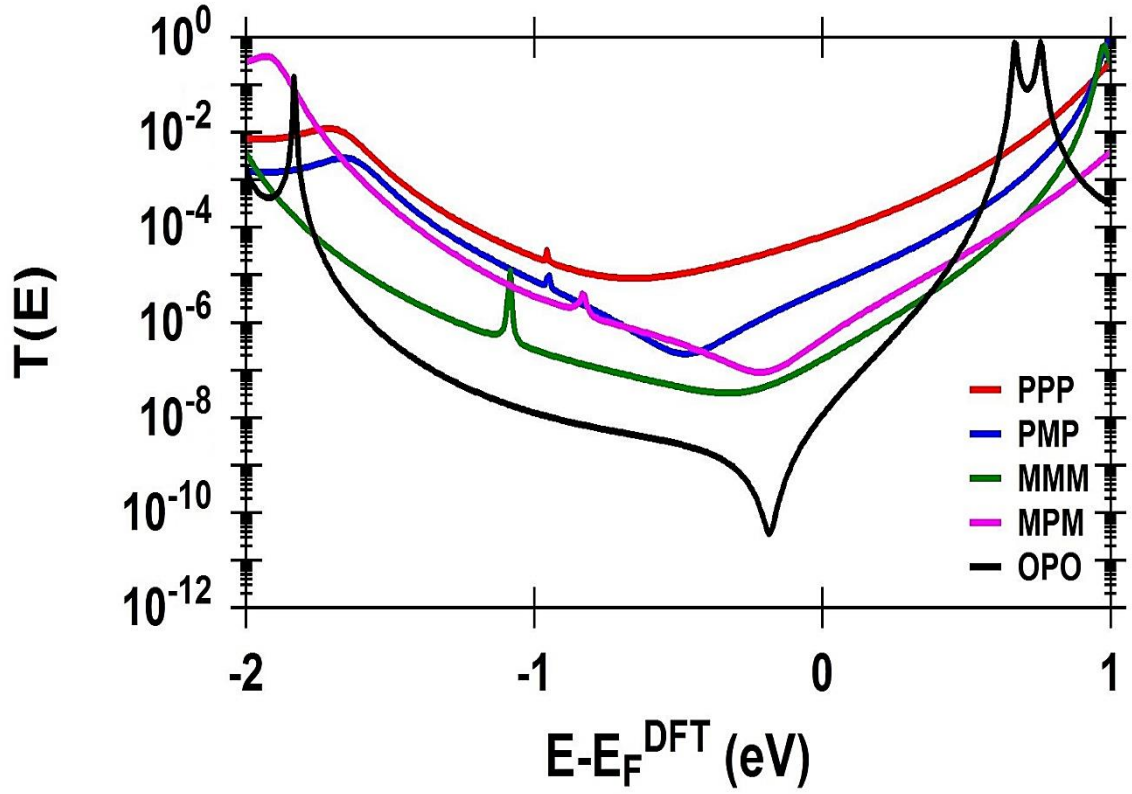

Figure 4.16. Represents the transmission coefficient as a function of the electrons energy of all molecular junctions.

Charge transport characteristics of single-molecule junctions formed from the molecules in Figure 4.15, were investigated using GOLLUM code [166] to simulate of scanning tunnelling microscopy (STM) technique.

Figure 4.16 displays the transmission coefficient T(E) versus the electrons energy of molecule PPP, PMP, MMM, MPM and OPO. The highest value (6.73×10^{-5}) of T (E) is presented via PPP molecule, which could be assign to a perfect formation of the single-molecule junction. Significant difference of T(E) are observed for other molecules, as shown in Figure 4.16 which ascribed to the the variety of connectivities of the central ring (see Figure 4.15) and locations of the nitrogen in the anchor units, while for

molecule PPP, the para connection in both central and terminal rings, which leads to the highest transmission coefficient. As shown in Table 4.7 and Figure 4.16, the lowest value (1.26×10^{-8}) of T(E) is exhibited by OPO molecule. These results could be understood in terms of the junction formation probability (JFP), since JFP is 100% for molecules PPP, PMP, MMM and MPM. Whereas, for OPO molecule the JFP decreased sharply to almost zero, and there is no junction as shown in Figure 4.15, because Nitrogen (N) atoms in the terminal ortho pyridyl is partially hidden from the electrode surfaces and therefore it is difficult to form a bridge between the two gold electrodes.

Table 4.7. L (N…N), is the molecule length, D (Au…Au), is the molecular length. X is the bond length (Au…N). Z (D – 0.25), is the theoretical electrodes separation. T(E) is the transmission coefficient.

Molecule	L (nm)	D (nm)	X (nm)	Z (nm)	T(E)
PPP	2.19	2.6	0.23	2.35	6.73×10^{-5}
PMP	2.19	2.6	0.23	2.35	5.02×10^{-6}
MMM	1.97	2.14	0.23	1.89	1.76×10^{-7}
MPM	1.97	2.14	0.23	1.89	4.43×10^{-7}
OPO	1.7	2.87	0.23	2.62	1.26×10^{-8}

Table 4.7 shows that theoretical electrode separations (Z) follow the trends $Z_{OPO} > Z_{PPP} = Z_{PMP}$ and $Z_{MMM} = Z_{MPM}$ that correlate with the molecular distance (D), demonstrating that the gold-anchor link is primarily controlled by the gold–nitrogen bonds. Therefore, it is clear that changes in the position of the N atom within the anchors affects both the JFP, as well as the transmission coefficient as shown in Figure 4.16. Unlike the PPP molecule, the other molecules possess anchoring nitrogen atoms located at meta or ortho positions within the terminal rings that do not naturally bind to electrode surfaces, as shown in Figure 4.15.

Another result has been reflected from Figure 4.16 which is worth to mention that the changing from para to meta in the central ring for molecules PPP and MMM, caused the transmission coefficient to drop by two orders of magnitude, and these results are consistent with previous studies [167,168,169,170]. On the other hand, the terminal ring of the MPM molecule reduces T(E) by an order of magnitude in comparing with that of PMP molecule. Thus, this study demonsterated the important contribution of constructive and destructive quantum interferences in the terminal and central aromatic rings to the transmission coefficient, which in turn with a collaboration of the JFP affacted the electrons transfer factor (Γ), which influenced the radiative recombination, and the latter impacted strongly the emission oscillator strength (f_{em}), and led to the results presented in figures 4.13 and 4.14.

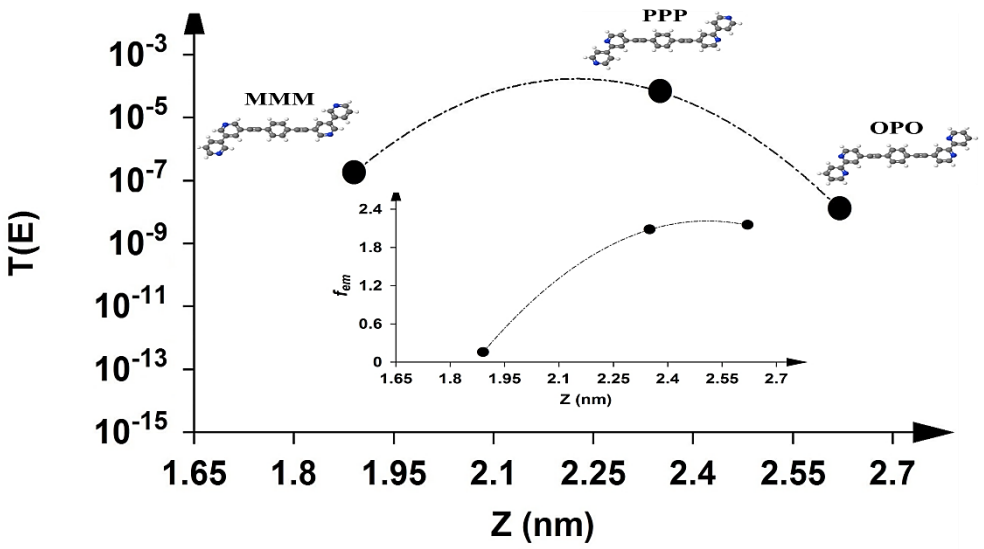

Figure 4.17. Represents the transmission coefficient T(E) as a function of the theoretical electrodes separation (Z) of molecules PPP, MMM and OPO. The insert figure shows the emission oscillator strength (f_{em}) as a function of Z for the same molecules.

The results shown in Figure 4.17 illustrate the confusion that may appear to the reader regarding the previous results of the molecules OPO and MMM for their transmission coefficient and emission oscillator strength values. First of all, the OPO molecule has the highest f_{em} and the lowest T(E), and this result in fact confirms an important role of the junction formation probability (JFP) in prevent the electronic transport between the molecule and electrodes, which in turn increased the radiative recombination, and the later led to high emission oscillator strength value.

On the other hand, the ortho and para connectivities of OPO molecule create a constructive quantum interference, which improves significantly the electronic transport between its atoms, which for sure increased the

emission intensity (3019 a.u.) of this molecule, as shown in Table 4.6 and Figure 4.13.

In contrast, Figure 4.17 shows the molecule MMM with meta connectivities possess the lowest f_{em}, and T(E). This result indicates to the effective influence of the destructive quantum interference in block the electroinc transport between molecule atoms, as well as between molecule and electrodes. As a consequence, the emission intensity (1036 a.u.) was very low, as shown in Table 4.6. For PPP molecule with para connectivities, the high junction formation probability (JFP) and the constructive quantum interference aided to increase both the transmission coefficient and the emission strength oscillator. Finally, These result bring us to an important fact that those molecules could be powerful for the optoelectronic applications such as light emitting diodes.

5.1. Conclusions

In conclusion, section 4.1 have described various features of the thiophene/phenylene co-oligomers (TPCO) materials. It includes the characteristics of the TPCO structures and their relevance to the structure/property relationship.

1- In relation to the important future application, we dealt with several features associated with the laser oscillation from the organic semiconductors, such as the emission oscillator strength, HOMO-LUMO gap, charges distribution and orbitals, as well as the transmission and seeback coefficients. It could be concluded that molecular length manipulation strategy is an effective method to control and enhance the properties of TPCO-based devices and their applications. Since, the increasing of molecule length enhances noticeably some of spectral, optical and thermoelectric (f_{em}, H-L gap and S) properties,

2- and on other hand it lowers some of electronic (T(E)) properties. We have stressed that the TPCO structures are exceptionally good for light emitting diode and thermoelectric applications. Their structures produce the effective optical quantum confinement and lasing characteristics within the structure, and thus may be an excellent candidates for the laser media.

3- In addition, the TPCO materials are expected to become important to a solar cell development. The TPCOs may play a pivotal role in the field of organic semiconductor materials and their optoelectronic device applications.

Section 4.2 of this thesis exhibites a theoretical study using the density functional theory methods of electronic and spectral properties for a family of Oligo(phenylene-ethynylene) OPEs with pyridyl linker groups, with different transport connections para, ortho and meta.

1- Based on the results that have been presented in this section, we can conclude that changing the transport connections from para to meta or ortho not only affects the intensity of the absorption, emission and emission oscillator strength but also leads to a displacement in wavelengths. Since, the molecules with para connection in the central part of molecule, PPP, MPM and OPO produce the highest f_{em}, while the molecules with meta connection in the central part of molecule, MMM and PMP, show the lowest f_{em}, as well as the maximum wavelength (λ_{max}) for all molecules lies in the visible region, and there are fluctuations depends on the connection transport point of the molecule.

2- On the other hand, the results of this section prove the influence of the constructive and destructive quantum interferences on the transmission coefficient, where the changing from para to meta in

the central ring for molecules PPP and MMM, caused the transmission coefficient to drop by two orders of magnitude.

3- Furthermore, it could be concluded that there is an important role of the junction formation probability (JFP) of molecule OPO in prevent the electronic transport between the molecule and electrodes, which in turn increased the radiative recombination, and the later led to high emission oscillator strength value.

4- Finally, this thesis introduces a successful and powerful strategies to develope the organic light-emitting diodes (OLEDs) in a single molecule technology, which can greatly simplify the display fabrication process and lead to new applications in electrically pumped organic lasers, and smart displays.

5.2. Future Works

Molecular Nanotechnology is a field that can be consider a source of scientific and cognitive inspiration and innovation, so I suggest some of ideas for the future work as follows:

1- Study the phonon transport properties of of the thiophene/phenylene co-oligomers (TPCO) structures, and Oligo(phenylene-ethynylene) OPE molecules, and their applications.

2- Investigation the electronic and thermoelectric properties of OPE molecules with different electrodes (carbon nanotubes and graphene).

3- Study the optoelectronics properties of TPCO molecules under magnetic field effects.

References

[1] R. Martel, T. Schmidt, H. R. Shea, T. Hertel, and Ph. Avouris., Single- and Multiwall Carbon Nanotube Field-Effect Transistors. App. Phys. Lett., 1998. p. 2447–2449.

[2] A. Kolmakov and M. Moskovits. , Chemical Sensing and Catalysis by One- Dimensional Metal-Oxide Nanostructures. Annu. Rev. Mater. Res., 2004. p.151–180.

[3] G. Raschke, S. Brogl, A. S. Susha, A. L. Rogach, T. A. Klar, J. Feldmann, B. Fieres, N. Petkov, T. Bein, A. Nichtl, and K. Kürzinger., Gold Nanoshells Improve Single Nanoparticle Molecular Sensors. Nano Lett., 2004. 4(10): p. 1853–1857.

[4] M. C. Petty., Molecular Electronics: From Principles to Practice. John Wiley &Sons, Ltd., 2007.

[5] J. R. Health and M. A. Ratner., Molecular electronics. Physics Today, 2003. p. 43–49.

[6] D. Fichou, S. Delysse, & Nunzi, J.-M., First evidence of stimulated emission from a monolithic organic single crystal: α-Octithiophene. Adv. Mater. 1997. p. 1178–1181.

[7] S. Chénais, & S. Forget, Recent advances in solid-state organic lasers. Polym.Int. 2012. p. 390–406.

[8] M. A. Baldo, O'Brien, D. F., Thompson, M. E. & Forrest, S. R. ,Excitonic singlet-triplet ratio in a semiconducting organic thin film. Phys. Rev. 1999. p. 14422–14428.

[9] C-S. Wang, A S. Batsanov, M. R. Bryce, S. Martin, R. J. Nichols, S. J. Higgins, V. M. García-Suárez and C. J. Lambert, Oligoyne Single Molecule Wires, Journal of the American Chemical Society 2009.

[10] E. Leary, H.Höbenreich, S. J. Higgins, H. van Zalinge, W. Haiss, R.J. Nichols, C. Finch, I. Grace and C.J. Lambert, Single- molecule, solvation-shell sensing, Phys Rev. Lett. 2009.

[11] G. Ashwell, B Urasinska, C Wang, MR Bryce, I Grace, CJ Lambert, ―Single-molecule electrical studies on a 7 nm long molecular wire‖ Chemical Communications. 2006. p. 4706-4708.

[12] R. Huber, M. T. Gonzalez, Wu, S.; Langer, M.; Grunder, S.; Horhoiu, V.; Mayor, M.; Bryce, M. R.; Wang, C. S.; Jitchati, R.; Schonenberger, C.; Calame, M. J. Am. Chem. Soc. 2008, 130: p.1080-1084.

[13] W. Hong, D. Z. Manrique, Moreno-Garca, P. Gulcur, M.; Mishchenko, A.; Lambert, C. J.; Bryce, M. R.; Wandlowski, T. J. Am. Chem. Soc. 2011. 134: p. 2292-2304.

[14] H. Sadeghi, S. Bailey, CJ Lambert, Silicene-based DNA nucleobase sensing. Applied Physics Letters 2014. 104 (10): p.103-104

[15] R. Martel, et al., Single- and multi-wall carbon nanotube field-effect transistors. Applied Physics Letters, 1998. 73(17): p. 2447-2449.

[16] A. DeHon, .Array-based architecture for FET-based, nanoscale electronics. IEEE Transactions on Nanotechnology. 2003. 2(1): p. 23-32.

[17] Z. J. Donhauser, et al., Conductance Switching in Single Molecules Through Conformational Changes. Science, 2001. 292(5525): p. 2303.

[18] Wang, C., et al., Ultrathin Au nanowires and their transport properties. J Am Chem Soc, 2008. 130(28): p. 8902.

[19] M. Tsutsui, and M. Taniguchi, Single Molecule Electronics and Devices. Sensors (Basel, Switzerland), 2012. 12(6): p. 7259-7298.

[20] R. Waser, and M. Aono, Nanoionics-based resistive switching memories. Nature Materials, 2007. 6 (3): p. 833.

[21] P. Franzon, et al., Molecular Electronics – Devices and Circuits Technology, in Vlsi-Soc: From Systems To Silicon: Proceedings of IFIP TC 10, WG 10.5, Thirteenth International Conference on Very Large Scale Integration of System on Chip (VLSI-SoC 2005),

October 17-19, 2005, Perth, Australia, R. Reis, A. Osseiran, and H.-J. Pfleiderer, Editors. 2007. Springer US: Boston, MA. p. 1-10.

[**22]** M.C. Petty, et al., Molecular Electronics, in Springer Handbook of Electronic and Photonic Materials, S. Kasap and P. Capper, Editors. 2017, Springer International Publishing: Cham. p. 1-1.

[23] J. Gierschner, Varghese, S. & Park, S. Y., Organic single crystal lasers.: a materials view. Adv. Opt. Mater. 2016. 4: p. 348–364

[24] C. Robert Neuman, Jr., Organic Molecules and Chemical Bonding. G. Somasundaram and A. Ramalingam, Chem. Phys. Lett.,2000, 324: p. 25–30.

[25] Changsheng Wang, Andrei S. Batsanov and Martin R. Bryce**.** ,Oligoyne Single Molecule Wires. . J.of the American Chemical Society. 2009. 131: p. 15647–15654.

[26] M. Pavel García, Murat G.and David Z. Manrique. "Single-Molecule Conductance of Functionalized Oligoynes: Length Dependence and Junction Evolution". J.of the American Chemical Society. July 22, 2013.

[27] Oday A. Al-Owaedi, David C. Milan, Marie-Christine Oerthel, Sören Bock, Dmitry S. Yufit, Judith A. K. Howard, Simon J. Higgins, Richard J. Nichols, Colin J. Lambert, Martin R. Bryce, Paul J. Low. Experimental and Computational Studies of the Single-

Molecule Conductance of Ru(II) and Pt(II) trans-Bis(acetylide) Complexes. Organometallics. 2016. 35: p. 2944−2954.

[28] Oday A. Al-Owaedi, Sören Bock, David C. Milan, Marie-Christine Oerthel, Michael S. Inkpen, Dmitry S. Yufit, Alexandre N. Sobolev, Nicholas J. Long, Tim Albrecht, Simon J. Higgins, Martin R. Bryce, Richard J. Nichols, Colin J. Lambert, Paul J. Low., Insulated molecular wires: inhibiting orthogonal contacts in metal complex based molecular junctions. Nanoscale. 2017. 9: p. 9902–9912.

[29] Mohsin Kadhim Abed Al-Khaykanee., Quantum Theory of Electronic and Thermal Transport through Nano-scale and Single-Molecule Devices. Department of Physics, Lancaster University, UK Ph.D. Thesis 2018.

[30] P. Guang- Zhanga, Yan-Qi Mua, Jin-M. Zhaoa and Hui Huang. ,Optimizing the conductance switching performance in photo switchable dimethyldihydropyrene/cyclophanediene single-molecule junctions. Physica E: Low-dimensional Systems and Nanostructures. 2019.

[31] Masoud Baghernejad, Yang Yang and Oday A. Al-Owaedi. ,Constructive Quantum Interference in Single-Molecule Benzodichalcogenophene Junctions. Chemistry - A European Journal • February 2020.

[32] Yi Jiang, Yuan-Y. Liu, Xu Liu, He Lin and Kun Gao., Organic solid-state lasers: a materials view and future development. Chem Soc RevDOI: 2020.10: p. 1039/d0cs00037j.

[33] Baraa A. Al-Mammory, Oday A. Al-Owaedi, Enas M. Al-Robayi. ,Thermoelectric Properties of Oligoyne-Molecular Wires. J. of Phys. Conference Series. 2021. 1818: p. 012095

[34] Rasool M. Al-Utayjawee, Oday A. Al-Owaedi., Enhancement of Thermoelectric Properties of Porphyrinbased Molecular Junctions by Fano Resonances. J. of Phys. Conference Series .2021. 1818: p. 012208.

[35] M. Naher et al., Molecular Structure–(Thermo) electric Property Relationships in Single-Molecule Junctions and Comparisons with Single-and Multiple-Parameter Models,.J. Am. Chem. Soc., , 2021. 143(10): p. 3817–3829.

[36] Bensalem Salaheddine, .Contribution to the study of physical properties of CZTX (X=S, Se) solar materials. Ph.D Thesis, Department of Physics, Faculty of Sciences. University Ferhat Abbas, Algeria, 2015.

[37] P. Hohenberg and W. Kohn, .Inhomogeneous Electron Gas. Phys. Rev. B. 1964. 136: p. 864-871.

[38] W. Kohn and L. J. Sham, .Self-Consistent Equations Including Exchange and Correlation Effects. Phys. Rev. A .1965. 140: p. 1133-1138.

[39] N. Argaman and G. Makov, . Density Functional Theory – an introduction. American Journal of Physics, arXiv.org:physics/9806013 .1999.

[40] M. Born,. and Oppenheimer, R. On the quantum theory of molecules. Annalen der Physik, 1927. 84(20): p. 1–32.

[41] Mel Levy. Universal variational functionals of electron densities, first order density matrices, and natural spin-orbitals and solution of the v-representability problem. Proc. Natl. Acad. Sci. USA. 1979. 76(12): p. 6062–6065.

[42] M. R. Dreizler, and Providencia, J. Density functional methods in physics. NATO ASI series. Series B, Physics, 1985.

[43] R.G. Parr, and Y. Weitao, Density-functional theory of atoms and molecules. Oxford University Press, USA. 1994.Vol. 16.

[44] E. K. Gross, and R. M. Dreizler, Density functional theory. Springer, 1995.

[45] M. Levy, Electron densities in search of Hamiltonians. Physical Review A, 1982. 26(3): p. 1200–1208.

[46] E. H. Lieb, Thomas-Fermi and related theories of atoms and molecules. Reviews of Modern Physics, 1981. 53(4): p. 603–641.

[47] Hartree, D. R. Proc. Cam. Phil. Soc. 1928. 24: p. 89–110.

[48] B. R.Cleydson Santos, Cleison C. Lobato, Francinaldo S. Braga, Sílvia S. S. Morais, Cesar F. Santos, Caio P. Fernandes, Davi S. B. Brasil, Lorane I. S. Hage-Melim, Williams J. C. Macêdo, José C. T. Carvalho . Application of Hartree-Fock Method for Modeling of Bioactive Molecules Using SAR and QSPR. 2014 (4)1 :p. 89-110.

[49] D. R. Hartree, Proc. Cam. Phil. Soc. 1928. 24: p.426–437.

[50] V. Fock, Z. Physik, 1930. 61: p. 126–148.

[51] D. R. Hartree, the Calculation of Atomic Structures; Structure of Matter Series; John Wiley & Sons Ltd.: London, 1957.

[52] D. Axel, Becke. Density-functional exchange-energy approximation with correct asymptotic behavior. Physical Review A, 1988. 38(6): p. 3098–3100.

[53] C. L. David, and Perdew, J. P. The exchange-correlation energy of a metallic surface. Solid State Communications, 1975. 17(11): p. 1425–1429.

[54] B. Hammer, Hansen, L. B.; Nørskov, J. K. Improved dsorption energetics within density-functional theory using revised perdew-

burke-ernzerhof functionals. Physical Review B, 1999. 59(11): p. 7413–7421.

[55] M. Richard Martin. Electronic structure: basic theory and practical methods. Cambridge university press, 2004.

[56] D. M. Ceperley, and Alder, B. Ground state of the electron gas by a stochastic method. Physical Review Letters, 1980. 45(7): p. 566–569.

[57] J. P. Perdew, and Zunger, A. Self-interaction correction to density-functional approximations for many-electron systems. Physical Review B, 1981. 23(10): p. 5048–5079.

[58] R. Q. Hood, M. Y. Chou, A. J. Williamson, G. Rajagopal and R. J. Needs. Quantum Monte Carlo investigation of exchange and correlation in silicon. Phys. Rev. Lett. 1997. 78(17): p. 3350–3353.

[59] R. Q. Hood, M. Y. Chou, A. J. Williamson, G. Rajagopal and R. J. Needs. Exchange and correlation in silicon. Physical Review B, 1998. 57(15): p. 8972–8982.

[60] R. Car, Quantitative Structure-Activity Relationships. 2002. 21(2): p. 97–104.

[61] P. Fulde, Electron Correlations in Molecules and Solids. 1995. Springer.

[62] L. Hedin, and S. Lundqvist, Effects of electron-electron and electron-phonon interactions on the one-electron states of solids. Solid State Physics, 1970. 23: p. 1–181.

[63] S. H. Vosko, L. Wilk, and M. Nusair, Accurate spin-dependent electron liquid correlation energies for local spin density calculations: a critical analysis. Canadian Journal of Physics, 1980. 58(8): p. 1200–1211.

[64] J. P. Perdew, K. Burke, and M. Ernzerhof, Generalized gradient approximation made simple. Physical Review Letters, 1996. 77(18): p. 3865–3868.

[65] J. P. Perdew, Ruzsinszky, A; Tao, J; Staroverov, V. N.; Scuseria, G. E.; Csonka, G. I. Prescription for the design and selection of density functional approximations: More constraint satisfaction with fewer fits. The Journal of Chemical Physics, 2005. 123(6): p. 062201–062209.

[66] D. Z. Manrique, Huang, C.; Baghernejad, M.; Zhao, X.; Al-Owaedi, O. A.; Sadeghi, H.; Kaliginedi, V.; Hong, W.; Gulcur, M.; Wandlowski, T.; Bryce, M. R. and Lambert, C. J. A Quantum Circuit Rule for Interference Effects in Single-Molecule Electrical Junctions. Nat. Commun. 2015. 6(6389): p. 1–8.

[67] J. M. Soler,; Artacho, E.; Gale, J. D.; Garcia, A.; Junquera, J.; Ordejon, P.; Sanchez-Portal, D. The SIESTA method for ab initio order-N materials simulation. J. Phys.: Condens. Matter, 2002. 14(11): p. 2745–2779.

[68] C. David, Milan; Oday, A., Al-Owaedi; Marie-Christine, Oerthe; Santiago, Marqués-González; Richard, J., Brooke; Martin, R., Bryce; Pilar, Cea; Jaime, Ferrer; Simon, J., Higgins; Colin, J., Lambert; Paul, J., Low; David, Zsolt, Manrique; Santiago, Martin; Richard, J., Nichols; Walther, Schwarzacher and Víctor, M. García-Suárez. J. Phys. Chem. C, 2016. 120(29): p. 15666–15674.

[69] Enrico Fermi. Sopra lo spostamento per pressione delle righe elevate delle serie spettrali. Il Nuovo Cimento, 1934. 11(3): p.157–166.

[70] Enrico Fermi. Motion of neutrons in hydrogenous substances. Ricerca sci. 1936. 7. p. 13–52.

[71] D. R. Hamann, M. Schlüter, and Chiang, C. Norm-conserving pseudopotentials. Physical Review Letters, 1979. 43(20): p.1494–1497.

[72] Norman Troullier and Jos´e Luriaas Martins. Efficient pseudopotentials for plane-wave calculations. Physical Review B, 1991. 43(3): p. 1993–2006.

[73] N. Troullier and Jos´eLu´ıs Martins. A straightforward method for generating soft transferable pseudopotentials. Solid State Communications, 1990. 74(7): p. 613–616.

[74] Leonard Kleinman and D. M. Bylander. Efficacious form for model pseudopotentials. Physical Review Letters, 1982. 48(20): p. 1425–1428.

[75] O. F. Sankey, and Niklewski, D. J. Ab initio multicenter tight-binding model for molecular-dynamics simulations and other applications in covalent systems. Physical Review B, 1989. 40(6): p. 3979–3995.

[**76]** S. Botti, .Applications of Time-Dependent Density Functional Theory. IOP Science, Physica Scripta, Vol. 2004.(109): p. 54-60 .

[77] M. Petersilka, U. J. Gossmann and E. K. U. Gross, .Excitation Energies from Time-Dependent Density-Functional Theory. Physical Review Letters, 1996. 76(8): p. 1212-1215.

[78] A. Szabo and N. S. Ostlund, .Modem quantum chemistry: Introduction to advanced electronic structure theory. Dover Publication, Inc. Mineola, New York, 2012. p. 484.

[79] R.Chandiramouli,. Structural and electronic properties of germanane nano-sheet upon molecular adsorption of alcohol and aldehyde

molecules: DFT comparative analysis. Elsevier, Journal of Molecular Liquids, 2017. (242): p. 571-579.

[80] W. J. Hehre, .A Guide to Molecular Mechanics and Quantum Chemical Calculations. Wave function, Inc., Printed in the USA, 2013. p. 796.

[81] M. J. Frisch, G. W. Trucks, H. B. Schlegel, G. E. Scuseria, M. A. Robb, J. R. Cheeseman, G. Scalmani, V. Barone, B. Mennucci, G. A. petersson, H. Nakatsuji, M. Caricato, X. Li, H. P. Hratchian, A. F. Izmaylov, J. Bloino, G. Zheng, J. L. Sonnenberg, M. Hada, M.Ehara, K. Toyota, R. Fukuda, J. Hasegawa, M. Ishid, T. Nakajima, Y. Honda, O. Kitao, H. Nakai, T. Vreven, J. A. Montgomery, Jr., J. E. Peralta, F. Ogliaro, M. Bearpark, J. J. Heyd, E. Brothers, K. N. Kudin, V. N. Staroverov, R. Kobayashi, J. Normand, K. Raghavacharii, A. Rendell, J. C. Burant, S. S. Iyengar, J. Tomasi, M. Cossi, N. Rega, J. M. Millam, M. Klene, J. E. Knox, J. B. Cross, V. Bakken, C. Adamo, J. Jaramillo, R. Gomperts, R.E Stratmann, O. Yazyev, A. J. Austin, R. Cammi, C. Pomelli, J. W. Ochterski, R. L. Martin, K. Morokuma, V. G. Zakrzewski, G. A. Voth, P. Salvador, J. J. Dannenberg, S. Dapprich, A.

D. Daniels, O. Farkas, J. B. Foresman, J. V. Ortiz, J. Cioslowski and D. J. Fox, .Gaussian 09, revision A. 02 Gaussian, Inc. Wallingford CT., 2009

[82] A. B. Pacheco, .Electronic Structure Calculations in Quantum Chemistry. HPC Training Louisiana State University, 2011.

[83] A. M. Pier and N. Kumar. ,Quantum transport in mesoscopic systems: complexity and statistical fluctuations. A Maximum Entropy Viewpoint (Mesoscopic Physics and Nanotechnology) Reissue Edition, Oxford University Press on Demand, 2010. p. 416.

[84] V. Sahni, .Quantal Density Functional Theory II: Approximation Methods and Applications. Springer Verlag, Berlin Heidelberg, 2009 p.426.

[85] O. Kwon, V. Coropceanu, N. E. Gruhn, J. C. Durivage, J. G., Katz H. E. Laquindanum, J. Cornil and J. L. Bredas,.Characterization of the Molecular Parameters Determining Charge Transport in Anthradithiophene. AIP, Journal Chemistry Physics, 2004. 120(17). p. 8186-8194.

[86] R. Landauer, .Spatial variation of currents and fields due to localized scatterers in metallic conduction. IBM Journal of Research and Development 1 1957. p. 223-231.

[87] M. Büttiker, Y. Imry, R. Landauer, S. Pinhas, .Generalized many-channel conductance formula with application to small rings. Physical Review B. 1985. 31: p. 6207.

[88] S. Datta, .Electronic transport in mesoscopic systems. (Cambridge university press, 1995.

[89] J. W. Negele and Orland H., Quantum Many-Particle Systems 1998. (New York Perseus Book Group) .

[90] S. Datta,. Electronic transport in mesoscopic systems. 1997.Cambridge university press.

[91] M. Büttiker,, et al., Generalized many-channel conductance formula with application to small rings. Physical Review B, 1985. 31(10): p. 6207.

[92] N. R. Claughton, M. Leadbeater, and C. J. Lambert, Theory of Andreev Resonances in Quantum Dots. Journal of Physics-Condensed Matter, 1995. 7(46): p. 8757– 8784.

[93] E.N. Economou, Green's functions in quantum physics1984. Springer.

[94] P.A. Mello, and N.K. Kumar, Quantum transport in mesoscopic systems: complexity and statistical fluctuations: a maximum-entropy viewpoint. 2004. 4. Oxford University Press on Demand.

[95] G. Sedghi, et al., Long-range electron tunnelling in oligo-porphyrin molecular wires. Nat Nanotechnol, 2011. 6(8): p. 517-23.

[96] X. Zhao, et al., Oligo(aryleneethynylene)s with Terminal Pyridyl Groups: Synthesis and Length Dependence of the Tunneling-to-Hopping Transition of Single-Molecule Conductances. Chemistry of Materials, 2013. 25(21): p. 4340-4347.

[97] M. Magoga, and C. Joachim, Conductance of molecular wires connected or bonded in parallel. Physical Review B, 1999. 59(24): p. 16011-16021.

[98] J. A. Mol, et al., Graphene-porphyrin single-molecule transistors. Nanoscale, 2015. 7(31): p. 13181-5.

[99] W. Hong, et al., An MCBJ case study: The influence of pi-conjugation on the single-molecule conductance at a solid/liquid interface. Beilstein J Nanotechnol, 2011.(2): p. 699-713.

[100] F. Prins, et al., Room-temperature gating of molecular junctions using few-layer graphene nanogap electrodes. Nano Lett, 2011. 11(11): p. 4607-11

[101] J. Xia, et al., Breakdown of Interference Rules in Azulene, a Nonalternant Hydrocarbon. Nano Letters, 2014. 14(5): p. 2941-2945.

[102] T. Markussen, R. Stadler, and K.S. Thygesen, The Relation between Structure and Quantum Interference in Single Molecule Junctions. Nano Letters, 2010. 10(10): p. 4260-4265.

[103] S. Sangtarash, et al., Searching the Hearts of Graphene-like Molecules for Simplicity, Sensitivity, and Logic. Journal of the American Chemical Society, 2015. 137(35): p. 11425-11431.

[104] C.J. Lambert, Basic concepts of quantum interference and electron transport in single-molecule electronics. Chem Soc Rev, 2015. 44(4): p. 875-88.

[105] G. Breit, and E. Wigner, Capture of slow neutrons. Physical Review, 1936. 49(7): p. 519.

[106] D. Z. Manrique, et al., A quantum circuit rule for interference effects in single-molecule electrical junctions. Nat Commun, 2015.

[107] Ke, S.-H., W. Yang, and H.U. Baranger, Quantum-interference-controlled molecular electronics. Nano letters, 2008. 8(10): p. 3257-3261.

[108] U. Fano, Effects of configuration interaction on intensities and phase shifts. Physical Review, 1961. 124(6): p. 1866.

[109] R. Stadler, Quantum interference effects in electron transport through nitrobenzene with pyridil anchor groups. Physical Review B, 2009. 80(12): p. 125401.

[110] J. Ferrer, C. Lambert, V. García-Suarez, S. Bailey, S. Hatef and D. Manrique, .GOLLUM version 1.0. Lancaster University, 2014.

[111] Sankey, Otto F., and David J. Niklewski,. Ab initio multicenter tight-binding model for molecular-dynamics simulations and other applications in covalent systems. Physical Review B 1989. 40(6): p. 3979.

[**112]** L. A. Algharagholy, Q. Al-Galiby, H. A. Marhoon, H. Sadeghi, H. M. Abduljalil, and C. J. Lambert, .Tuning thermoelectric properties of graphene/boron nitride heterostructures. Nanotechnology, 2015. 26(47): p. 475401.

[113] C.-X. Liu, X.-L. Qi, H. Zhang, X. Dai, Z. Fang, and S.-C. Zhang, .Model Hamiltonian for topological insulators. Phys. Rev. B, 2010. 82(4): p. 45122.

[114] S. Mao, A. Yamakage, and Y. Kuramoto, .Tight-binding model for topological insulators: Analysis of helical surface modes over the whole Brillouin zone. Phys. Rev. B, 2011. 84(11): p. 115413.

[115] D. Fichou, S. Delysse, and Nunzi, J.-M. First evidence of stimulated emission from a monolithic organic single crystal: α-Octithiophene. Adv. Mater. 9, 1997 . p. 1178–1181

[116] Samuel, I. D. W. and Turnbull, G. A. Organic semiconductor lasers. Chem. Rev. 107. 2007. p.1272–1295.

[117] S. Chénais, and S. Forget, Recent advances in solid-state organic lasers. Polym. Int. 61, 2012. p . 390–406.

[118] Cui, Q. H., Zhao, Y. S. and Yao, J. Controlled synthesis of organic nanophotonic materials with specific structures and compositions. Adv. Mater. 26, 2014. p. 6852–6870 .

[119] A. J. C. Kuehne, and Gather, M. C. Organic lasers: recent developments onmaterials, device geometries, and fabrication techniques. Chem. Rev. 116, 2016. p .12823–12864.

[120] J. Gierschner, S. Varghese, and Park, S. Y. Organic single crystal lasers: amaterials view. Adv. Opt. Mater. 4, 2016. p.348–364.

[121] H. Nakanotani, et al. Extremely low-threshold amplified spontaneous emission of 9,9′-spirobifluorene derivatives and electroluminescence from field-effect transistor structure. Adv. Funct. Mater. 17. 2007. p. 2328–2335 .

[122] A. S. D. Sandanayaka, et al. Quasi-continuous-wave organic thin-film distributed feedback laser. Adv. Opt. Mater. 4, 2016. p. 834–839 .

[123] Baldo, M. A., O'Brien, D. F., Thompson, M. E. & Forrest, S. R. Excitonic singlet-triplet ratio in a semiconducting organic thin film. Phys. Rev. B 60, 1999. p. 14422–14428 .

[124] A. S. D. Sandanayaka, et al. Indication of current-injection lasing from an organic semiconductor. Appl. Phys. Express 12, 2019. p. 061010 .

[125] K. N. Baker, A. V. Fratini, T. Resch, H. C. Knachel, W. W. Adams, E. P. Socci and B. L. Farmer, Polymer, 1993, 34, 1571–1587.

[126] S. Hotta and K. Waragai, J. Mater. Chem., 1991. 1: p. 835–842.

[127] S. Hotta and K. Waragai, Adv. Mater., 1993. 5: p. 896–908.

[128] S. Hotta and M. Goto, Adv. Mater., 2002.14: p. 498–501.

[129] S. Hotta, M. Goto, R. Azumi, M. Inoue, M. Ichikawa and Y. Taniguchi, Chem. Mater., 2004. 16: p. 237–241.

[130] T. Yamao, Y. Taniguchi, K. Yamamoto, T. Miki, S. Ota, S. Hotta, M. Goto and R. Azumi, Jpn. J. Appl. Phys., 2007.46: p. 7478–7482.

[131] T. Yamao, Y. Nishimoto, K. Terasaki, H. Akagami, T. Katagiri, S. Hotta, M. Goto, R. Azumi, M. Inoue, M. Ichikawa and Y. Taniguchi, Jpn. J. Appl. Phys., 2010. 49: p. 04DK20.

[132] Ou, Q., Peng, Q., & Shuai, Z. .Computational screen-out strategy for electrically pumped organic laser materials. Nature communications, 2020. 11 (1) :p. 1-10 .

[133] H. Nakanotani, Furukawa, T., Hosokai, T., Hatakeyama, T., & Adachi, C. . Light amplification in molecules exhibiting thermally

activated delayed fluorescence. Advanced Optical Materials, 2017. 5 (12).

[134] H. Huang, Yu, Z., Zhou, D., Li, S., Fu, L., Wu, Y. & Fu, H. , Wavelength-Turnable organic microring laser arrays from thermally activated delayed fluorescent emitters", Acs Photonics, 2019. 6 (12) :p. 3208-3214 .

[135] Ye, H., Kim, D. H., Chen, X., Sandanayaka, A. S., Kim, J. U., Zaborova, E. & Adachi, C. .Near-infrared electroluminescence and low threshold amplified spontaneous emission above 800 nm from a thermally activated delayed fluorescent emitter. Chemistry of Materials, 30 (19): p. 6702-6710, 2018.

[136] D. Kim, H. D'aléo, A., Chen, X. K., Sandanayaka, A. D., Yao, D., Zhao, L. & Adachi, C. . High-efficiency electroluminescence and amplified spontaneous emission from a thermally activated delayed fluorescent near-infrared emitter. Nature Photonics. 2018. 12(2): p. 98-104.

[137] M. A. Abdulsattar, S. A. Majeed and A. M. Saeed .Electronic, structural, and vibrational properties of α-sn Nano crystals built from diamonded structures: Ab initio study. IEEE Trans. Nanotechnology., 13 . 2014. p.1186-1193.

[138] D. Zhang, Huang, T., Duan, L. .Emerging Self-Emissive Technologies for Flexible Displays. Adv. Mater. 2020, 32: p. 1902391.

[139] A. J. Heeger, Semiconducting and Metallic Polymers: The Fourth Generation of Polymeric Materials (Nobel Lecture). Angew.Chem., Int. Ed. 2001, 40: p. 2591−2611.

[140] H. Sirringhaus, 25th Anniversary Article: .Organic Field-Effect Transistors. The Path Beyond Amorphous Silicon. Adv. Mater. 2014. 26: p.1319−35.

[141] Y. Zhao, Guo, Y.; Liu, Y. 25th Anniversary Article .Recent Advances in N-Type and Ambipolar Organic Field-Effect Transistors.Adv. Mater. 2013. 25: p.5372−91.

[142] Y. Ren, Yang, X.; Zhou, L.; Mao, J. Y.; Han, S. T.; Zhou, Y. Recent Advances in Ambipolar Transistors for Functional Applications. Adv. Funct. Mater. 2019. 29: p.1902105.

[143] C. Zhang, Chen, P.; Hu, W. .Organic Light-Emitting Transistors: Materials, Device Configurations, and Operations. Small 2016. 12: p.1252−94.

[**144]** Liu, C. F.; Liu, X.; Lai, W. Y.; Huang, W. . Organic Light-Emitting Field-Effect Transistors: Device Geometries and Fabrication Techniques. Adv. Mater. 2018.30: p.1802466.

[145] J.Zaumseil, Recent Developments and Novel Applications of Thin Film, Light-Emitting Transistors. Adv. Funct. Mater. 2020. 30: p.1905269.

[146] A. Hepp, H. Heil, Weise, W.; Ahles, M.; Schmechel, R.; von Seggern, H. .Light-Emitting Field-Effect Transistor Based on a Tetracene Thin Film. Phys. Rev. Lett. 2003. 91: p.157406.

[147] S. Toffanin, Capelli, R.; Koopman, W.; Generali, G.; Cavallini,S.; Stefani, A.; Saguatti, D.; Ruani, G.; Muccini, M. Organic Light-Emitting Transistors with Voltage-Tunable Lit Area and Full Channel Illumination. Laser & Photonics Reviews 2013. 7: p. 1011−1019.

[148] W. A. Koopman, Natali, M.; Donati, G. P.; Muccini, M.;Toffanin, S. .Charge−Exciton Interaction Rate in Organic Field-Effect Transistors by Means of Transient Photoluminescence Electromodulated Spectroscopy. ACS Photonics 2017. 4: p.282−291.

[149] A. S. D. Sandanayaka, Matsushima, T.; Bencheikh, F.; Terakawa, S.; Potscavage, W. J.; Qin, C.; Fujihara, T.; Goushi, K.; Ribierre, J.-C.; Adachi, C. . Indication of Current-Injection Lasing from an Organic Semiconductor. Appl. Phys. Express 2019. 12: p. 061010.

[150] Liu, D.; De, J.; Gao, H.; Ma, S.; Ou, Q.; Li, S.; Qin, Z.; Dong, H.; Liao, Q.; Xu, B.; Peng, Q.; Shuai, Z.; Tian, W.; Fu, H.; Zhang, X.; Zhen, Y.; Hu, W. .Organic Laser Molecule with High Mobility, High Photoluminescence Quantum Yield, and Deep-Blue Lasing Characteristics.J. Am. Chem. Soc. 2020. 142: p.6332−6339.

[151] L. Hou, Zhang, X.; Cotella, G. F.; Carnicella, G.; Herder, M.; Schmidt, B. M.; Patzel, M.; Hecht, S.; Cacialli, F.; Samori, P. .Optically Switchable Organic Light-Emitting Transistors. Nat. Nanotechnol. 2019. 14: p.347−353.

[152] D. Yuan, Sharapov, V.; Liu, X.; Yu, L. .Design of High-Performance Organic Light-Emitting Transistors. ACS Omega 2020. 5: p.68.

[153] C. J. Lambert, Liu, S.-X. Chem. Eur. J. 2018, 24, 4193-4201;K.Yoshizawa, T. Tada, and A. Staykov, J. Am. Chem. Soc. 2008. 130: p.9406

[154] R. Stadler, Jacobsen, K. W. Phys. Rev. B 2006. 74: p.161405.

[155] S. Huzinaga and S. Narita. Mulliken Population Analysis and Point Charge Model of Molecules. Israel Journal of Chemistry 1980. 19: p. 242-254.

[156] Peng, Q., Yi, Y., Shuai, Z. & Shao, J.. Toward quantitative prediction of molecular fluorescence quantum efficiency: role of duschinsky rotation. J. Am. Chem. Soc. 2007. 129: p. 9333–9339 .

[157] P. Hohenberg and W. Kohn, Phys. Rev., 1964. 136: p. B864–B871.

[158] W. Kohn and L. J. Sham, Phys. Rev., 1965. 140: p. A1133–A1138.

[159] K. Capelle, Braz. J. Phys., 2006. 6: p.1318–1343.

[160] J. P. Perdew, K. Burke and M. Ernzerhof, Phys. Rev. Lett.,1996. 77: p. 3865–3868.

[161] N. Troullier and J. L. Martins, Phys. Rev. B: Condens. Matter Mater. Phys., 1991. 43: p.1993–2006.

[**162]** P. Ordejo´n, E. Artacho and J. M. Soler, Phys. Rev. B: Condens.Matter Mater. Phys., 1996.53: p. R10441–R10444.

[163] D. Sa´nchez-Portal, P. Ordejo´n, E. Artacho and J. M. Soler, Int. J. Quantum Chem., 1997. 65: p.453–461.

[164] E. Artacho, D. Sa´nchez-Portal, P. Ordejo´n, A. Garcia and J. M. Soler, Phys. State Solid. B, 1999. 215: p. 809–817.

[165] H. J. Monkhorst and J. D. Pack, Phys. Rev. B: Solid State, 1976.13: p. 5188–5192.

[166] J Ferrer, C J Lambert, V M García-Suárez, D Zs Manrique, D Visontai, L Oroszlany, R Rodríguez-Ferradás, I Grace, S W D

Bailey, K Gillemot, Hatef Sadeghi and L A Algharagholy ,. "GOLLUM: a next-generation simulation tool for electron, thermal and spin transport." New Journal of Physics , 2014.16 (9): p.93029 .

[167] S. V. Aradhya, et al. Dissecting contact mechanics from quantum interference in single-molecule junctions of stilbene derivatives. Nano Lett. 2012. 12: p. 1643–1647.

[168] C. R. Arroyo, et al. .Signatures of quantum interference effects on charge transport through a single benzene ring. Angew. Chem. Int. Ed. 2013. 52: p.3152–3155 .

[169] J. S. Meisner, et al. Importance of direct metalp coupling in electronic transport through conjugated single-molecule junctions. J. Am. Chem. Soc. 2012. 134: p. 20440–20445 .

[170] C. R. Arroyo, et al, .Quantum interference effects at room temperature in OPV-based single-molecule junctions. Nanoscale Res. Lett. 2013. 8: p.1–6.